Trends of Oxygen with Bidecadal Oscillations in the Western North Pacific

January 2016

Daisuke SASANO

Trends of Oxygen with Bidecadal Oscillations in the Western North Pacific

A Dissertation Submitted to
the Graduate School of Life and Environmental Sciences,
the University of Tsukuba
in Partial Fulfillment of the Requirements
for the Degree of Doctor of Environmental Studies
(Doctoral Program in Sustainable Environmental Studies)

Daisuke SASANO

Contents

Abbreviations

AL: Aleutian Low

AOU: Apparent Oxygen Utilization

CFCs: Chlorofluorocarbons

DIC: Dissolve Inorganic Carbon

DSW: Dense Shelf Water

EUC: Equatorial Undercurrent

KEF: Kuroshio Extension Front

NEC: North Equatorial Current

NPCMW: North Pacific Central Mode Water

NPI: North Pacific Index

NPIW: North Pacific Intermediate Water

NPSTMW: North Pacific Subtropical Mode Water

NLS: Nonlinear Least Squares

OHC: Ocean Heat Content

OML: Oxygen Minimum Layer

OSIW: Okhotsk Sea Intermediate Water

OSP: Ocean Station Papa

OUR: Oxygen Utilization Rate

PV: Potential Vorticity

QC: Quality Control

WSAG: Western Subarctic Gyre

WSAW: Western Subarctic Water

Abstract

Dissolved Oxygen (O_2) is a fundamental biogeochemical parameter in oceanic systems. The distribution of O_2 concentration in the ocean is controlled by biological processes (photosynthesis and remineralization) and physical processes (air-sea interaction and water transport). Over the past few decades, secular trends due to climate change of dissolved O_2 have been observed in a variety of regions and depths in the North Pacific, but it is necessary to improve our understanding of these controlling factors. In the present study, the controlling factors of secular trends in dissolved O_2 was demonstrated based on long-term hydrographic and hydrochemical observations in the western North Pacific.

In Chapter 1, a quick response dissolved O_2 sensor "RINKO" was evaluated, which was under development at that time, to determine its in situ response and applicability to hydrographic and hydrochemical observations. The response time of the RINKO sensor to ambient O_2 changes was demonstrated at about 1 sec in these in situ experiments. RINKO data were calibrated to temperature, pressure, and bottle sample O_2 data obtained by conventional Winkler method, yielding a precision of $< \pm 1$ μmol kg^{-1}, except in the upper layers of the ocean where vertical O_2 variations are large. Although the sensor was subject to instrumental drift during the period of a cruise (equivalent to < 6 μmol kg^{-1} in O_2) and to pressure hysteresis between downcasts and upcasts (< 4 μmol kg^{-1} in O_2), the RINKO sensor is capable of observing continuous vertical O_2 profiles with a precision that is sufficient for most practical purposes.

In Chapter 2, the rate of change of dissolved O_2 concentrations was analyzed over 1987–2011 for the high-frequency repeat section along 165°E in the western North Pacific. Significant trends toward decreasing O_2 were detected in the northern subtropical to

subtropical-subarctic transition zones over a broad range of isopycnal horizons. On 25.3σ_θ between 25°N and 30°N in North Pacific Subtropical Mode Water, the rate of O_2 decrease reached -0.45 ± 0.16 μmol kg^{-1} yr^{-1}. It is largely attributed to a deepening of isopycnal horizons and to a reduction in oxygen solubility associated with ocean warming. In North Pacific Intermediate Water, the rate of O_2 decrease was elevated (-0.44 ± 0.14 μmol kg^{-1} yr^{-1} on 26.8σ_θ) and was associated with net increases in apparent oxygen utilization in the source waters. On 27.3σ_θ in the subtropical Oxygen Minimum Layer (OML) between 32.5°N and 35°N, the rate of O_2 decrease was significant (-0.22 ± 0.05 μmol kg^{-1} yr^{-1}). It was likely due to the increases in westward transport of low-oxygen water. These various drivers controlling changes in O_2 along the 165°E section are the same as those acting along 137°E [*Takatani et al.*, 2012] and also account for the differences in the rate of O_2 decrease between these sections. Additionally, in the tropical OML near 26.8σ_θ between 5°N and 10°N, significant trends toward increasing O_2 were detected in both sections (+0.36 ± 0.04 μmol kg^{-1} yr^{-1} in the 165°E section). These results demonstrate that warming and circulation changes are causing multidecadal changes in dissolved O_2 over wide expanses of the western North Pacific.

In Chapter 3, the rates of change of dissolved O_2 concentrations were analyzed over 1954–2014 for the high-frequency observation in the Oyashio region in the western subarctic North Pacific. Significant linear trends toward decreasing O_2 were detected between 26.6σ_θ and 27.5σ_θ. The largest decreasing rate in O_2 was found on 26.7σ_θ at -0.72 ± 0.11 μmol kg^{-1} yr^{-1} while it was attributed to a deepening effect of isopycnal horizons by approximately 33%. Additionally, the decreasing O_2 around these densities would be attributed to a reduction of ventilation because surface density in winter have been decreasing and the density is corresponding to temperature minimum layer which is formed in winter convection. Furthermore, O_2 decrease in deep densities up to 27.5σ_θ would be attributed to signals from

the Sea of Okhotsk which is propagated by diapycnal mixing, and to strengthening of the Aleutian Low. In the Oyashio region, bidecadal oscillations of O_2 were determined in 26.6σ_θ–27.5σ_θ. The cycles of oscillations were almost constant at 16.4–19.6 years, and were vertically synchronized within 1 year. Along the 165°E section, the bidecadal oscillations were also found horizontally in 30°N–42.5°N on 26.8σ_θ with a lag of 1–3 years from the Oyashio region, and vertically in 40°N up to the subtropical OML at 27.5σ_θ. It suggests that the bidecadal oscillations are extended horizontally and vertically to the region where the subarctic water influences. Since the amplitude of oscillations of O_2 in 165°E is as half as those in the Oyashio region, variation of O_2 found in the eastern subarctic North Pacific is not propagated directly from the Oyashio region. These results demonstrate that the western subarctic North Pacific plays an important role of the origin for secular trends and natural climate variability in dissolved O_2. In this study, the controlling factor of long-term changes in dissolved O_2 was indicated in the western subtropical and subarctic North Pacific, and the extension of bidecadal oscillations of O_2 from the Oyashio region together with consideration in change in physical field. These comprehensive analyses lead a new insight of picture about O_2 change in the North Pacific.

General Introduction

Dissolved oxygen (O_2) is a fundamental biogeochemical parameter in oceanic systems. For all aerobic organisms, O_2 is closely linked parameter to survive. Generally, their essential activities are photosynthesis and remineralization. Through photosynthesis for which phytoplankton is responsible, O_2 is produced and thereby is released to ambient water. Concurrently, other biogeochemical parameters, such as carbon dioxide (CO_2), phosphate (PO_4), and nitrate (NO_3), are consumed. On the other hand, remineralization including aerobic respiration, which is generally accompanied by both autotrophic and heterotrophic organisms, is an inverse reaction to photosynthesis, meaning that O_2 is consumed and CO_2 and other related parameters are produced. Therefore, oxygen plays central roles directly in the biogeochemical cycles of carbon, nitrogen, and other important elements (P, Fe, Mn, etc.). Additionally, O_2 has another function to indirectly control nitrogen cycle in the ocean. Under suboxic environment (< ~5 μmol kg^{-1}), denitrification is superior to respiration, and thereby NO_3 is converted to gaseous nitrogen which is finally released to the atmosphere; denitrification affects a cycle of nitrate, and therefore productivity in the ocean.

The distribution of O_2 concentration in the ocean is controlled by biological processes (photosynthesis and remineralization) and physical processes (air-sea interaction and water transport). Therefore, O_2 concentration in the ocean interior is used as an indicator of water masses. As mentioned above, photosynthesis and remineralization act as source and sink of O_2, respectively. Because photosynthesis is driven by solar light, O_2 production occurs only in euphotic layers. In contrast, O_2 consumption through remineralization occurs in almost any region where bacteria live. Air-sea interaction controls O_2 concentration in near surface waters. When O_2 in the ocean is supersaturated against the atmosphere, the ocean loses O_2 to

the atmosphere. On the other hand, when O_2 in the ocean is undersaturated, the ocean gains O_2 from the atmosphere. This is mainly determined by the saturation concentration of O_2 (O_2^{sat}), that is, mainly controlled by the distribution of sea surface temperature (when temperature is low, O_2^{sat} increases). O_2 exchange between the atmosphere and ocean is relatively rapid; it usually takes about a month to be equilibrated sufficiently [e.g., *Broecker and Peng*, 1974]. Although dissolved O_2 concentration is typically close to O_2^{sat}, it is not perfectly equilibrated. Generally, near surface waters are slightly supersaturated due to production of O_2 by photosynthesis. In subarctic region, near surface waters are typically undersaturated in winter, reflecting high O_2^{sat} due to low temperature and deep convection which moves up low O_2 water from deeper layer to take more time to equilibrate. Water transport, such as vertical mixing, diffusion, lateral transport, and oceanic circulation, controls vertical and horizontal distributions of O_2. For example, vertical mixing and subsequent subduction supply high O_2 water from near surface to subsurface waters. However, water transport does not act as source and sink of O_2 practically, but it distributes waters and subsequently changes the concentration through mixing with ambient water. As another function, water transport induces the change of residence time of water. When the elapsed time after the water is last in contact with the atmosphere is extended by slowdown in ocean circulation, O_2 concentration is decreased due to accumulation of bacterial remineralization with time.

Measurement method of dissolved O_2, “Winkler titration”, has been developed in the end of nineteenth century [*Winkler*, 1888]. After that, the method was modified [*Carpenter et al.*, 1965, 1966], but the principle of measurement was the same as before. Superiority of this method is that it is simple and the precision is relatively high even in historical data although there are no certified reference material of dissolved O_2 to achieve detectable

measurement of long-term trends. For example, *Aoyama et al.* [2008] have estimated the precision of O_2 analysis as 0.5% in the cruises conducted by Nagasaki Marine Observatory from 1965 to 1999. As a result, data with relatively good qualities are archived over the long period. In World Ocean Database 2013, while physical parameters of temperature and salinity have the largest number of the observation data (over 2,850,000 and 2,380,000 by 2012, respectively), oxygen data set has the largest number of observation data (~900,000) among biochemical parameters [*Boyer et al.*, 2013]. It means that oxygen data have been accumulated historically with relatively good quality. Although other biochemical parameters, such as PO_4 and NO_3, also have the next largest number of observations (over 576,000 and 353,000, respectively), these historical parameters have some problems in data quality. Considering these advantages, oxygen data set is the most suitable among the biogeochemical parameters to determine the variability in a long period. An O_2 sensor is another powerful tool for determination of O_2 concentrations in seawater because the sensor allows continuous automated observations. The sensor can determine O_2 variability in great detail vertically and horizontally if the sensor is calibrated appropriately to obtain precise measurements and its response time is quick. Although some sensors for biochemical parameters have been developed, they have some problems in reliability in precision and/or stability to determine long-term variability today. Although O_2 sensors with good qualities were recently developed, these data help us to understand O_2 variability in the ocean.

The distributions of physical parameters of temperature and salinity controls vertical structure and flow field in the ocean. Therefore the studies for long-term trends in these parameters are critical to forecast the environment in the future. By contrast, there are many phenomena in the ocean which cannot be detected by physical parameters but can be detected by biogeochemical parameters. For these reasons, oxygen data set is suitable to

investigate more information about climate change. One of the most serious findings from long-term O_2 data set is “ocean deoxygenation”, meaning that dissolved O_2 have been decreased in the world’s ocean over the past few decades [*Keeling et al.*, 2010, and references therein]. Deoxygenation is considered as one of the serious consequences of climate change driven by human activities. One of the problems of deoxygenation is to change ocean environment to be difficult to survive for aerobic organisms. Therefore, deoxygenation is considered as the serious stressor to affect ecosystem together with the warming and acidification of the ocean [*Gruber,* 2011]. Indeed, deoxygenation has already led to serious affection to ecosystem in freshwater and coastal regions [*Diaz and Rosenberg*, 2008]. These changes are usually caused by eutrophication by agricultural runoff or sewage inputs. Changing in ocean current system is another factor of controlling deoxygenation. In California coastal region in 2002, change in upwelling system developed transports of deep water with low O_2 onto continental shelves, which induced mass die-offs fish and invertebrates [*Grantham* al., 2004]. In an open ocean, the decrease of O_2 level today would not affect ecosystem immediately. However, in the future, progress in deoxygenation may affect the ecosystem even in an open ocean by sensitivity to O_2 concentration and living area of species. Another problem of deoxygenation is the extension of Oxygen Minimum Layer (OML). In several ocean basins, OMLs are expected at intermediate depth. Due to deoxygenation, OMLs have expanded vertically and their O_2 concentrations have been decreased [*Stramma et al.*, 2008]. The extension of low O_2 layers accelerates denitrification as mentioned above. Increase in denitrification not only affects the nitrogen cycle in the ocean but also increases the oceanic production of nitrous oxide (N_2O) which is produced as a by-product of denitrification. Because N_2O is a powerful greenhouse gas, deoxygenation may accelerate global warming. Understanding deoxygenation is also crucial for carbon

cycle studies because decrease in dissolved O_2 in the ocean implies increase in CO_2. The concentration of CO_2 in the atmosphere has been increased after industrial revolution in middle of eighteenth century by the combustion of fossil fuels and by the change in land use change through human activities. For the decadal mean during 2002–2011, global CO_2 emissions from fossil fuel combustion (including cement production) and land use change were 8.3 ± 0.4 PgC yr^{-1} and 1.0 ± 0.5 PgC yr^{-1}, respectively, and the ocean CO_2 sink was 2.5 ± 0.5 PgC yr^{-1} [*Le Quéré et al.*, 2013], meaning that 27% of anthropogenic CO_2 has been absorbed and stored in the ocean. It indicates that the ocean moderates global warming. Understanding changes in dissolved O_2 in the ocean are necessary to distinguish the change in dissolved inorganic carbon due to biological activity from that due to the anthropogenic CO_2 invasion into the ocean interior [e.g., *Brewer*, 1978; *Gruber et al.*, 1996].

Together with secular trends due to climate change, natural climate variability is usually found in an environment. When the variability is considerably large, it is necessary to evaluate the natural variability to distinguish the secular trends properly. In the Oyashio region in the western North Pacific, O_2 decrease with bidecadal oscillations have been reported [*Ono et al.*, 2001]. The oscillations in O_2 were also reported in other regions in the subarctic western and eastern North Pacific [*Andreev and Kusakabe*, 2001; *Whitney et al.*, 2007]. Although bidecadal oscillations in other parameters have been reported such as potential temperature in the Sea of Okhotsk [*Osafune and Yasuda*, 2006] and PO_4 in the Oyashio region [*Tadokoro et al.*, 2009], the oscillations in O_2 is fairly clear in their large amplitude and data precision. It means that oxygen data set is also applicable to detect natural variability in the ocean.

This study focuses on the western North Pacific. In the region, the density outcropped to sea surface in winter is the densest typically up to $26.6\sigma_\theta$ in the open ocean in the North

Pacific [*Reid*, 1965]. In the marginal sea of the Sea of Okhotsk, denser water up to 27.0σ_θ is ventilated through the sea ice formation [*Martin et al.*, 1998; *Gladyshev et al.*, 2000], and then this ventilated water is outflowed to the western North Pacific at the Kuril Straits through tidal mixing processes [*Nakamura et al.*, 2000]. It means that O_2 source for the North Pacific deeper than depth of 26.6σ_θ is generally limited to the western North Pacific. Additionally, some dominant water masses observed in the North Pacific are formed in the region such as North Pacific Intermediate Water. Therefore, it is crucial to examine of O_2 change in the region to understand its extension to the whole North Pacific. Furthermore, some regions in the subarctic western North Pacific are known that bidecadal oscillations in dissolved O_2 have been determined such as the Oyashio region [*Ono et al.*, 2001] and the Sea of Okhotsk [*Osafune et al.*, 2006]. Because whole pictures about the extensions of the bidecadal oscillations to the North Pacific has not been clarified, the study about the oscillations will promote the better understanding of O_2 variation including long-term trends in the North Pacific.

To understand secular trends and natural climate variability in dissolve O_2, it is necessary to investigate data which have high quality and cover high spatial and temporal density datasets in space and time. The Japan Meteorological Agency (JMA) has been conducting time-series hydrographic and biogeochemical measurements along many sections. Notably, the relatively high frequency temporal sampling along meridional sections at 165°E and 137°E in the western North Pacific offers a number of globally unique opportunities for evaluating biogeochemical variability over a broad range of timescales and regions. Additionally, numerous data have been accumulated in the Oyashio region. The region is close to the region where the densest density is outcropped in the open ocean in the North Pacific, and therefore the analysis in dissolve O_2 in the region leads to understanding the

controlling factor of change in O_2 in the North Pacific. Through the comparison between these data, secular trends and natural climate variability in the western North Pacific were evaluated.

The aim of Chapter 1 is to evaluate the performance of the O_2 sensor “RINKO” (JFE Advantech Co., Ltd.). RINKO sensor has a quick response time to changes in O_2 concentrations (< 1 sec, 90% response at 25°C, according to the manufacturer’s specifications). This feature is superior to other sensors. If RINKO sensor is applicable to shipboard hydrographic observations with sufficient precision, we can acquire continuous data with detailed structure of vertical O_2 profiles. The aim of Chapter 2 is to analyze the rate of change of dissolved O_2 concentrations along the 165°E section in the western North Pacific. Significant trends towards decreasing dissolved O_2 were identified in the principal water masses at 165°E. Through the comparison with the results documented by *Takatani et al.* [2012] for 137°E, large-scale controls of the O_2 decreases in the western North Pacific were evaluated. In Chapter 3, long-term trends and bidecadal oscillations in dissolved O_2 in the Oyashio region were evaluated. Although the oscillations have been reported in the Oyashio region, more detailed analysis than the previous study was conducted. Furthermore, the oscillations along the northern part of the 165°E section were also evaluated. Through comparison of the oscillations between the Oyashio region and the 165°E section, the expansion of the oscillations in the western North Pacific was examined.

Chapter 1

Testing a new quick response oxygen sensor, “RINKO”

1.1. Introduction

Dissolved oxygen (O_2) is a fundamental biogeochemical parameter in oceanic systems, reflecting biological activity, air–sea interactions and oceanic circulation. In the ocean interior, changes in dissolved O_2 are closely related to changes in other biogeochemical parameters, such as nitrate, phosphate, and dissolved inorganic carbon (DIC). The inverse relationship between O_2 and DIC is of particular importance; in the euphotic zone, O_2 is produced (and DIC consumed) as a consequence of photosynthesis and is consumed (and DIC produced) by the respiratory processes of autotrophic and heterotrophic organisms. Therefore, observations of O_2 in the ocean are crucial for discriminating changes in ocean carbon content due to the increase in anthropogenic CO_2 from those due to biological activity and/or ocean circulation [e.g., *Gruber*, 1998].

Concentrations of dissolved O_2 in seawater in a discrete sample bottle have been determined using a titration technique developed by *Winkler* [1888]; because dissolved O_2 concentrations can be determined with high precision (< 1 μmol kg^{-1}) with this relatively simple method, it has been widely used for oceanographic observations, and is the basis for a large, good quality, historical dissolved O_2 database. However, an inherent disadvantage of titration methods using discrete sampling bottles is that the resulting data inevitably represent rather sparse sampling intervals, both spatially and temporally.

O_2 sensors are another powerful tool for determination of O_2 concentrations in seawater. O_2 sensors allow continuous automated observations and thus the determination of O_2 variability in great detail. Recently, Argo floats with attached O_2 sensors have been deployed in the oceans, thus facilitating the collection of high spatial and temporal density datasets in space and time [*Gruber et al.*, 2007; *Körtzinger et al.*, 2008].

Several types of O_2 sensors have been developed. The SBE-43 (SeaBird Electronics Inc.) is commonly used for hydrochemical observations because the instrument has a quick response time (< 7 sec at 29.2°C and < 28 sec at 1.7°C, for a 99% nominal response); however, it is subject to long-term instability and pressure hysteresis. The Aanderaa optode (Aanderaa Data Instruments AS) is another widely used sensor, exhibiting excellent temporal stability and suitability for mooring observations; however, the sensor is less suitable for hydrochemical observations because its response time is slow relative to the O_2 change during the CTD's motion [*Uchida et al.*, 2008]. Appropriate calibration can largely compensate for the limitations of the SBE-43 and Aanderaa optode sensors [*Uchida et al.*, 2010]. However, the response time of O_2 sensors in response to rapidly changing O_2 concentrations is critical for collection of shipboard vertical hydrographic and hydrochemical observations using CTD systems, because the quick response yields high resolution data that clarify the detailed structure of vertical O_2 profiles.

Recently, a new optical O_2 sensor, "RINKO" (JFE Advantech Co., Ltd.), was developed on the basis of fluorescence quenching of a pressure sensitive paint layer. The RINKO sensor is outstanding for its quick response time to changes in O_2 concentrations (< 1 sec, 90% response at 25°C, according to the manufacturer's specifications), and is therefore considered applicable for continuous and highly accurate shipboard vertical observations in conjunction with CTD measurements. RINKO sensors have already been used for basin-scale hydrographic observations [*Murata et al.*, 2009], and *Uchida et al.* [2010] have proposed a sophisticated calibration procedure. However, information on the performance of RINKO sensors is still insufficient to identify its constraints and full range of applications; further studies are required to suggest improvements to the RINKO sensor system. In this study, RINKO was used for shipboard hydrographic observations in the subarctic to subtropical

western North Pacific and in the Sea of Japan. On the basis of the results, RINKO's performance was evaluated and a simple calibration procedure have been proposed for convenient use in hydrographic observations.

1.2. Materials

A series of experiments with a RINKO sensor in conjunction with a CTD system were conducted on board the R/V *Ryofu maru*, R/V *Keifu maru*, and R/V *Seifu maru* of the Japan Meteorological Agency (JMA) between April and June 2009 in the western North Pacific and in the Sea of Japan (Table 1-1, Fig. 1-1). The RINKO sensor (RINKO III, JFE Advantech Co., Ltd) was connected to the CTD system (SBE 911plus, Sea-Bird Electronics, Inc.) with a carousel multi-sampler. RINKO and CTD data were processed and acquired at a vertical interval of 1 dbar [JMA, 1999]. The pressure data were filtered by using a low pass filter with a time constant of 0.15 sec, as recommended by SBE. Temperature and salinity data were obtained by the CTD sensor. Raw RINKO output was converted to percent oxygen saturation by DO Converter software (JFE Advantech Co., Ltd.), which uses an algorithm based on inputs of raw RINKO data, temperature, and pressure. Dissolved O_2 concentrations (μmol kg^{-1}) were then calculated as the product of the percent oxygen saturation and the saturation concentration of O_2 [*Garcia and Gordon*, 1992]. To assess the response time of RINKO sensors, the serial output of the CTD and RINKO sensor data (24 Hz; 0.0417 s) were sampled to create datasets representing output streams at three frequencies: (1) the first dataset represents an 8-Hz frequency (0.125-sec), chosen to approximately correspond with the sampling rates of the RINKO sensor (ca. 10 Hz), reflecting high frequency (short interval)

data acquisition; (2) the second dataset represents 1-sec output intervals, chosen to evaluate the rate of change in each 1-sec; (3) the third dataset represents 7-sec running averages calculated from (2), chosen to smooth out fluctuations associated with the frequency of the ship's roll (5–9-sec cycle).

At hydrographic/hydrochemical stations, the CTD underwater unit was winched down (downcast) into the sea at a speed of ca. 0.8 m sec^{-1} to the maximum depth of observation; the unit was then winched up (upcast) at a speed of ca. 1.0 m sec^{-1}, while stopping at sampling depths to enclose water samples in Niskin bottles mounted to the carousel multi-sampler. To collect the water samples, the upcast speed of the unit was gradually decreased over a depth interval corresponding to ca. 10 dbar; the unit was stopped for about 20 sec at each sampling depth to close the bottle.

After the CTD unit arrived on deck, the Niskin bottles were sub-sampled into precalibrated glass bottles for dissolved O_2 analyses by a modified Winkler method [*Carpenter*, 1965]. The repeatability of measurements inferred from replicate analyses was 0.35 μmol kg^{-1} (n = 23).

1.3. Results and discussion

1.1.1. Rapid response of the RINKO sensor

Rapid response time is a key property of sensors designed to obtain precise measurements in variable environments. To evaluate the in situ response time of the RINKO sensor, the rate of change of RINKO output was examined at hydrographic stations showing large depth-related O_2 variations. One such station (RF-3369; 37°N, 147°E) in the Kuroshio–

Oyashio Transition Zone was observed in April 2009 during the R/V *Ryofu maru*'s RF09-04 cruise. Within the upper layer at this station, calibrated RINKO O_2 (see next section) showed large and rapidly changing depth-dependent variations in O_2 concentrations: 140–268 μmol kg^{-1} at pressures of 280–150 dbar, and 206–283 μmol kg^{-1} at pressures of 50–25 dbar; these variations are related to horizontal advection of the Kuroshio current (low O_2 and saline water) and the Oyashio current (high O_2 and fresh water) (Fig. 1-2). At this station, the CTD underwater unit was stopped on the upcast for about 20 sec at pressures of 500, 400, 300, 250, 200, 150, 125, 100, 75, 50, 25, and 10 dbar (see horizontal steps in the thick gray line, Fig. 1-3a) to collect water samples in Niskin bottles. The rates of change of pressure, raw RINKO output, and RINKO O_2 concentration were examined using a 7-sec running average of the data resampled at 1 sec intervals. The rate of pressure change was approximately −1 dbar sec^{-1}, except when the CTD underwater unit was stopped to collect water samples (thick gray line, Fig. 1-3b). In regions with steep O_2 gradients, the rate of change of raw RINKO output and calibrated RINKO O_2 values (thin and thick black lines, respectively, Fig. 1-3b) showed large time-dependent variations, with rates of change of O_2 concentration of up to 7 μmol kg^{-1} sec^{-1} (data sampled at 1-sec intervals); the calibrated RINKO O_2 closely track the pressure change variations, without showing any marked delays in response to the pressure changes associated with deceleration or acceleration of the CTD underwater unit when the upcast was paused for sampling (Fig. 1-3b). When the CTD underwater unit stopped ascending at 50 dbar (approximately 100 sec before the end of observations), the O_2 concentration decreased sharply and the rate of change in the raw RINKO output and the calibrated RINKO O_2 showed a slight delay relative to the pressure. However, the CTD temperature measurement, with response time nominally 0.065 sec, also showed a similar delay and the temperature–pressure relationship was also changed at this time (data not shown). This suggests that the raw

RINKO output delay was not due to a delay in response but was likely caused by spatial O_2 variations.

To assess the response of the RINKO sensor in more detail, data at 8-Hz frequencies (0.125-sec intervals) were examined in the vicinity of the 400-dbar depth, where the CTD underwater unit stopped ascending for about 40 sec and the variability of dissolved O_2 gradient was small (Fig. 1-4). The raw RINKO output and pressure data show approximately synchronous fluctuations, but the raw RINKO output shows a phase delay relative to pressure; note that the pressure sensor is considered temporally more stable because its response time (nominally 0.015 sec) is much faster than that of the RINKO sensor (manufacturer specifications: < 1 sec for 90% response at 25°C). To compare the in situ response time of the RINKO sensor with that of the pressure sensor, the lag correlations between the raw RINKO output and pressure data were examined using a dataset with an 8-Hz frequency (0.125-sec sample interval). The lag correlation, plotted as a function of lag time (Fig. 1-5), shows smoothly fluctuating variations with a peak lag correlation at approximately 1 sec (average temperature was 4.7°C) and a period (ca. 7 sec) corresponding with the ship's roll (5–9 sec). This result indicates that the in situ response time of the RINKO sensor to ambient O_2 changes is approximately 1 sec at 4.7°C, which is comparable to the manufacturer's specifications derived from laboratory tests (< 1 sec for 90% response at 25°C).

1.1.2. In-situ RINKO sensor calibration

RINKO O_2 concentrations calculated using the algorithm provided by the manufacturer (hereinafter RINKO-O_2) systematically differed from values obtained directly using the Winkler method (hereinafter Winkler-O_2). The differences between RINKO-O_2 and Winkler-O_2 values were depth-dependent and were particularly large at pressures less than 1000 dbar

where O_2 and temperature were highly variable (Fig. 1-6). In contrast, differences between RINKO-O_2 and Winkler-O_2 values at pressures greater than 1000 dbar were relatively small, and showed systematic variations with depth. In addition, the magnitude of the differences gradually changed during the course of each cruise, indicating that the RINKO sensor is subject to instrumental drift and requires periodic calibration to obtain precise measurements.

This study attempted to calibrate the RINKO sensor using in situ Winkler-O_2 data, first using a quadratic regression of Winkler-O_2 values against corresponding RINKO-O_2 values (open circles, Fig. 1-7). Adding the first-order terms for temperature (T) and pressure (P) values to the quadratic expression for RINKO-O_2 yielded a corrected RINKO-O_2 estimate (hereinafter cor$RINKO_0$-O_2), given by

$$\text{cor}RINKO_0\text{-}O_2 = a\ \text{RINKO-}O^2 + b\ \text{RINKO-}O_2 + c\ T + d\ P + e, \quad (1)$$

where a, b, c, d, and e are coefficients. O_2 values calculated on the basis of the calibration showed a strong correspondence with Winkler-O_2 values, as represented by the 1:1 correspondence between cor$RINKO_0$-O_2 and Winkler-O_2 (closed circles, Fig. 1-7). The multiple regression compensates for nonlinear changes in raw RINKO output in response to ambient oxygen saturation and for dependence to ambient temperature, and pressure.

Using the above calibration equations, differences between cor$RINKO_0$-O_2 and Winkler-O_2 values were mostly reduced to $< \pm 5$ μmol kg^{-1}. However, the targeted difference between RINKO and Winkler O_2 values ($< \pm 1$ μmol kg^{-1}) was not achieved. Furthermore, the magnitude of the differences changed with time (< 6 μmol kg^{-1}) during the course of a cruise because of instrument drift (Fig. 1-8); this could not be corrected using a single set of coefficients for the period of a cruise. It was difficult to estimate the magnitude and persistence of instrument drift because the drift varied during different cruises. However, it was observed that the magnitude of instrument drift was less towards the end of a long cruise

(Fig. 1-8c), suggesting that the RINKO sensor might stabilize during long-term use.

Next, this study attempted to calibrate the RINKO O_2 values for each sampling cast to remove the biases caused by instrument drift (hereinafter corRINKO-O_2), by incorporating time-dependent changes in the values of the regression coefficients in the quadratic multiple regression equation (Fig. 1-9; data for cruise RF09-04). The variations in the coefficients during the course of the cruise were relatively small. However, by calibrating the RINKO data to the Winkler data for each hydrocast, differences between corRINKO-O_2 and Winkler-O_2 were mostly reduced to $< \pm 1$ μmol kg^{-1} over the water columns from near-surface to deep layers at ca. 6000 dbar (Fig. 1-10).

During the cruises, bottle samples were collected at least every few sampling stations, and at least once a day. For stations with no bottle sampling, RINKO-O_2 values were calibrated to Winkler-O_2 data by using both preceding and succeeding sampling stations, since the RINKO-O_2 drift between neighboring sampling stations was expected to be $< \pm 1$ μmol kg^{-1} (Fig. 1-8). The values of the calibration coefficients for stations without bottle-sampling were usually the values of preceding and succeeding sampling stations (Fig. 1-9).

Despite the corrections, large discrepancies ($> \pm 3$ μmol kg^{-1}) between corRINKO-O_2 and Winkler-O_2 were sometimes observed in the upper layers, especially in the Kuroshio–Oyashio Transition Zone (Fig. 1-10a and b). It is likely that these large discrepancies can be attributed to large variations in dissolved O_2 concentrations with depth. In the Kuroshio–Oyashio Transition Zone, vertical O_2 profiles showed O_2-depth gradients that exceeded 10 μmol kg^{-1} $dbar^{-1}$ at a pressure of approximately 50 dbar (Fig. 1-2). If the CTD underwater unit was stopped at a depth corresponding to a large O_2 gradient, the differences between RINKO-O_2 and Winkler-O_2 data might be attributed to the physical distance between the RINKO sensor and the Niskin bottles, which was more than a few tens of centimeters

vertically. Reducing this difference in the upper layers is difficult, especially in the area where the dissolved O_2 profile is largely variable.

Finally, it is possible that some large discrepancies between corRINKO-O_2 and Winkler-O_2 data observed in both shallow and deep water layers were caused by sampling errors or analytical errors in the Winkler method. If an error in the Winkler-O_2 value is suspected, the data should be carefully compared with the RINKO-O_2 profile, as the RINKO-O_2 data may be helpful for detecting such errors.

1.1.3. Pressure hysteresis

In the previous section, it was demonstrated that high-precision RINKO sensor calibration ($< \pm 1$ μmol kg^{-1}) at a sampling station can be achieved by using dissolved O_2 data from bottle samples analyzed with the Winkler titration. However, the bottle samples are generally collected on the upcasts, and it is not certain whether output of the RINKO sensor would vary depending on its direction of motion (descent versus ascent). To determine whether the RINKO sensor was properly calibrated for downcasts, it was examined that the differences between vertical corRINKO-O_2 profiles obtained on downcasts and upcasts in deep layers where the vertical O_2 gradient was gentle and temporal variability is expected to be negligible.

Data from all three cruises showed that corRINKO-O_2 values from downcasts were systematically larger than those from upcasts; in deep layers, the differences were up to 4 μmol kg^{-1} (Fig. 1-11). The greater the maximum pressure on a hydrocast, the greater the magnitude of the differences between the corRINKO-O_2 values from downcasts and upcasts (Fig. 1-11a, c, and e), indicating that the differences were dependent on the magnitude of the maximum pressure in each cast and were probably not artifacts of pressures encountered in

previous casts. Even on shallower casts in which the maximum observed pressure was only about 2000 dbar at the last 18 stations on KS09-04, the differences were still not negligible (Fig. 1-11c). In addition, in the Sea of Japan (cruise SM09-04; Fig. 1-11e and f) where dissolved O_2 concentrations were essentially constant (Winkler-O_2 variations were less than 4 μmol kg^{-1}) at pressures greater than about 2000 dbar (corresponding to the Japan Sea Proper Water, JSPW; Fig. 1-11f), the upcast–downcast differences in deep layers changed almost linearly with pressure (Fig.1-11e), suggesting that the differences are primarily dependent on pressure and change almost linearly under conditions where dissolved O_2 concentrations are constant.

Although the differences in the upper layers might be partly attributable to spatial and temporal O_2 variability, these systematic differences indicate that the RINKO sensor is subject to pressure-induced time-dependent memory effects (i.e., pressure hysteresis) that cause output differences between descending (pressurizing) and ascending (depressurizing) casts. Because RINKO sensor output from downcasts was not calibrated with dissolved O_2 data from bottle samples, the downcast data should be used with caution. Note, however, that the response of the RINKO sensor to ambient O_2 variations is likely to be unaffected by pressure hysteresis, since similar fine-scale patterns of vertical O_2 structures were observed in both downcasts and upcasts (Fig. 1-2).

This study also attempted to calibrate the RINKO O_2 data obtained on the downcast using previously described methods that combined RINKO-O_2, temperature, and pressure data on the downcast with Winkler-O_2 data obtained on the upcast. A subset of the CTD/RINKO data obtained on the downcast was chosen such that the potential density matched that of bottles sampled on the upcast. However, at pressures greater than 2000 dbar, the resulting corRINKO-O_2 values obtained using downcast data had a somewhat larger

uncertainty (< ±4 μmol kg^{-1}) than values obtained on the upcast (Fig. 1-12). At pressures less than 2000 dbar, the uncertainty of corRINKO-O_2 values on the downcast was even greater than that for values obtained on the upcast. Because the vertical structure of the upper layer during downcasts was not necessarily the same as the structure during upcasts, the calibration on downcasts using bottle data obtained on upcasts might generate unreliable results.

Uchida et al. [2010] present a sophisticated algorithm for RINKO sensor calibration that gives accurate O_2 profiles on both downcasts and upcasts. Their algorithm is most helpful when the O_2 profile is merged with CTD data from downcasts (as are usually reported). However, the relatively simple method described above facilitates the collection of O_2 profiles obtained on the upcast with precisions < ± 1 μmol kg^{-1}. Detailed O_2 profiles acquired on the upcast are important because other biogeochemical parameters closely coupled with O_2 concentrations (e.g., nutrient, CO_2 system parameters, dissolved organic carbon, etc.) can only be obtained by bottle sampling on the upcast. It is suggested that CTD and RINKO data be reported not only from downcasts but also from upcasts, in order to give O_2 results that can be compared with data for other biogeochemical parameters obtained on the upcast.

1.4. Conclusion

A new quick response dissolved O_2 sensor (RINKO) developed by JFE Advantech Co., Ltd., was mounted on a CTD system. With this sensor, we successfully obtained high quality O_2 data from shipboard hydrographic and hydrochemical observations in the western North Pacific and in the Sea of Japan. My results demonstrated that the RINKO sensor responds to ambient O_2 changes within about 1 sec, which compares favorably with the manufacturer's

specifications. Although dissolved O_2 values calculated using the manufacture's algorithm are biased in comparison with bottle sample O_2 data, and some problems such as instrument drift and pressure hysteresis were identified, these issues could mostly be corrected by calibrating the instrument with a multiple regression equation with CTD temperature and pressure data and O_2 values obtained by bottle sampling and Winkler titration analyses on the upcast. Using this method, we were able to obtain continuous reliable high precision O_2 data ($< \pm 1$ μmol kg^{-1}) in most environments, except where O_2 concentrations change rapidly with depth. When the RINKO sensor is further improved and the problem of instrument drift is resolved, it will be possible to use Winkler-O_2 data from multiple sampling stations within a certain time interval or leg of the cruise to calibrate the RINKO-O_2 within the targeted resolution of less than 1 μmol kg^{-1}.

The instrument's quick response is the RINKO sensor's main advantage over other O_2 observation instruments, and my results confirmed the RINKO sensor's superior performance as a dissolved O_2 observation instrument. Application of the RINKO sensor to oceanographic observations will clarify and provide details about the vertical structures of dissolved O_2 concentrations, which are difficult to detect with CTD sensor and other sensors. Full utilization and application of the RINKO sensor will contribute to our understanding of dissolved O_2 variability.

Tables and Figures of Chapter 1

Table 1-1. Japan Meteorological Agency cruises on which RINKO sensors were tested.

Ship	Cruise	Date	Area	CTD stations without bottle samplings	CTD stations with bottle samplings
Ryofu maru	RF09-04	22 April – 12 May 2009	south of the Kuroshio – the Kuroshio–Oyashio Transition Zone	15	16
Keifu maru[*]	KS09-04	23 April – 13 May 2009	western North Pacific (137°E)	8	25
Seifu maru	SM09-04	24 April – 8 June 2009	Sea of Japan	5	74

[*] Only upper water layers (pressures < 2000 dbar) were observed at the last 18 stations.

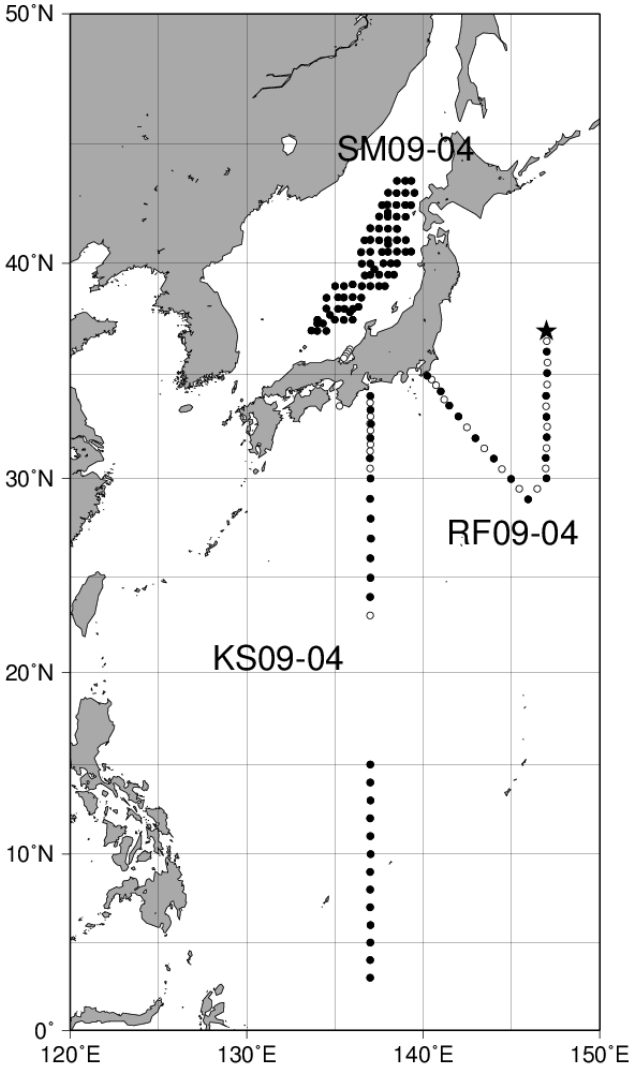

Fig. 1-1. Locations of sampling stations in the western North Pacific and the Sea of Japan. Filled and open circles indicate locations of Conductivity Temperature Depth (CTD) measurements with and without bottle sampling, respectively. The star indicates the location of station RF-3369 (see Figs. 1-2 to 1-5).

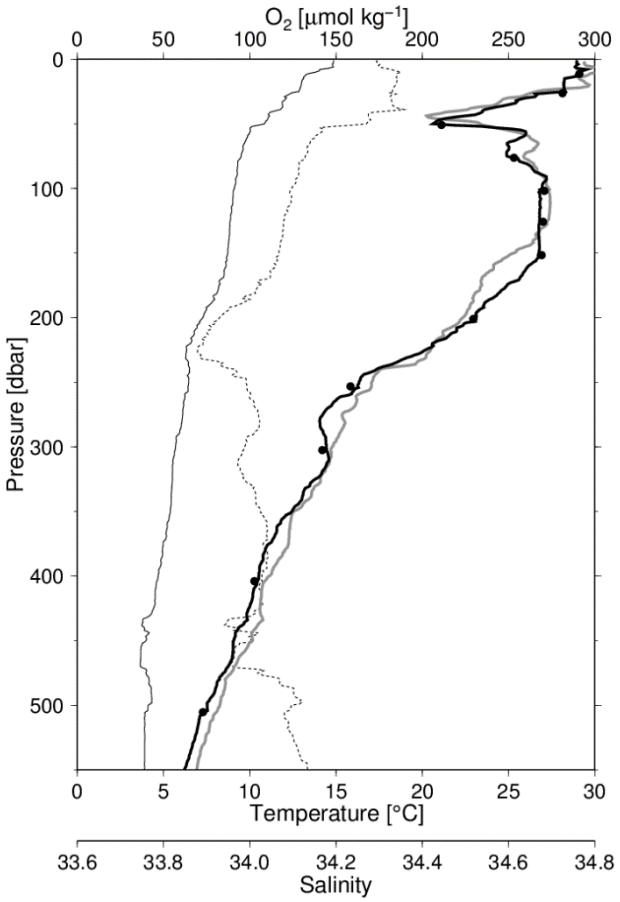

Fig. 1-2. Vertical profiles of dissolved O_2, temperature, and salinity above 550 dbar at station RF-3369 (37°N, 147°E) in the Kuroshio–Oyashio Transition Zone. The thick black line, thin line, and dotted line represent, respectively, dissolved O_2, temperature, and salinity data obtained in the upcast. The thick gray line represents dissolved O_2 data obtained in the downcast, calculated using the same coefficients as in the upcast. Filled circles indicate Winkler O_2 data for samples collected in the upcast.

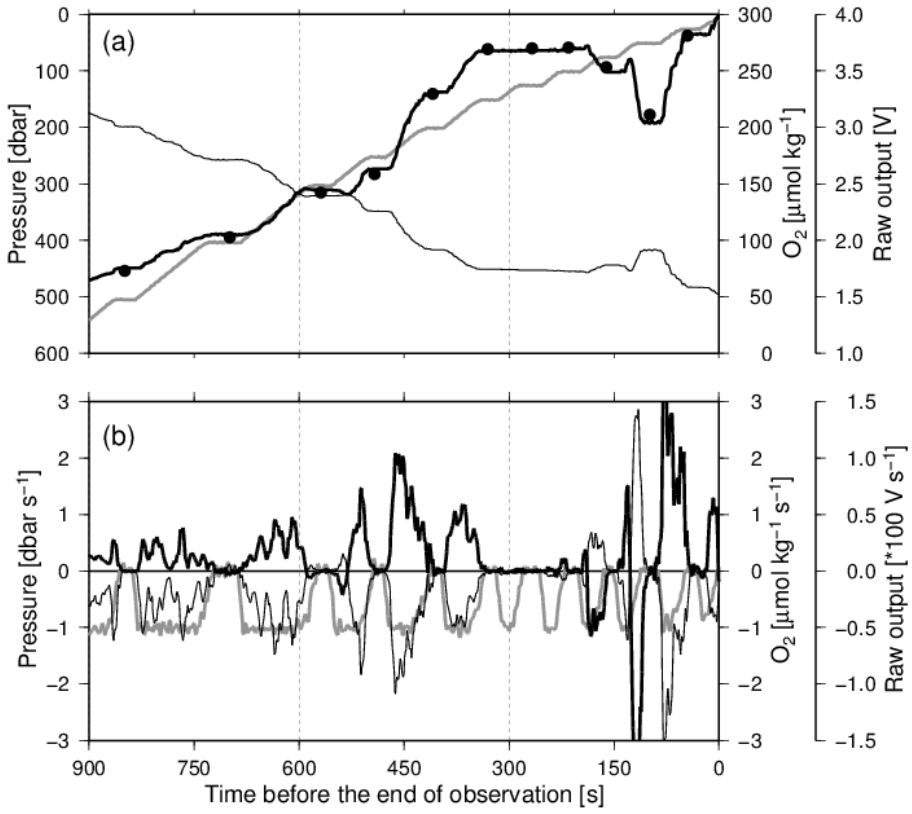

Fig. 1-3. (a) Changes in pressure (thick gray line), raw RINKO output (thin line), and calibrated RINKO O_2 concentrations (thick black line) as a function of observation time (1-sec sample interval); filled circles represent Winkler O_2 measurements. (b) Rate of change of the same parameters as a function of time (data represent 7-sec running averages). Data are from station RF-3369, at pressures less than 550 dbar (also see Figs. 1-1 and 1-2).

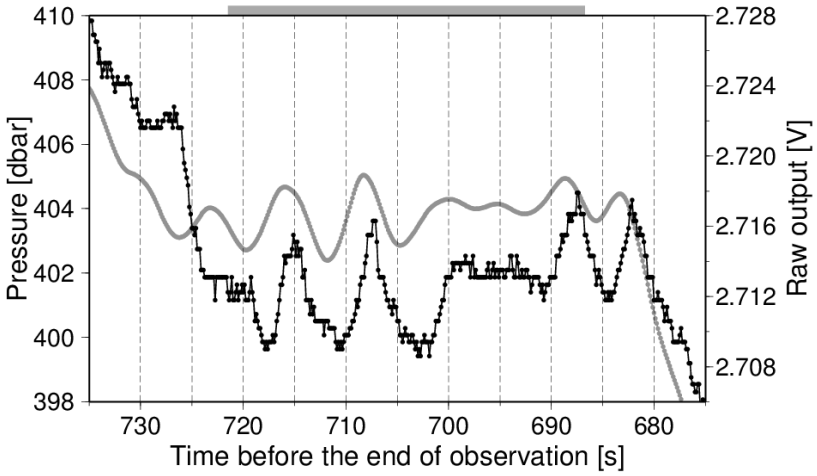

Fig. 1-4. Details of pressure (gray line) and raw RINKO output (thin line) at 735–675 sec, bracketing the time when the CTD underwater unit was stopped for sample collection at the 400 dbar depth, at station RF-3369 (also see Figs. 1-1–3). Data represent a 0.125-sec sampling interval (8 Hz). The gray bar at the top of the graph represents the time span sampled for the analysis in Fig. 1-5.

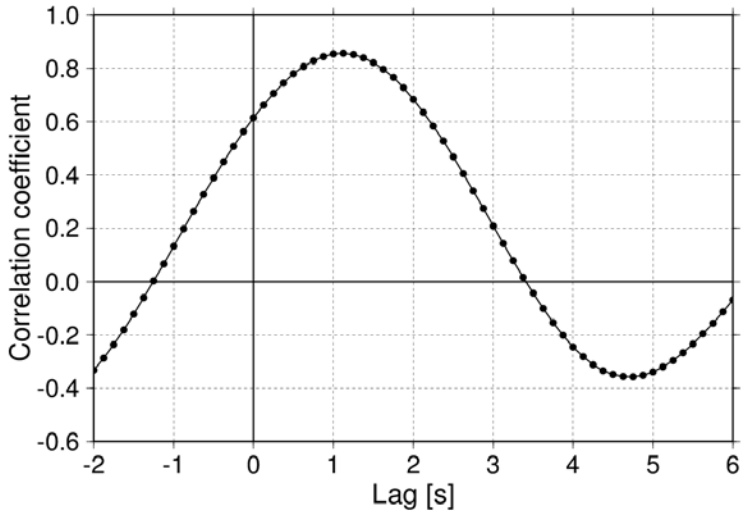

Fig. 1-5. Lag correlation between raw output of RINKO and pressure in the span shown in Fig. 1-1–4.

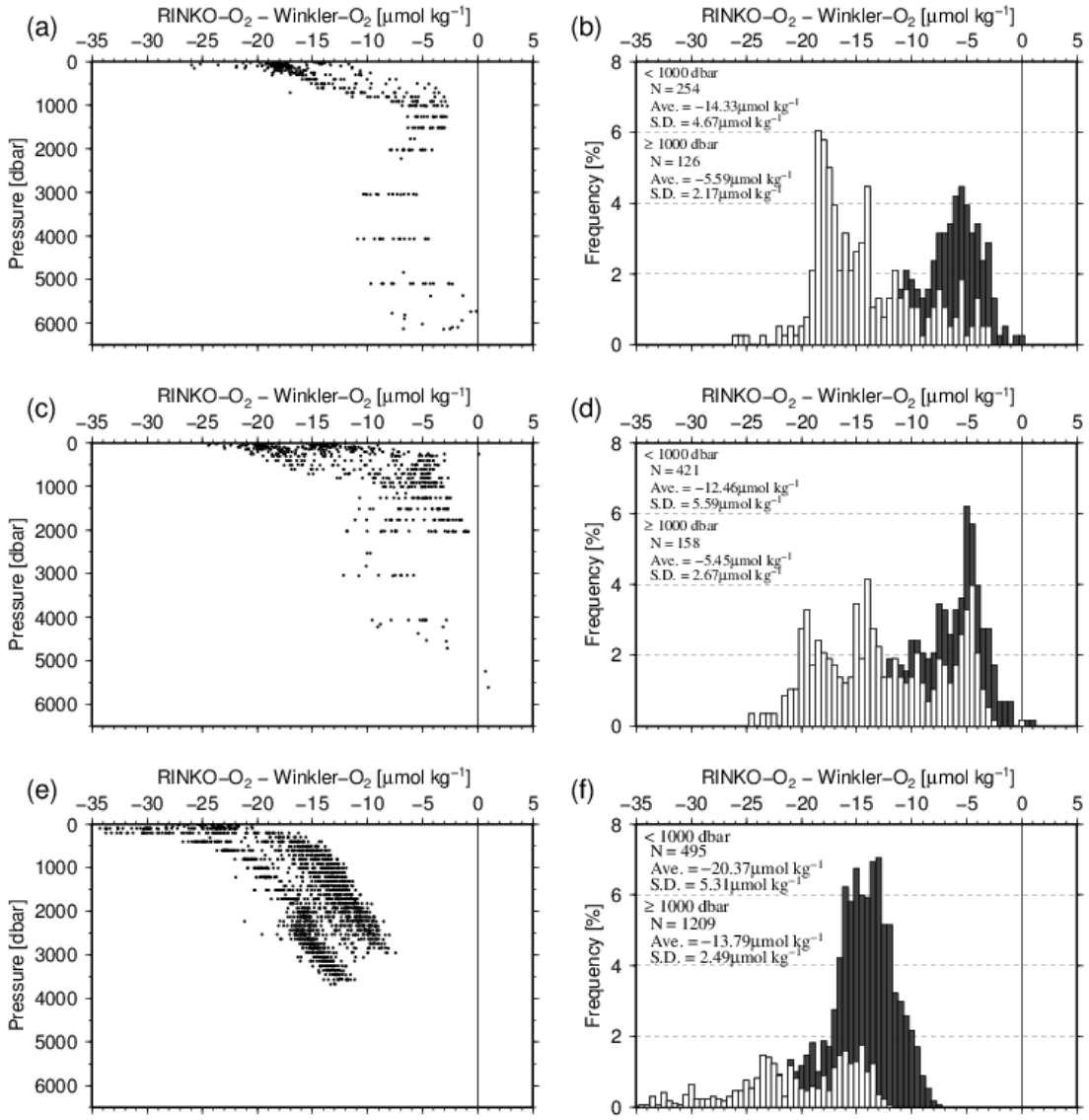

Fig. 1-6. Depth profiles (left panels) and corresponding histograms (right panels) of the differences between RINKO-O_2 and Winkler-O_2 values obtained on cruises RF09-04 (top), KS09-04 (middle), and SM09-04 (bottom). On the histograms, white and black bars indicate values greater than 1000 dbar and less than 1000 dbar, respectively.

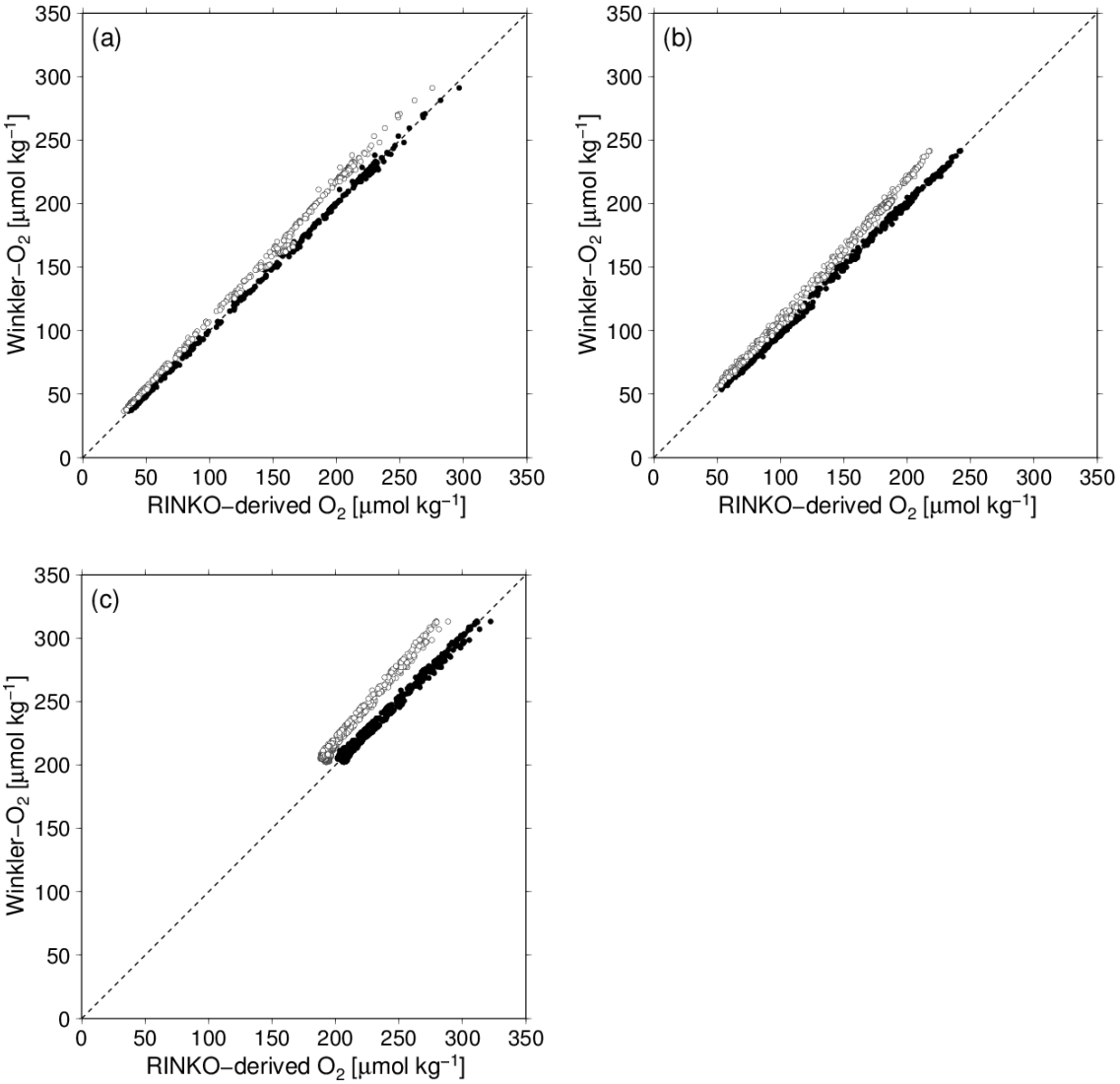

Fig. 1-7. In situ Winkler-derived O_2 values (Winkler-O_2) plotted as a function of RINKO-derived O_2 values obtained using the manufacturer's calibration (RINKO-O_2; open circles). The RINKO-O_2 values were corrected using a quadratic multiple regression that included first order temperature and pressure terms (corRINKO$_0$-O_2; closed circles). The dashed line shows equivalency (1:1 relationship) between RINKO-derived and Winkler-derived O_2 values. The data are from cruises (a) RF09-04, (b) KS09-04, and (c) SM09-04. Values of corRINKO-O_2 were calculated for each sampling cast, using a calibration curve obtained with in situ Winkler-O_2 values.

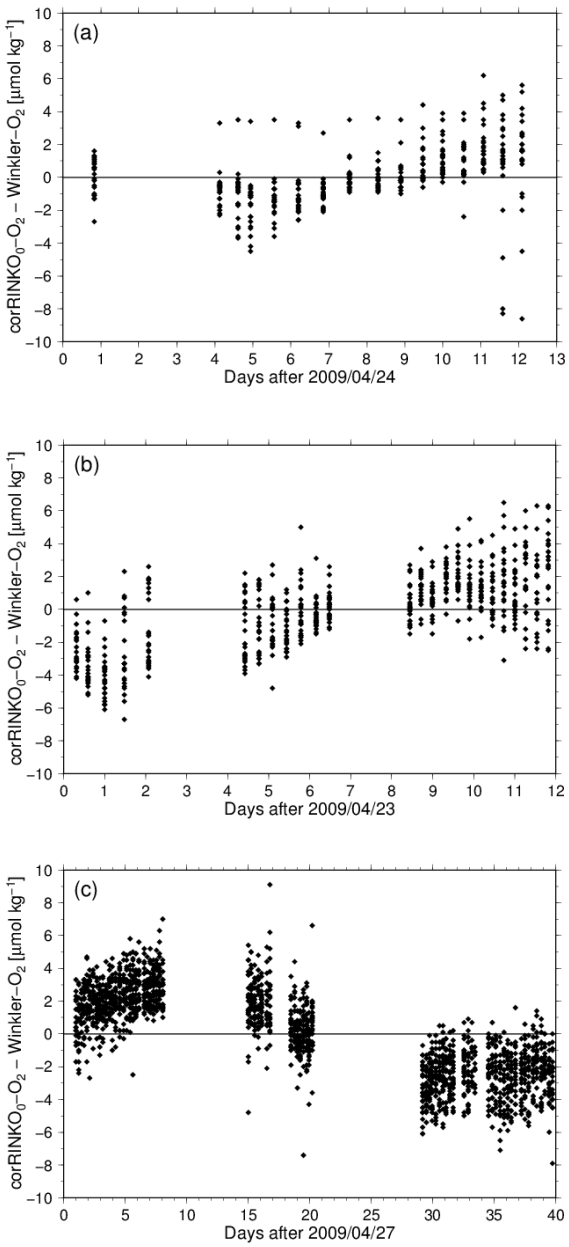

Fig. 1-8. Temporal changes in the difference between corrected RINKO O_2 data (corRINKO$_0$-O_2) and Winkler O_2 data (Winkler-O_2) during the course of cruises (a) RF09-04, (b) KS09-04, and (c) SM09-04. The corRINKO$_0$-O_2 data represent calibrations using a single set of coefficients for the duration of each cruise.

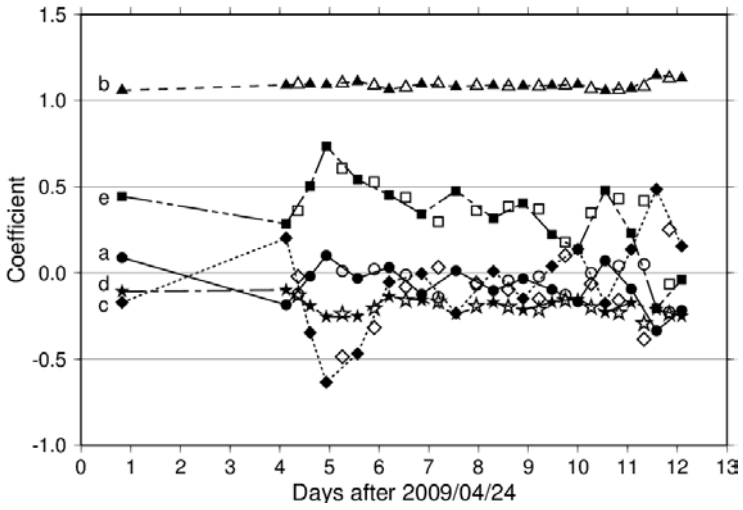

Fig. 1-9. The regression coefficients of the multiple regression equation for each sampling station during the RF09-04 cruise. The coefficients are represented by the following symbols: a (circles), b (triangles), c (diamonds), d (stars), and e (squares); values of coefficients have been adjusted to fit on the same scale: a, d, and e have been divided by 10, 10^{-2}, and 10^{-3}, respectively. Filled and open symbols indicate sampling stations with and without bottle sampling, respectively. Coefficients for stations without bottle sampling were calculated using Winkler-O_2 data from nearby stations with bottle sampling.

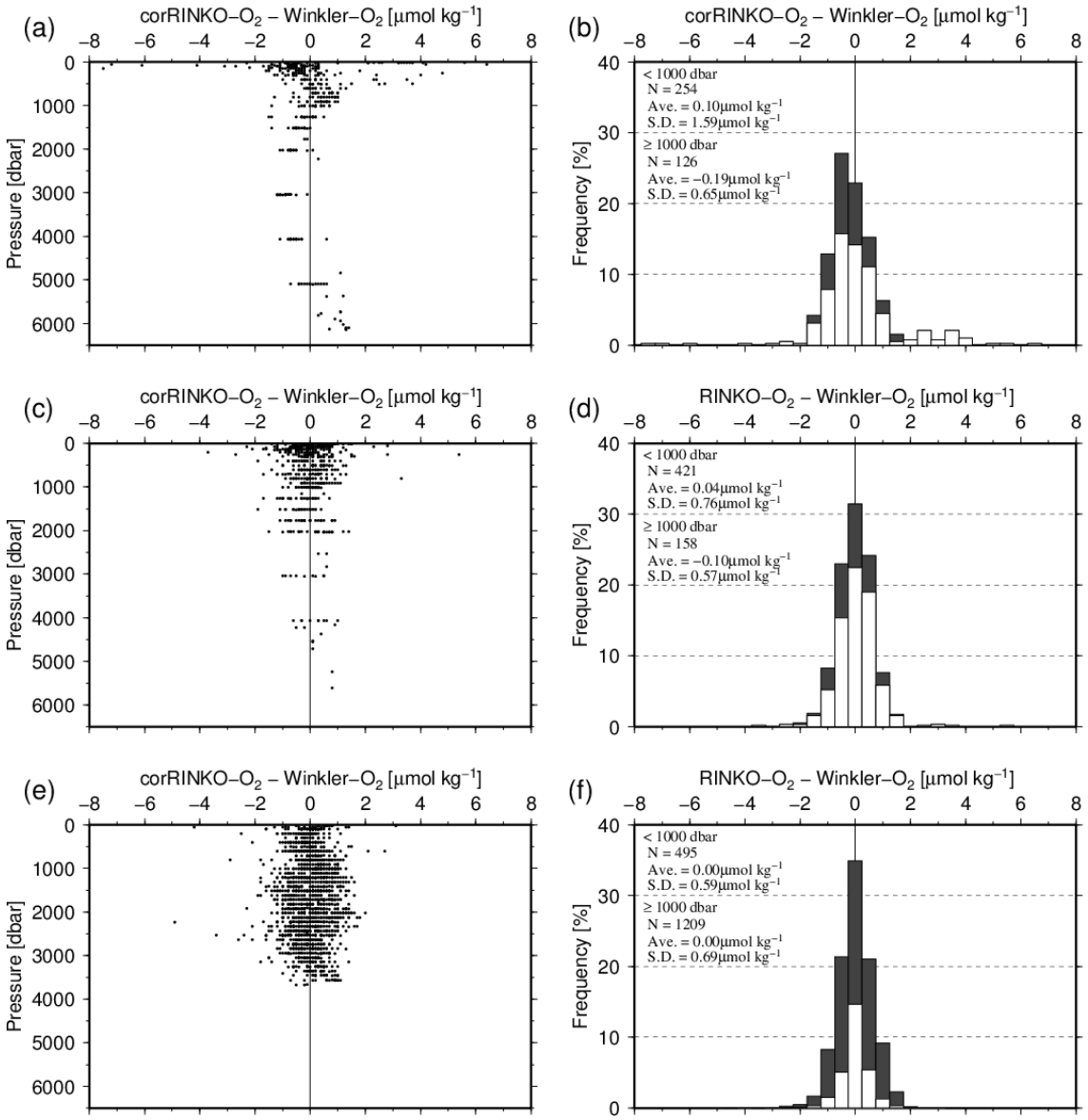

Fig. 1-10. Vertical profiles (left) and histograms (right) of the differences between corRINKO-O_2 and Winkler-O_2 on cruises RF09-04 (top), KS09-04 (middle), and SM09-04 (bottom). On the histograms, white and black bars indicate the differences observed at pressures less than 1000 dbar and greater than 1000 dbar, respectively and each bar's total height corresponds to the sum of the values for the white and black bars.

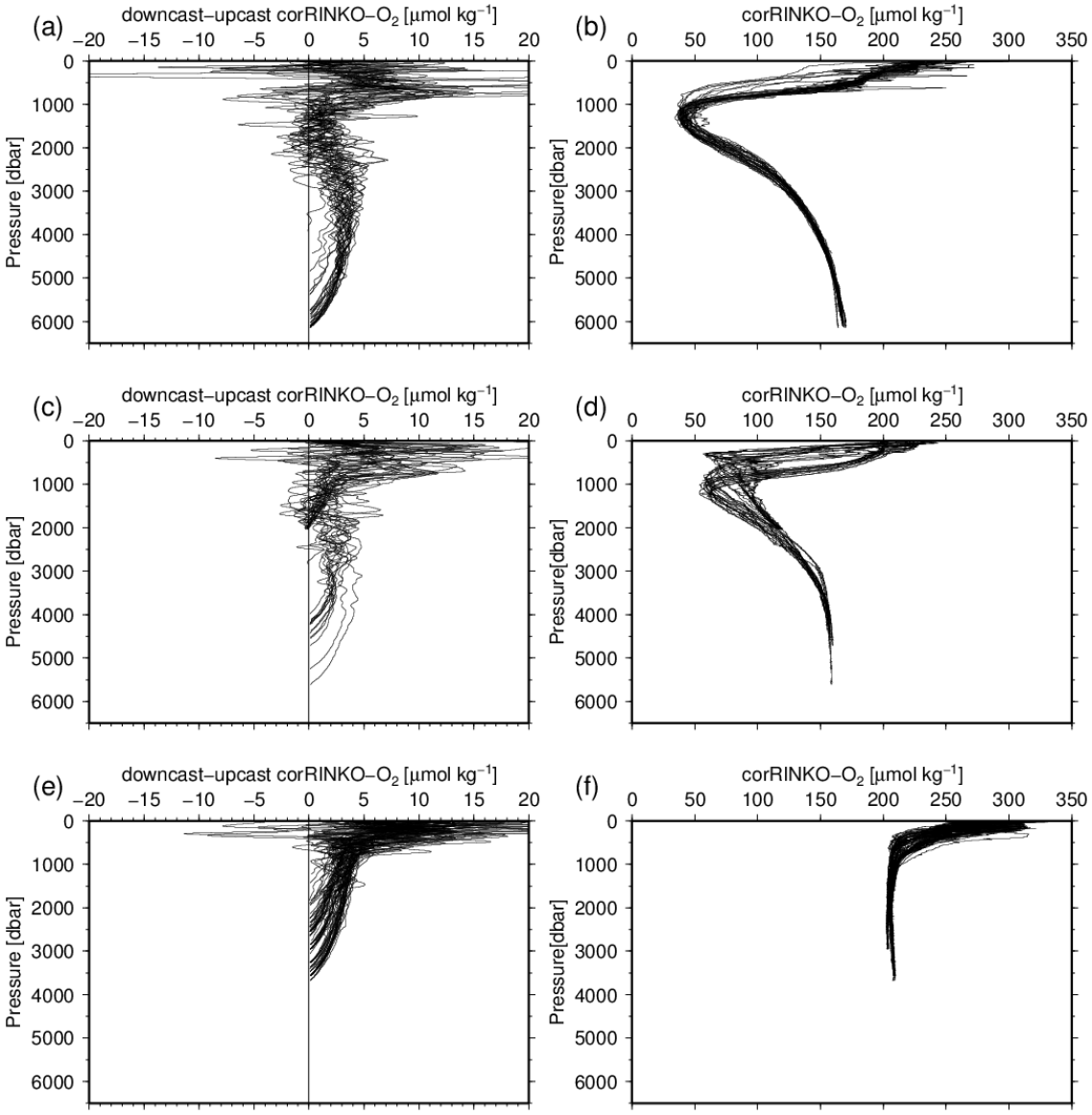

Fig. 1-11. Vertical profiles of the differences between coefficient-corrected RINKO-O_2 values (corRINKO-O_2) obtained on the downcast and on the upcast (left panels) and vertical profiles of corRINKO-O_2 values obtained on the upcast (right panels); the data are from all three cruises: RF09-04 (top), KS09-04 (middle), and SM09-04 (bottom). The profiles of the RINKO differences were smoothed to 1 dbar intervals using a Gaussian filter with a 100-dbar half length.

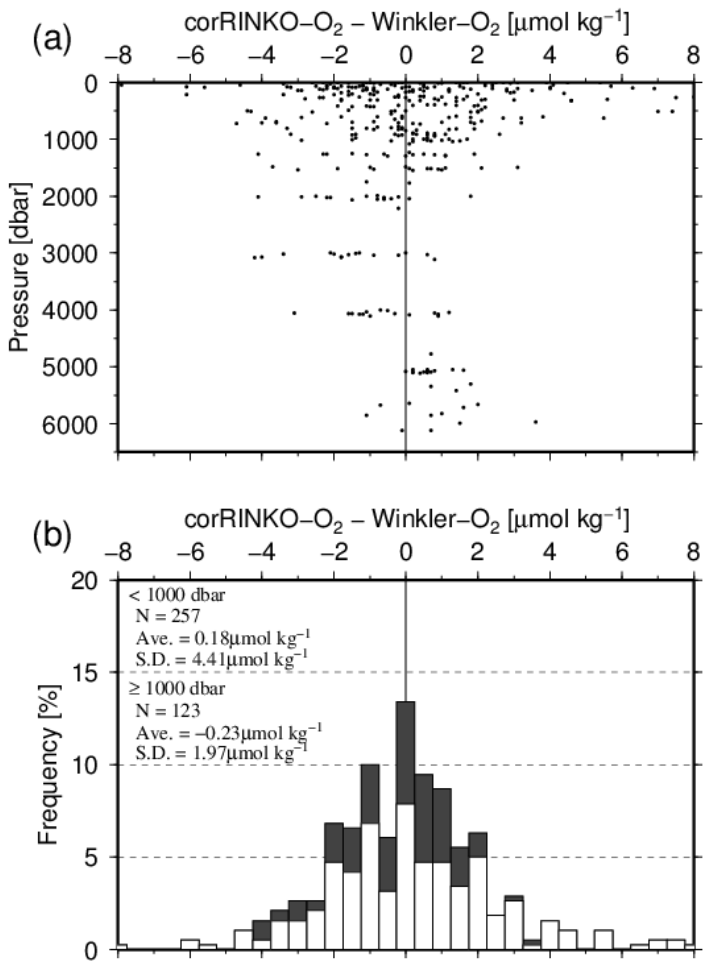

Fig. 1-12. (a) Differences between coefficient-corrected RINKO-O_2 values (corRINKO-O_2) obtained on the downcast and Winkler-O_2 obtained on the upcast (RINKO data is chosen on the same potential density layer from which the Winkler-O_2 data were obtained). (b) Histogram showing the difference values in (a); white and black bars indicate the differences above 1000 dbar and below 1000 dbar, respectively. Each bar's total height corresponds to the sum of the values for the white and black bars. Data are from cruise RF09-04.

Chapter 2
Multidecadal trends of oxygen and their controlling factors in the western North Pacific

2.1. Introduction

Over the past few decades, trends toward decreasing concentrations of dissolved oxygen (O_2) have been observed in a variety of regions and depths in the North Pacific and in the tropical oceans [*Keeling et al.*, 2010, and references therein]. Together with the warming and acidification of the ocean that are occurring concurrently, the trend toward dissolved O_2 decline (i.e., ocean deoxygenation) is considered as one of the serious consequences of climate change on the marine environment driven by human activities [*Gruber*, 2011]. Since O_2 is fundamental to the survival of aerobic organisms and biogeochemical cycling of carbon as well as nitrogen and phosphorus, a decline in dissolved O_2 has potentially profound implications for ecosystems in the ocean. The decreasing trend in O_2 is likely to continue over the coming decades. It underscores the need to improve our understanding of the trends, drivers, as well as impacts through an optimization of the ocean observing network for physics, biogeochemistry, and biology and through models. Understanding the trends and factors controlling the O_2 changes is also crucial for carbon cycle studies. Changes in dissolved O_2 through photosynthesis (source) and respiration (sink) are linked with changes in dissolved inorganic carbon (DIC) and are thereby useful for evaluating the change in DIC due to biological activity and distinguishing it from that due to the anthropogenic CO_2 invasion into the ocean interior [e.g., *Brewer*, 1978; *Gruber et al.*, 1996].

Taken together, the western North Pacific subtropical to subarctic zones comprise a region where a significant trend toward dissolved O_2 decrease has been detected over the past several decades. However, physical and biological processes controlling the decrease in O_2, and their link to natural climate variability and/or secular trends are not yet well understood. In previous studies, it has been argued that the main cause of O_2 decrease in the ocean interior

is a reduction of ventilation as a result of intensified stratification due to warming. For instance, *Watanabe et al.* [2001] have shown that apparent oxygen utilization (AOU), defined as the difference between the measured O_2 concentration and the saturation concentration of O_2 (O_2^{sat}) with respect to the atmosphere that usually occurs through respiration, and chlorofluorocarbon-derived tracer ages increased concurrently between mid-1980s and the end of 1990s on isopycnal horizons spanning $26.4\sigma_\theta$–$27.4\sigma_\theta$ along the 165°E section. According to their interpretation, the decrease in dissolved O_2 is the result of a reduction in ventilation. *Ono et al.* [2001] have also demonstrated an increasing trend in AOU in the subsurface of Oyashio Current (Kurile Current) off the eastern coast of northern Japan on isopycnals spanning $26.7\sigma_\theta$–$27.2\sigma_\theta$ over 1968–1999. They speculated that vertical exchanges of water in the upper layers of the subarctic North Pacific have diminished, and thereby, the O_2 content in the subsurface has been reduced. *Emerson et al.* [2004] also suggested the possibility that isopycnals in the vicinity of $26.6\sigma_\theta$, i.e., the maximum outcrop density in the North Pacific, ceased to outcrop in the late twentieth century. Results from a three-dimensional ocean biogeochemistry model have also been invoked to support the idea that a reduction in ventilation was the dominant cause of dissolved O_2 decline, rather than the changes in biological processes [*Deutsch et al.*, 2005, 2006]. Thereafter, *Kouketsu et al.* [2010] documented AOU increases on isopycnal density horizons near the salinity-minimum core of North Pacific Intermediate Water (NPIW) ($\sim 26.8\sigma_\theta$) in the western North Pacific (25°N–40°N, west of 170°W), along with a density decrease of NPIW associated with rising temperatures. However, they refrained from attributing the AOU increase around this density class to a reduction of ventilation and rather pointed to the possibility that the change in AOU is associated with changes in the formation and modification processes of NPIW within the Oyashio. These previous studies have been based on the repeat hydrographic/biogeochemical

measurements on the same sections made several years apart, and to date it has proven difficult to deconvolve the long-term secular trend from shorter-term natural variability. Similarly, time series measurements that resolve long-term trends cannot resolve spatial structures of variability.

Oxygen Minimum Layers (OMLs; O_2 < 70 μmol kg^{-1}) are also domains where trends in O_2 have been reported. In the North Pacific, two OMLs extend from the coastal zone of the North America to the west; one is the Eastern Tropical North Pacific OML near 26.8σ_θ (around 250 m at the 165°E section), and the other is the Eastern Subtropical North Pacific OML at approximately 27.4σ_θ (about 600–1300 m) in the subtropical and subarctic North Pacific in Fig. 2-1a (see also Fig. 3 in *Keeling et al.* [2010]). While the minimum O_2 concentrations increase in their absolute concentrations with mixing with ambient water as one moves to the west, these OMLs extend into the western North Pacific [*Paulmier and Ruiz-Pino*, 2009]. For the Eastern Tropical North Pacific OML, *Stramma et al.* [2008] have documented the vertical expansion of the low-oxygen zone and its O_2 concentration decrease (the trends were not significant but decreased at a rate of -0.19 to -0.13 μmol kg^{-1} yr^{-1}) for the past 50 years. Ocean models predict that the O_2 content will continue to decrease and OMLs will continue to expand in the coming decades along with warming in the upper layers of the ocean [e.g., *Bopp et al.*, 2002; *Oschlies et al.*, 2008]. An O_2 decline in the OML would impact the ocean's nitrogen cycle through an increase of denitrification [e.g. *Codispoti et al.*, 2001]. However, a significant increase in O_2 has also been observed in the tropical OML (8°N–9°N at 26.8σ_θ) in the western North Pacific at the 137°E section [*Takatani et al.*, 2012]. For the subtropical OML, little to date has been published regarding an O_2 decline. *Takatani et al.* [2012] identified a decreasing trend in O_2 (~ -0.1 μmol kg^{-1} yr^{-1}) over the past 25 years in the subtropical OML (10°N–34°N at 27.3σ_θ) along 137°E to the south of Japan. As the OMLs

expand broadly in places where the ocean circulation stagnates, further investigation will be needed to identify and understand scientifically the O_2 changes in the OML, particularly in poorly studied regions such as in the western tropical and in the subtropical OML.

The Japan Meteorological Agency (JMA) has been conducting time-series hydrographic and biogeochemical measurements along a meridional section at 137°E in the western North Pacific to the south of Japan since the late 1960s. On the basis of the time-series data set at this section, *Takatani et al.* [2012] identified decreasing trends of dissolved O_2 after the mid-1980s on a range of isopycnal horizons. They suggested that the factors controlling the decline in O_2 include deepening of isopycnals due to warming in the upper layers, changes in source waters, and ocean circulation in intermediate to deeper layers. Their contributions differ among the isopycnal horizons. However, as the 137°E section is confined to the latitudinal bands of the subtropical and tropical regions, the degree to which this signal finds expression in broader expanses in the western Pacific remains unexplored.

In 1996, the JMA initiated another time-series of annual and biannual hydrographic and biogeochemical observations along 165°E (WHP-P13). This section extends from the equatorial zone at 5°S across the subtropical gyre to the center of western subarctic gyre at 50°N (Figs. 2-1 and 2-2). The relatively high frequency temporal sampling along 165°E offers a number of globally unique opportunities for evaluating biogeochemical variability over a broad range of timescales and regions. For this study the principal water masses of interest along 165°E as well as along 137°E include North Pacific Subtropical Mode Water (NPSTMW; observed as thermostad of 16–18°C around $25.0\sigma_\theta$–$25.6\sigma_\theta$, e.g., *Hanawa and Talley* [2001] and *Suga* et al. [2004]), NPIW (observed as the salinity minimum layer with $S < 34.2$), and the subtropical OML ($O_2 < 70$ μmol kg^{-1}), the focus of *Takatani et al.* [2012]. Comparisons between these two sections are expected to advance understanding of the

mechanistic drivers and the spatial extent of the dissolved O_2 decline in the western North Pacific. In particular, as NPIW is formed in the Kuroshio-Oyashio Interfrontal Zone east of northern Japan [*Talley*, 1993] and then spreads over intermediate depth horizons over the North Pacific, the 165°E section monitors waters that are closer to NPIW formation regions downstream from the Oyashio region, thereby providing a view that is complementary to that observed along 137°E. The same is true for the NPSTMW being formed in the regions to the south of the Kuroshio Extension at around 165°E and spreads over the subsurface horizons in the northwestern portion in the subtropical gyre [*Oka and Qiu*, 2012]. After conducting rigorous data quality control to correct for the analytical offsets, I performed a comprehensive analysis on the rate of dissolved O_2 change in the high-frequency repeat section at 165°E over the tropical, subtropical, and subarctic regions, combining this with data from several other cruises (Figs. 2-1b and 2-3). Through the comparison with the results documented by *Takatani et al.* [2012] for 137°E, large-scale controls of the O_2 decreases in the western North Pacific were evaluated.

2.2. Data and methods

2.2.1. Data Sources

JMA has been conducting hydrographic/biogeochemical observations routinely along the section at 165°E (5°S–50°N) in the western Pacific since 1996 on R/V *Ryofu Maru* and R/V *Keifu Maru* (http://www.data.jma.go.jp/gmd/kaiyou/db/vessel_obs/data-report/html/ship/ship_e.php). Although the frequency of measurements varies with latitude, a total of 44 cruises had been conducted by the end of the year 2011 (Fig. 2-1b). Methods of measurements have been summarized in *Takatani et al.* [2012]. Analysis of dissolved O_2 has been conducted

with a modified Winkler's titration [*Carpenter et al.,* 1965, 1966]. Before 2003 its standard deviation (SD) was less than 1.6 μmol kg^{-1} and after 2004 that was 0.60 μmol kg^{-1} [*Takatani et al.*, 2012], reflecting differences in sampling procedures for the evaluation of SD and precision enhancements in O_2 measurements. Temperature and salinity were measured with a Seabird SBE-911 plus CTD system manufactured by Sea-Bird Electronics, Inc. I also used measurements that have been collected through other programs such as four WOCE P13 (165°E) cruises conducted in the early 1990s, WOCE and Repeat Hydrography cruises at zonal sections (P01–P04) that have cross-over stations with P13, and others conducted along the same section (Figs. 2-1b and 2-3). The data at stations located within the meridional band of 165.0°E ± 2.5° were used for the analysis. As a result, data from a total of 1220 stations from 57 cruises that have been conducted over the period 1987–2011 were used in this study. The majority of these data sets (44 cruises) have been archived in the PACIFICA database for the Pacific Ocean interior carbon and biogeochemical variables [*Suzuki et al.,* 2013] but the others (13 cruises) have not, since water column carbon measurements have not been performed during these cruises.

2.2.2. Data Quality Control

Rigorous quality control (QC) is a critical process in assuring the highest possible quality of data. First, it is necessary that all dissolved O_2 data are subjected to go through a procedure to identify the outliers and data from erroneous samplings and measurements are rejected (primary QC). Then, systematic errors in data were evaluated and corrected for (secondary QC).

For primary QC, I applied a statistical method and identified O_2 data that lie out of the mean ±3SD profiles with respect to pressure and potential density in the same manner as

described in *Takatani et al.* [2012]. With this method, I can evaluate individual data components objectively as to whether they are outliers or not. However, improper judgments of rejection could be made for outlying data associated with large natural variability in ocean tracer fields. In order to reduce the risk of screening real natural variability, I also invoked quasi-conservative fields of NO (= $9 \cdot NO_3 + O_2$) and PO (= $135 \cdot PO_4 + O_2$) [*Broecker*, 1974]. More details of the methods are described in Appendix A. Through these procedures, a total of 191 data out of 29,260 were flagged as outliers, but 61 data were objectively determined as outliers due to a natural variability and were used for the analysis of the rate of dissolved O_2 changes. In addition, I visually inspected all profiles of dissolved O_2, NO, and PO, focusing particularly on the flagged data and on the layers where applying the criterion of mean ±3SD appears questionable in determining outliers due to the paucity of data (e.g., in the upper tropics with respect to potential density and in abyssal layers with respect to pressure). Consequently, a total of 252 data (0.86%) were rejected.

The data that have passed through the primary QC were interpolated vertically at intervals of 5 m and $0.1\sigma_\theta$ for each station using the Akima spline method [*Akima*, 1991]. Secondary QC procedures were then applied to the interpolated data. An offset in O_2 data was evaluated for each cruise data set of the 165°E section on the basis of the cross-over analysis [*Tanhua et al.*, 2010]. Procedures of calculation have been modified to compare each cruise only with a “core cruise” with the best data quality so that it becomes more appropriate for time-series data acquired in a single section (see Appendixes B1 and B2 for more details). Values of multiplicative adjustment to correct for the offsets in dissolved O_2 data (0.963 to 1.045) well agreed with those provided in PACIFICA regardless of data distributions in the cruises (Fig. 2-3). Offsets were then adjusted in all data sets from the 165°E section.

2.2.3. Computation of the Rate of Change

Linear rates of potential temperature, salinity and dissolved O_2 changes for the period spanning 1987–2011 were computed for each latitudinal band along 165°E in intervals of 2.5° in latitude and at intervals of $0.1\sigma_\theta$ in density. These rates were considered significant when *p*-value was less than 0.05, although the rates with the *p*-value less than 0.1 were also shown in Fig. 2-4 to exhibit their patterns broadly. In this analysis, anomalies of each parameter from its mean value for the entire period were calculated at intervals of 1° and $0.1\sigma_\theta$. A least squares fitting was then applied to the annual mean anomaly in each 2.5° band on each $0.1\sigma_\theta$. In general, the choice of narrower latitudinal intervals helps to capture changes in parameters in finer spatial scales, but the choice of rather broad latitudinal intervals of 2.5° in this work has the advantage of reducing biases associated with the unevenly distributed measurements in space and time (Fig. 2-1b).

2.3. Results

2.3.1. Trends of Temperature and Salinity

For the past 25 years, decreasing trends in potential temperature and salinity are evident in the subtropical zone (10°N–32.5°N) of the 165°E section on isopycnal horizons above the salinity minimum layer of NPIW ($\sigma_\theta < 26.5$) (Figs. 2-4a and 2-4b). These decreasing trends in temperature and salinity are perfectly correlated with each other to remain on a constant density. It should be noted that these trends toward decreasing temperature/salinity on isopycnal horizons indicate warming and/or freshening in the upper layer of the ocean where salinity decreases with depth (see Fig. 2-2b). In fact, at a constant depth of 190 m in 25°N–30°N corresponding to around $25.3\sigma_\theta$ in NPSTMW, potential temperature was increasing and

salinity was decreasing at a mean rate of +0.035 ± 0.008 °C yr^{-1} and -0.0025 ± 0.0009 yr^{-1}, respectively (Fig. 2-5). This trend of warming in the upper ocean is consistent with trends identified by *Levitus et al.* [2009] and *Rhein et al.* [2013] in which the trend of warming is pronounced in the north-western subtropics in the North Pacific. Warming and freshening both reduce a density of the upper ocean and thereby are associated with deepening of isopycnal horizons. Accordingly, the isopycnal horizon of $25.3\sigma_\theta$ is also deepening at a rate of +3.01 ± 0.55 m yr^{-1} on average (Fig. 2-6a).

In the northern subtropics at 25°N–32.5°N, warming and freshening trends are seen up to the layers just below the winter mixed layer ($24.5 \leq \sigma_\theta \leq 26.5$). It suggests that the signal of warming/freshening spreads from the winter mixed layer in these zones into the ocean interior through the subduction and formation of waters such as NPSTMW and North Pacific Central Mode Water (NPCMW) as an interior equatorward component of shallow meridional overturning circulation in the North Pacific. The rate of decrease in temperature and salinity is higher on the relatively light isopycnals ($24.5\sigma_\theta$–$25.8\sigma_\theta$; -0.018 ± 0.001 °C yr^{-1} and -0.0056 ± 0.0003 yr^{-1}, respectively) in shallower layers than on the relatively heavy isopycnals ($25.9\sigma_\theta$–$26.5\sigma_\theta$; -0.010 ± 0.001 °C yr^{-1} and -0.0026 ± 0.0002 yr^{-1}, respectively) in deeper layers.

By contrast, trends toward increasing temperature/salinity are usually found below the salinity-minimum layer of NPIW in the subtropical (27.5°N–35°N) and subtropical-to-subarctic transition (37.5°N–50°N) zones, where salinity increases with depth. *Kouketsu et al.* [2010] documented the consistent trends of temperature and salinity changes at several repeat sections in the western North Pacific (25°N–40°N, west of 170°W from 1980s to 2000s) including 165°E for the period of 1996–2007 and ascribed these changes to a density decrease in the NPIW core. These trends were clearly confirmed in this work with time-series

data for prolonged period extending to 2011.

A trend toward salinity/temperature decreases is also evident at 2.5°N on isopycnal horizons satisfying $\sigma_\theta < 26.6$. In contrast, a trend toward salinity/temperature increases is seen in the upper layers in the southern rim of the subtropical gyre ($24.8 > \sigma_\theta$, 7.5°N–15°N). In these domains, meridional gradients of salinity/temperature on isopycnal horizons are large, and these trends are consistent with the southward expansion of North equatorial current (NEC) [*Qiu and Chen*, 2012]. Trends toward warmer and saltier waters are also seen in the latitudinal band of 5°S–0°. This suggests a potential increase in mass transport from the South Pacific into the tropics through the Equatorial Undercurrent (EUC).

2.3.2. Trend of Dissolved Oxygen

A significant multidecadal trend toward decreasing dissolved O_2 as well as a significant increase O_2 were detected on a variety of isopycnal horizons in a variety of the latitudinal zones in the 165°E section (Fig. 2-4c). In addition, it appears that the mean rate of O_2 change (-1.3 to +0.9 μmol kg^{-1} yr^{-1}) reveals heterogeneity and significant differences when evaluated for distinct water masses along 165°E, as opposed to temperature and salinity. Changes in dissolved O_2 are particularly notable in NPSTMW (~$25.3\sigma_\theta$), NPIW (~$26.8\sigma_\theta$), and subtropical OML (~$27.3\sigma_\theta$) in the northern subtropics, and around the northern boundary of the EUC ($24.7\sigma_\theta$–$26.4\sigma_\theta$) and in the tropical OML (~$26.8\sigma_\theta$) in the northern flank of the tropics. Here, this study focuses on the dissolved O_2 trends in the northern subtropics and tropical zone.

2.3.2.1. Northern Subtropics

The upper ocean is relatively well ventilated in the northwestern region of the

subtropical gyre in the North Pacific, with this finding expression in a relatively deep permanent thermocline. In the 165°E section, the contour lines of multidecadal mean O_2 concentrations at 200 μmol kg^{-1} and at 150 μmol kg^{-1} reached their deepest layer (> 400 m and > 600 m, respectively) at 30°N (Fig. 2-2c). In the shorter term, these contours of dissolved O_2 and other ocean variables fluctuate in space and time due to the passage of mesoscale eddies and the north–south shift in the path of the Kuroshio Extension Current. However, with respect to dissolved O_2 on isopycnal horizons, their meridional gradients are small in the northern subtropics (Fig. 2-4c). The vertical gradient of O_2 concentrations with respect to depth is small in the upper layers above the isopycnal horizon of $26.3\sigma_\theta$ (< -0.2 μmol kg^{-1} m^{-1}) contrary to the larger gradient (~ -0.5 μmol kg^{-1} m^{-1}) in the deeper layer between $26.4\sigma_\theta$ and $27.2\sigma_\theta$.

In NPSTMW around the $25.3\sigma_\theta$ horizon, the mean rate of O_2 decrease was among the highest (-0.45 ± 0.16 μmol kg^{-1} yr^{-1}) at 25°N–30°N (Figs. 2-4c and 2-6a). At this density, potential temperature and salinity were also decreasing (-0.0173 ± 0.0040 °C yr^{-1} and –0.0054 ± 0.0013 yr^{-1}, respectively). The interannual and decadal-to-interdecadal variations were determined in both temperature/salinity and oxygen (Fig. 2-6a). These variations were similar to those between 20°N and 25°N along 137°E [*Takatani et al.*, 2012], indicating that the controlling factors are the same in both sections. Cooling and freshening raise O_2^{sat} (+0.09 ± 0.02 μmol kg^{-1} yr^{-1}) (primarily driven by cooling), and thereby, the decrease in O_2 should not be attributed to a change in O_2^{sat} but rather to an increase in AOU (+0.55 ± 0.16 μmol kg^{-1} yr^{-1}). It is conceivable that the AOU increase here is related to the deepening of isopycnal horizons due to the warming in the upper ocean (see section 2.3.1), since the elapsed time after the water was last in contact with the atmosphere is expected to be shorter in shallower layers (see section 2.4 for more detail). On the other hand, on isopycnal horizons between

$26.0\sigma_\theta$ and $26.2\sigma_\theta$ in NPCMW, the change in dissolved O_2 was not significant over the past 25 years. On these isopycnal horizons, the vertical gradient of O_2 with respect to depth is also small and the rate of temperature/salinity decrease is lower. Consequently, the effect of the deepening of isopycnal horizons due to warming on O_2 decline is expected to be smaller than in NPSTMW.

For NPIW near $26.8\sigma_\theta$, a significant trend toward decreasing O_2 was again detected broadly between 25°N and 40°N (Fig. 2-4c). Although the long-term component of O_2 changes on $26.8\sigma_\theta$ exhibited decadal-timescale variability, this quasi time-series dataset of 25 years duration from 1987 to 2011 revealed a mean rate of change of O_2 of -0.44 ± 0.14 μmol kg^{-1} yr^{-1} over 25°N–30°N (Fig. 2-6b). The increase in AOU was significant (+0.46 ± 0.13 μmol kg^{-1} yr^{-1}) and attributable to the O_2 decrease, but neither changes in potential temperature and salinity (-0.0016 ± 0.0022 °C yr^{-1} and -0.0002 ± 0.0004 yr^{-1}, respectively) nor changes in the depth (-0.05 ± 0.47 m yr^{-1}) were significant near this isopycnal horizon.

In the subtropical OML near $27.3\sigma_\theta$, decline of O_2 was significant between 32.5°N and 35°N. In this zone, dissolved O_2 was decreasing at a mean rate of -0.22 ± 0.05 μmol kg^{-1} yr^{-1}, which is approximately half of that in NPSTMW and in NPIW described above. On the other hand, the rate of O_2 decrease was even lower (-0.07 ± 0.05 μmol kg^{-1} yr^{-1} on the average) for the same isopycnal horizon over 25°N–30°N (Fig. 2-6c), with this O_2 decrease being not statistically significant. Interannual variability in dissolved O_2 was smaller than in the shallower isopycnal horizons, and rates of change in potential temperature, salinity, depth of this isopycnal horizon, and AOU were also not significant.

It is notable that these trends toward decreasing O_2 in the northern subtropics of the 165°E section are comparable with those found along the 137°E section for the corresponding period after the mid-1980s [*Takatani et al.*, 2012]. The study of *Takatani et al.* [2012] also

found a decreasing trend in O_2 in three water masses in the northern subtropics (20°N–25°N) along the 137°E section, i.e., -0.28 ± 0.08 μmol kg^{-1} yr^{-1} on 25.5σ_θ in NPSTMW, -0.36 ± 0.08 μmol kg^{-1} yr^{-1} on 26.8σ_θ in NPIW, -0.23 ± 0.04 μmol kg^{-1} yr^{-1} on 27.3σ_θ in the subtropical OML. For both sections, the rate of decrease of O_2 is relatively high in NPSTMW and in NPIW. The rate of O_2 decline in NPSTMW appears higher at 165°E (-0.45 ± 0.16 μmol kg^{-1} yr^{-1}) than at 137°E. Results derived from quasi time-series measurements in these sections suggest that the causes of O_2 decline on respective isopycnal horizons are common to both sections, and dissolved O_2 decline was occurring extensively in the northern subtropics of the western North Pacific, in particular on isopycnal horizons of NPSTMW, NPIW, and the subtropical OML.

2.3.2.2. Tropical Zone

Trends of significant O_2 decline, with rates exceeding -0.6 μmol kg^{-1} yr^{-1}, were also observed over isopycnal horizons from 24.7σ_θ through 26.4σ_θ along the northern flank of the EUC at 2.5°N and 5°N. In this domain, the trend toward temperature/salinity decreases has been concurrently observed at 2.5°N whereas it shows no significant change at 5°N (Fig. 2-4a). Here, meridional gradients on isopycnal horizons are large for dissolved O_2 at 2.5°N–5°N and temperature/salinity at 2.5°N, and these trends are likely to be attributable to the equatorward shift of the front at the northern flank of the EUC.

In contrast, an increasing trend is clear for dissolved O_2 in the tropical OML over 26.6σ_θ–27.3σ_θ at 5°N–10°N. In both the OML core and its flank, profiles of 3 year means of dissolved O_2 concentrations at 165°E for 1985–1987 to 2009–2011 reveal large interannual variability but clearly changed toward increasing O_2 (Fig. 2-7). The mean rate of O_2 increase reached +0.36 ± 0.04 μmol kg^{-1} yr^{-1}. A similar trend toward increasing O_2 in the tropical OML

has also been detected along the 137°E section further to the west [*Takatani et al.*, 2012]. However, it is intriguing that these multidecadal trends of O_2 increase in the tropical OML in the western Pacific are opposed to those reported for the central (170°W) and eastern Pacific (110°W), where the tropical OML is vertically expanding and dissolved O_2 is declining at a rate of -0.19 ± 0.20 μmol kg^{-1} yr^{-1} and -0.13 ± 0.32 μmol kg^{-1} yr^{-1}, respectively [*Stramma et al.*, 2008].

2.4. Discussion

Long-term changes in the O_2 content of the ocean reflect changes in the air-sea O_2 exchange, vertical exchanges of water through mixing, ocean circulation, and biological activity [*Keeling et al.*, 2010]. A number of studies to date have attributed long-term O_2 decreases to ocean warming through a reduction in ventilation [e.g., *Watanabe et al.*, 2001; *Mecking et al.*, 2008]. Recently, *Takatani et al.* [2012] proposed a distinct mechanism associated with "the deepening effect of isopycnal surfaces" due to upper ocean warming and freshening. They quantified the effect of various factors contributing to changes in dissolved O_2 concentration on isopycnal horizons, with the essential concepts conveyed in the following equation.

$$\frac{\partial O_2}{\partial t} = \left(\frac{\partial O_2}{\partial z} \cdot \frac{\partial z}{\partial t} \right) + \left(\frac{\partial O_2^{sat}}{\partial t} \right)_{net} - \left(\frac{\partial (AOU)}{\partial t} \right)_{net}, \quad (1)$$

and consequently, they proposed the following equation:

$$\frac{\partial O_2}{\partial t} = \left(\frac{\partial O_2}{\partial z} \cdot \frac{\partial z}{\partial t} \right) + \left(\frac{\partial O_2^{sat}}{\partial t} - \frac{\partial O_2^{sat}}{\partial z} \cdot \frac{\partial z}{\partial t} \right) - \left(\frac{\partial (AOU)}{\partial t} - \frac{\partial (AOU)}{\partial z} \cdot \frac{\partial z}{\partial t} \right) \quad (2)$$

(i) (ii) (iii) (iv) (v) (vi).

The underlying processes and the derivation of the equations are described in Appendix C.

In these equations, $\partial X/\partial t$ (X = O_2, O_2^{sat}, AOU) and $\partial z/\partial t$ represent the mean rate of change in the variable X and the depth of isopycnal horizon z, respectively. They were calculated from the data associated with time-series measurements interpolated onto isopycnal horizons. The term $\partial X/\partial z$ represents the vertical gradient of a variable X with respect to depth at an isopycnal horizon. This work used its mean values over the past 25 years. The term $(\partial X/\partial t)_{net}$ represents the net change in a variable X ("net" means here the result of the removal of apparent change of the deepening effect of isopycnal horizon). This was calculated as a difference between observed change ($\partial X/\partial t$) and the effect of deepening ($\partial X/\partial z \cdot \partial z/\partial t$). By applying equation (2) to the time-series data, the rate of O_2 change on each isopycnal horizon (i) was attributed to the three factors, i.e., the apparent effect of the deepening of isopycnal horizon due to warming/freshening (ii), the net change in O_2^{sat} (iii – iv) due to temperature/salinity changes, and the net change in AOU (v – vi) due to changes other than those in O_2^{sat} such as in disequilibrium with atmosphere, biological activities, lateral advection, and/or the circulation (the elapsed time after the water lost contact with the atmosphere).

To understand multidecadal O_2 changes along the 165°E section, equation (2) is applied for three water masses, i.e., NPSTMW, NPIW, and subtropical OML in the northern subtropics (Fig. 2-8a) that have previously been considered by *Takatani et al.* [2012] in the 137°E section. The region between 25°N and 30°N along 165°E highlighted here is thought to be a region where equation (2) is appropriately applicable, as the Kuroshio Extension Front (KEF), the nearest front to my target region, is usually positioned to the north of 33°N [*Oka and Suga*, 2005], and thereby, its variations are considered to have a negligible effect on $\partial z/\partial t$ (see Appendix C). Over this region, a large number of hydrographic/biogeochemical data have been acquired over the past several decades (Fig. 2-1b). Furthermore, *Nakano et*

al. [2007] have shown that the depths of isopycnal horizons reveal a deepening trend at a rate over 1 m yr^{-1} at 25°N, 137°E above the salinity minimum layer associated with the increase of ocean heat content (OHC). Since the increase in OHC is remarkable to the south of the Kuroshio and the KEF [*Levitus et al.*, 2009], deepening of isopycnal horizons due to warming/freshening and its apparent effect on O_2 changes are also expected to be significant along the 165°E section. Moreover, my target region between 25°N and 30°N along 165°E is connecting with the regions between 20°N and 25°N along 137°E evaluated by *Takatani et al.* [2012] (it can be seen that geostrophic stream lines at 165°E are shifted to the north in Fig. 2-1a). The comparison of the results between the 165°E and 137°E sections will aid in understanding the controlling factors of multidecadal O_2 decline in the northern subtropics of the western North Pacific.

2.4.1. Oxygen Decline in the Mode Waters

For NPSTMW observed along 165°E over 25°N–30°N, potential temperature at a depth of approximately 200 m has been rising significantly (+0.035 °C yr^{-1}) over the past 25 years, while on a corresponding isopycnal horizon of 25.3σ_θ it was rather decreasing (-0.017 °C yr^{-1}) (Fig. 2-5a). These changes in temperature were also associated with freshening on both pressure and isopycnal horizons (i.e., freshening on a constant density inherently accompanies cooling) (Figs 2-4a and 2-4b). It is evident that these changes are driven by warming and/or freshening in the upper ocean and result in the deepening of isopycnal horizons (see Appendix C). For instance, in the subtropical zone of the western North Pacific at the 137°E section, *Nakano et al.* [2007] have shown on the basis of the repeat hydrographic measurements since early 1970s that ocean warming (+0.01 °C yr^{-1}) and freshening (0.0015 yr^{-1}) are simultaneously occurring in the upper water column (~700 m) above the salinity

minimum of NPIW. As a consequence, isopycnal horizons are deepening, further freshening, and thereby cooling.

The effect of the deepening of an isopycnal horizon due to warming/freshening on the long-term decline of dissolved O_2 is significant for NPSTMW. On $25.3\sigma_\theta$, the mean rate of deepening ($\partial z/\partial t$) exceeded 2 m yr^{-1} and was the highest among all isopycnal horizons considered (Fig. 2-8b). Accordingly, the trend in dissolved O_2 that was analyzed following equation (2) shows that more than half of the O_2 decline (~0.2 μmol kg^{-1} yr^{-1}) on this isopycnal horizon can be attributed to the effect of the deepening of the isopycnal horizon (ii) (Fig. 2-8a). The net reduction of O_2^{sat} (iii – iv) also contributed approximately 30% (~0.1 μmol kg^{-1}) to the O_2 decline. The significant contributions of these two factors that are associated with ocean warming/freshening in NPSTMW have also been identified at 137°E by *Takatani et al.* [2012]. However, the decline of dissolved O_2 on isopycnal horizons corresponding to NPSTMW was faster at 165°E than at 137°E, reflecting the higher rate of deepening ($\partial z/\partial t$) at 165°E (2.3 ± 0.5 m yr^{-1}) than at 137°E (0.9 ± 0.3 m yr^{-1}) for $25.5\sigma_\theta$ (to compare the rate of change at 137°E, this study focuses on this density which *Takatani et al.* [2012] highlighted).

In the upper layers of the western North Pacific subtropical gyre, both warming [*Levitus et al.*, 2012] and freshening [*Boyer et al.*, 2005] have been reported, and the higher rate of $\partial z/\partial t$ in NPSTMW at 165°E relative to 137°E is attributed to the higher rate of warming/freshening on isopycnals along 165°E. To evaluate the relative contributions of warming and freshening to the long-term mean $\partial z/\partial t$, I reconstructed linear trends of potential temperature (θ) and salinity (S) with depth and have represented the temporal evolution within a θ-S diagram (Fig. 2-9). The $25.3\sigma_\theta$ horizon has deepened from approximately 150 m in 1987 to approximately 225 m in 2011 as a consequence of warming and freshening. As a consequence of warming alone (taking the combination of temperature in 2011 and salinity

in 1987), this isopycnal horizon would have deepened to about 210 m, whereas it would have deepened only to about 165 m when only the contribution from freshening (taking the combination of temperature in 1987 and salinity in 2011) was considered. The contribution of warming to $\partial z/\partial t$ accounts for about 80% of the change, indicating that warming is more important than freshening in the deepening of isopycnals and thereby of the decline in dissolved O_2 on isopycnals in NPSTMW.

While the decrease of dissolved O_2 in NPSTMW can largely be explained by the deepening of the isopycnal horizons and the reduction of O_2^{sat} due to warming, a portion of the O_2 decline at approximately -0.15 μmol kg^{-1} yr^{-1} appears to be attributable to the effect of net AOU increase (Fig. 2-8a). The effect of a net AOU increase of approximately -0.1 μmol kg^{-1} yr^{-1} has also been quantified for the O_2 decline at 137°E [*Takatani et al.*, 2012]. Although these contributions of the net AOU increase are within the uncertainty range of the estimate, it is possible that the net AOU increase has been caused by the aging of NPSTMW due to the change in the formation rate and/or formation region and the increase in the remineralization of organic matters through bacterial activity due to the increase in export flux of biological organic carbon from upper layers and/or the rise of water temperature. Here, I briefly examine the possibility of an AOU increase due to the enhanced enzyme reaction of bacteria. As mentioned in section 2.3.1, the temperature of NPSTMW is increasing significantly at a mean rate of +0.035 °C yr^{-1} on the depth of the $25.3\sigma_\theta$ horizon along 165°E (see Fig. 2-5a) and +0.035 °C yr^{-1} in the NPSTMW core along 137°E (calculate based on Fig. 9 in *Takatani et al.* [2012]). *Christian and Karl* [1995] showed that bacterial ectoenzyme activity increases with the rise of temperature in the subtropical North Pacific near Hawaii. According to their result, the activity of ectoenzyme is estimated to increase biochemically by 0.5% per 0.05 °C at around 17°C. Since the O_2 utilization rate (OUR) in NPSTMW is 20 μmol kg^{-1} yr^{-1} [*Suga et*

al., 1989], the increase of AOU due to the bacterial activity associated with warming is likely to amount to changes of order -0.1 μmol kg^{-1} yr^{-1} and is comparable to the rate of net AOU change analyzed in this work.

Over the density range $25.7\sigma_\theta$–$26.2\sigma_\theta$ between 25°N and 30°N, the change in dissolved O_2 concentrations was slower (-0.14 ± 0.05 μmol kg^{-1} yr^{-1}; see Fig. 2-8a) than for other density horizons. These density horizons roughly correspond to NPCMW that is being formed just to the north of the KEF [*Oka and Suga*, 2005; *Oka et al.*, 2011]. Here, the deepening of isopycnal horizons and the reduction of O_2^{sat} have minor contributions, indicating that the effect of warming is smaller than in NPSTMW (Fig. 2-5a). The insensitivity of dissolved O_2 to climate change here is also ascribed to the small vertical gradient of dissolved O_2 across these isopycnal horizons (Fig. 2-8b). On the other hand, the concave structure of the rate of O_2 change with respect to the density around NPCMW was unclear at 137°E [*Takatani et al.*, 2012]. It would be mainly ascribed to the larger net AOU change at 137°E and would reflect the longer distance from the formation region of NPCMW to 137°E.

2.4.2. Oxygen Decline in NPIW

The rate of dissolved O_2 decline also showed its extremum (-0.42 ± 0.06 μmol kg^{-1} yr^{-1}) in intermediate layers spanning $26.6\sigma_\theta$–$26.9\sigma_\theta$ between 25°N and 30°N at 165°E. This density-space domain corresponds to the salinity-minimum core of NPIW (Fig. 2-8a). The dominant factor controlling the O_2 decline here is the net increase of AOU, while the effect of the deepening of isopycnal horizons and reduction of O_2^{sat} were minor. However, the O_2 utilization in NPIW by bacterial activity would need to be an order of magnitude larger in order to explain the net increase of AOU with the change of in situ OUR by an export flux of organic matter or in the remineralization of organic matter through bacterial activity

[*Watanabe et al.*, 2001]. In addition, it is unlikely that the net AOU increase can be attributed directly to a reduction in ventilation, since the isopycnal horizons denser than $26.7\sigma_\theta$ do not typically outcrop in the open North Pacific [*Reid*, 1965; *Talley*, 1993].

It is known that NPIW is formed in the subsurface of the Kuroshio-Oyashio Interfrontal Zone in the region offshore of northern Japan [*Talley*, 1993]. One of the main sources of NPIW is the Oyashio (Kuril Current) [*Yasuda*, 1997], where dissolved O_2 has been declining over the past several decades [*Ono et al.*, 2001]. Once it is formed, NPIW is thought to be advectively transported to the subtropical zones at 165°E and also to 137°E through the Kuroshio recirculation [*Fujii et al.*, 2013] (see also Fig. 2-1a) while mixing with surrounding waters. Therefore, the signal of decreasing dissolved O_2 in the Oyashio is thought to propagate to NPIW at 165°E and then further downstream to 137°E. Indeed, it was found that the decline in dissolved O_2 on $26.8\sigma_\theta$ in NPIW at 165°E was slower than that in the Oyashio region (1.04 ± 0.33 μmol kg^{-1} yr^{-1} in AOU) [*Ono et al.*, 2001] but was faster than that at 137°E (-0.36 ± 0.08 μmol kg^{-1} yr^{-1} in dissolved O_2) [*Takatani et al.*, 2012]. Through the analysis of several data sets from infrequent but basin-wide observations in repeat hydrography sections, *Kouketsu et al.* [2010] reported a significant increase in AOU in NPIW between 25°N and 40°N and west of 170°W. This work reinforces their findings and suggests a large-scale propagation of decreasing dissolved O_2 in the Oyashio to NPIW in the western North Pacific along its interior ventilation pathway. Furthermore, the long-term component of O_2 changes on $26.8\sigma_\theta$ between 25°N and 30°N at 165°E exhibited decadal-like variability (Fig. 2-6b). Bidecadal cycles have previously been reported for the Oyashio region [*Ono et al.*, 2001] and in the eastern North Pacific [*Whitney et al.*, 2007]. The cycles are thought to be related to the strength of the Aleutian Low [*Ono et al.*, 2001; *Watanabe et al.*, 2008] or to 18.6 year nodal tides [*Yasuda* et al., 2006; *Osafune and Yasuda*, 2006]. The decadal-like variability found at

165°E is expected to reflect a connection with the Oyashio region. These oscillations are discussed in Chapter 3.

The Oyashio water itself has its sources in the Okhotsk Sea Mode Water (OSMW) and in Western Subarctic Gyre water (WSAG). Since a decrease in dissolved O_2 has also been found for both the OSMW [*Nakanowatari et al.*, 2007] and WSAG [*Andreev and Watanabe*, 2002], the decline of O_2 in the Oyashio is likely to be a result of the O_2 decline in these source waters. In addition, WSAG water contains less dissolved O_2 than OSMW, and the increase in the mixing ratio of WSAG water associated with a strengthening of the Aleutian Low is also thought to be a factor contributing to the O_2 decline in Oyashio [*Takatani et al.*, 2007; *Takatani et al.*, 2012].

In the eastern North Pacific, the highest rate of decreasing O_2 has also been reported on $26.6\sigma_\theta$ [*Emerson et al.*, 2004; *Mecking et al.*, 2008]. *Mecking et al.* [2008] reported that maximum changes on $26.6\sigma_\theta$ occurred along the 30°N section to the east of ~160°W and along the 152°W section. They attributed these O_2 decreases to a reduction of ventilation, because this density is the maximum density that outcrops in the western North Pacific. The highest rate of decrease in dissolved O_2 was also identified on $26.6\sigma_\theta$ in upper NPIW between 25°N and 30°N along the 165°E section, and this may also be connected with the O_2 decrease in the same density in the eastern North Pacific. However, *Kouketsu et al.* [2010] have investigated the data from several repeat sections in the North Pacific and pointed out that the relationship between the change in potential density and that in AOU to the west of 170°W is different from that to the east of 170°W over the latitudinal band of 25°N–40°N. It suggests that the O_2 changes on $26.6\sigma_\theta$ in the western North Pacific evaluated in this study would not propagate directly to the eastern North Pacific. Clarification of the connection between the changes in O_2 between the western and eastern North Pacific near $26.6\sigma_\theta$ is left as a subject

for further investigation.

2.4.3. Oxygen Changes in the OML

Trends toward decreasing dissolved O_2 were also found in the subtropical OML between 25°N and 40°N at 165°E (Fig. 2-4c). In the northern subtropics (25°N–30°N), decreasing dissolved O_2 was attributed mostly to a net increase of AOU (Fig. 2-8a). As shown in Figs 2-1a, 2-2c, and 2-4c, the subtropical OML penetrates to the western North Pacific at deeper depths (900–1500 m) on higher densities ($27.3\sigma_\theta$–$27.6\sigma_\theta$) than the tropical OML (at 250–700 m on $26.5\sigma_\theta$–$27.2\sigma_\theta$) (see also Fig. 10 in *Takatani et al*. [2012]). Accordingly, the radiocarbon age in the subtropical OML is much older (1600–1800 years on $27.3\sigma_\theta$) than in the tropical OML (700–800 years on $26.8\sigma_\theta$) in the 165°E section [*Key et al*., 2004]. In previous studies, the O_2 decline in the OML has been considered as resulting from decreased ventilation associated with intensified stratification, with the stratification changes themselves driven by warming (e.g., *Oschlies et al.* [2008]; *Stramma et al.* [2008]). However, they focused mainly on the tropical OML, with this being lighter and younger than the subtropical OML. It is questionable as to whether the warming being transmitted from upper layers can sufficiently account for the O_2 decline in the denser and older subtropical OML.

Decline of O_2 in the subtropical OML has also been identified along the 137°E section further to the west by *Takatani et al.* [2012]. They suggested that the O_2 decline in the subtropical OML at 137°E is a result of an enhanced westward advection of lower-O_2 water that expands sluggishly from the coastal zone of the North America over a great distance. The enhanced westward advection is associated with the strengthening of the North Pacific subtropical gyre associated with a strengthening of Westerlies over the past 40 years [e.g., *Yasuda and Sakurai*, 2006]. The O_2 decline in the subtropical OML identified here along the

165°E section can also be attributed to the same mechanism. On the other hand, the strengthening of the subtropical gyre does not account for the O_2 decline in NPIW above the subtropical OML, as upstream O_2 concentrations are in fact higher.

In order to evaluate whether the westward advection of low-O_2 subtropical OML water is increasing or not, the latitudinal distributions of dissolved O_2 on an isopycnal horizon of 27.3σ_θ were compared among several latitudinal sections in the western North Pacific with 3 year means of dissolved O_2 concentrations along 165°E for 1991–1993 to 2009–2011 (Fig. 2-10). Dissolved O_2 over 29°N–41°N was low at 179°E (25–35 μmol kg^{-1}) and was relatively high in the western section at 150°E (40–45 μmol kg^{-1}). In the region where a significant decrease of dissolved O_2 concentration was determined locally along 165°E, dissolved O_2 was higher than that at 179°E and gradually decreasing toward concentrations at 179°E with time from 1991–1993 to 2009–2011. These variations of dissolved O_2 in space and time suggest that the trend of declining O_2 at 165°E can be attributed to an increase in the transport of low-O_2 water to the west. The faint trends toward decreasing O_2 between 25°N and 30°N can also be explained by the same controlling factor, as the zonal gradient south of 27°N had vanished. In contrast, this does not explain the O_2 increase observed at 47.5°N (Fig. 2-4c) since dissolved O_2 at 47°N, 165°E, is higher than that at 179°E. This increase can potentially be explained by a northward shift of the subarctic gyre, as dissolved O_2 along 47°N in 2000s was nearly equal to that along 46°N in the 1990s and the meridional gradient in dissolved O_2 on the isopycnal horizon is large.

At 137°E, the decreasing trend in O_2 has also been identified throughout the subtropical OML (see Fig 3 in *Takatani et al.*, [2012]). Along this section, dissolved O_2 concentrations are higher (55–65 μmol kg^{-1}) than at 150°E and 165°E (Fig. 2-10). This is consistent with the large zonal gradient of O_2 increasing toward the west that is seen at the Izu-Ogasawara Ridge

located just to the east of the 137°E section (see vertical section of dissolved O_2 concentration at WHP-P02) [*Talley* 2007]. These facts imply that dissolved O_2 in the OML along the 137°E section is sensitive to changes in the westward advection of low-O_2 water from the east. Consequently, O_2 decreases in the subtropical OML in the western North Pacific can likely be attributed to the west–east gradient of dissolved O_2 and the increase in the westward advection of low-O_2 water due to the strengthening of the subtropical gyre.

On the other hand, significant increases of dissolved O_2 were found in the tropical OML over $26.8\sigma_\theta$–$27.2\sigma_\theta$ between 5°N and 10°N. In particular, the O_2 increase was prominent in the northern part of the tropical OML at 10°N. A similar pattern has been found in the tropical OML along the 137°E section (see Fig. 3 in *Takatani et al.*, [2012]). These results suggest that the same drivers are causing the O_2 increases in the tropical OML in the two sections in the western Pacific. Near the tropical OML core at 165°E, the dissolved O_2 concentrations revealed large interannual variability within the range of 10–30 μmol kg^{-1} (Fig. 2-7). These variations were larger than those in the subtropical OML (Fig. 2-10). In addition, the vertical structure of the tropical OML was temporally variable. This suggests that isopycnal deepening and changes in O_2^{sat} associated with temperature/salinity changes contribute little to the observed changes in O_2, and large-scale changes in ocean circulation contribute more to the O_2 increases. *Qiu and Chen* [2012] suggested that the NEC and North Equatorial Countercurrent have migrated southward and strengthened in the western North Pacific over the period of 1993–2009. Because the OML penetrates sluggishly westward between two tongues of high O_2 water extending eastward from the western boundary [*Reid*, 1997], the southward migration and strengthening of the NEC would interrupt westward and northward expansion of the OML and therefore result in O_2 increases in the western tropical Pacific, particularly in the northern part of the OML near the NEC. This is supported by the long-term

trend toward decreasing salinity within similar isopycnal horizons and latitudinal zones, as salinity is lower and O_2 is higher in the northern and western regions of the tropical OML (Figs. 2-1a and 2-4b).

2.5. Conclusions

Significant trend towards decreasing dissolved O_2 were identified over the past 25 years between 1987 and 2011 in several domains on density-latitude space from the tropical through the subarctic zones at 165°E in the western North Pacific. While long-term changes in biological activity and their impact on the dissolved O_2 warrants further investigation, the driver of the decrease in dissolved O_2 appears to be primarily linked with the ocean warming and circulation changes in the western North Pacific. On the isopycnal horizons of NPSTMW, the average rate of decrease in dissolved O_2 reached -0.45 μmol kg^{-1} yr^{-1} and can largely be attributed to the deepening of isopycnal horizons and the reduction of O_2^{sat} due to warming of the upper ocean layers. These findings suggest that dissolved O_2 in NPSTMW will continue to decline in the coming decades, on average, as global warming progresses. For NPIW, the decreasing trend in dissolved O_2 was also remarkable. Its rate at 165°E (-0.44 μmol kg^{-1} yr^{-1} in the NPIW core on $26.8\sigma_\theta$) was lower than in the subsurface of Oyashio near the NPIW formation region [*Ono et al.*, 2001] and was higher than it is downstream at 137°E [*Takatani et al.*, 2012]. Furthermore, the decreasing trend in O_2 in NPIW along 165°E is consistent with the results for NPIW in other repeat sections in the western North Pacific [*Kouketsu et al.*, 2010]. These results from observations suggest that the multidecadal decline of O_2 in NPIW has its origin in the Oyashio and is propagating over the western North Pacific while attenuating its signal. The decline of dissolved O_2 was also found on deeper isopycnal

horizons in the subtropical OML, although the signal of O_2 decline was weaker than in the 137°E section further to the west. The O_2 decline in the subtropical OML was attributed to the increase in westward transport of low-O_2 water due to the strengthening of the subtropical gyre. Since the subtropical OML is associated with a large volume of water and its O_2 concentration is low (< 40 μmol kg^{-1}), the decline of O_2 in the subtropical OML may have a large impact on the ocean biogeochemistry. By contrast, an increasing trend in O_2 was found in the tropical OML in the western Pacific, while the expansion of the OML has been documented in the central and eastern Pacific [*Stramma et al.*, 2008]. An assessment of the drivers of O_2 changes over the tropical OML is left as a subject for future investigation.

This study evaluated not only the trend in dissolved O_2 concentrations but also the trends in temperature and salinity on isopycnal horizons. It is important to consider these trends simultaneously as the analysis on isopycnal horizons could be misleading given that biogeochemical as well as physical properties on isopycnals are subject to change due to circulation changes and ocean warming/freshening. These effects should also complicate the interpretation of changes in other biogeochemical parameters such as nutrients and DIC. Under global warming, the analysis on isopycnal horizons should be performed carefully, especially in the upper layers. As there are long historical records of dissolved O_2 concentrations in the ocean with relatively high quality, most often with contemporaneous temperature and salinity measurements, it is generally possible to consider the changes in dissolved O_2 within the context of non-stationary ocean density structures. Moreover, changes in dissolved O_2 will continue to be central to a number of methods to quantify the changes in DIC in the ocean interior associated with the invasion of anthropogenic CO_2 [e.g., *Gruber et al.*, 1996]. This also has implications for efforts to detect and attribute ocean acidification [*Byrne et al*., 2010]. Therefore, analyses that contribute to the attribution of changes in

dissolved O_2 in the ocean interior can be also of value for a number of questions related to the interpretation of the entry of anthropogenic CO_2 into the ocean.

Finally, the high-frequency repeat section at 165°E, along with the high-frequency repeat section at 137°E, provides a unique opportunity to systematically evaluate the evolution of tracers over both interannual and decadal timescales. For the case where the secular decadal trend is the signal to be detected, they provide a means to identify and understand the noise (interannual variability) against which the signal is to be detected. It is my intention that the results here be more generally applicable to the case of WOCE, CLIVAR to GO-SHIP CO_2/Repeat Hydrography changes. Additionally, these points apply to the specific water masses considered here, with the formation history of these water masses varying in time in ways that are not yet well characterized by the scientific community. These high-frequency repeat sections also complement the larger-scale observing network where sampling occurs on decadal timescales.

Appendix A: Method of Primary QC Considering Natural Variability

I first conducted data quality control for dissolved O_2 following the method presented in *Takatani et al.* [2012]. I also calculated NO (= $9 \cdot NO_3 + O_2$) and PO (= $135 \cdot PO_4 + O_2$) [*Broecker*, 1974] and applied the same method of data quality control to these tracers. Because these tracers are considered quasi-conservative with respect to biological activity, these profiles are expected to change smoothly with depth. For example, Fig. 2-A1 shows profiles of dissolved O_2, PO_4, and PO at 165°E, 21°N, in July 2011. The vertical profiles of O_2 and PO_4 measured through discrete bottle samplings are somewhat scattered, and some are even lying out of the mean ±3SD profiles. However, all PO data ranged within the mean

±3SD profiles and varied smoothly with depth. This suggests that these outliers of dissolved O_2 are not analytical errors but show natural variability. This was confirmed by measurements with an O_2 sensor that agreed with all discrete bottle data including outliers (Fig. 2-A1a). The evaluation of data quality of dissolved O_2 combined with quasi-conservative tracers NO and PO helps to distinguish between erroneous measurements and natural variability in ocean biogeochemistry. These processes are equivalent to examine the data quality with property-property plots of O_2 against NO_3 and PO_4.

Appendix B1: Method of Secondary QC

I evaluated systematic errors (offsets) occurring in the measurements of dissolved O_2 and salinity for each data set of the cruises conducted along 165°E assuming that the each data set has a single offset value for each parameter. First, I applied the cross-over analysis [*Tanhua et al.*, 2010] for data under the assumption that water properties in deep layers are stable over time at the same station. The evaluation of water properties was conducted in depth-, theta-, and sigma4-spaces below 1500 m. Second, I evaluated the differences in dissolved O_2 and salinity from those in the data set of the "core cruise" (see Appendix B2) with the best data quality. Finally, adjustment values, multiplicative for O_2 and additive for salinity, were determined and applied to each data set. The procedure is essentially the same used for the secondary data quality control of CARINA [*Tanhua et al.*, 2010] and PACIFICA [*Suzuki et al.*, 2013] except that (1) data from a station in a cruise was compared with the data from the same station in the "core cruise" located at each 1° of latitude on 165°E, (2) then a single offset value was evaluated for each cruise against the data from the core cruise (i.e., the inversion technique that has been applied to CARINA and PACIFICA was not executed

to determine the offsets), (3) for the cruises in which the maximum depth of measurement was shallower than 2100 m, the calculation of offset in depth-space was not made because the offset value in depth-space was often biased largely to both those in theta- and sigma4-spaces, and (4) no minimum adjustment value (e.g., 0.01 for dissolve O_2 defined in CARINA and PACIFICA as a border dividing natural variability and analytical offset) was assigned, because to define a border might introduce artificial differences among cruises in m target region where natural variability is large (see Appendix B2).

Appendix B2: Calculation Procedure

The Japan Meteorological Agency conducted a research cruise along the repeat section WHP-P13 (165°E) spanning the tropical to the subarctic zones of the North Pacific in May–August 2011 as one of the Global Ocean Ship-based Hydrographic Investigations Program (GO-SHIP) cruises (http://www.go-ship.org/). The data set from this cruise is the most recent one I used in this study and is the one with the highest data quality, just as the data set from the cruise conducted along the repeat section WHP-P09 in July–August 2010 [*Nakano*, 2010] provided the one with the highest data quality in that section. In the WHP-P13 cruise, the reproducibility of dissolved O_2 analysis by titration as determined from many pairs of replicate samples was as good as 0.19 ± 0.17 μmol kg^{-1}. In addition, rigorous quality control procedures including the measurements of several working standards made it possible to confirm that there was no systematic drift in the quality of dissolved O_2 measurements during the cruise [*Nakano*, 2012; to be revised to include the description for O_2 measurements; the quality of dissolved O_2 measurements was comparable to that in the WHP-P09 cruise in 2010].

Furthermore, vertical profiles of dissolved O_2 in deep layers agreed well with those in other GO-SHIP sections (WHP-P01 in 2007, WHP-P02 in 2004, and WHP-P03 in 2005/2006) in 2000s at their cross-over stations within the range of analytical uncertainty. Accordingly, I defined this cruise as the “core cruise” to which the offsets in other cruises are adjusted.

Prior to the evaluation of offsets in the data of dissolved O_2, analytical offsets in salinity data were evaluated. For most cruises, additive offsets in salinity were within ±0.005 and no adjustments were applied. For other cruises in which the offsets were larger, they were corrected (applied adjustments were -0.005 for TEW cruise and -0.006 for CO2-87 cruise). Subsequently, multiplicative offsets were evaluated for dissolved O_2. For the cruises in which measurements were conducted only within the upper 2100 m to the north of 28°N, the adjustment values tended to be systematically lower (about 0.03 on the average) than those of PACIFICA. Even for the P13 cruise conducted in 1992 with no significant offsets, the experimental calculation using the same procedure but with limited data distributions within the upper 2100 m to the north of 28°N yields a relatively large offset. It suggests that dissolved O_2 in the layers in the depth range 1500–2100 m in the northern part of the western North Pacific includes natural variability. Therefore, I calculated the mean vertical profiles of dissolved O_2 for each 1° in latitude using the offset-adjusted data from the measurements when they have been done to the depths below 2100 m. I then reevaluated offset values for all cruises using these time-averaged profiles instead of the profiles from just one cruise (WHP-P13 in 2011) as references in order to avoid introducing the natural variability into the analytical offset.

Appendix C: Mechanism of the deepening of isopycnal horizons

In quantifying the net temporal changes of biogeochemical properties in the ocean interior over decades, analyses of data are often made on isopycnals rather than on isobaths. This is because the isopycnals are the preferred horizons for transport and mixing of properties, while the depths of isopycnals fluctuate largely over a range of time scales due to ocean circulation processes including the passage of cyclonic/anticyclonic eddies, internal waves, and gyre wobble. However, in the upper layers of the oceans, this conventional approach begins to waver as changes in temperature and salinity on constant density horizons would drive isopycnal displacements. *Bindoff and McDougall* [1994] divided these changes into the three processes which could occur in the water mass formation region: cooling/warming, freshening/salting, and heaving. This interpretation is useful in quantifying changes of physical and biogeochemical parameters on isopycnal horizons.

For instance, in the subtropical zone of the western North Pacific at the 137°E section, *Nakano et al.* [2007] have shown that ocean warming and freshening are simultaneously occurring in the upper water column above the salinity minimum of NPIW. As a consequence of this warming and freshening, isopycnal horizons are deepening, further freshening, and thereby cooling. They suggested that the rate of deepening of isopycnals exceeds 1 m yr^{-1} between the main thermocline and the salinity minimum layer. The trend of ocean warming in the upper layers has also been reported over the broad expanse of the western North Pacific, in particular, in the region to the south of the Kuroshio Extension Current where NPSTMW is being formed [*Levitus et al.*, 2009; *Rhein et al.*, 2013]. These findings suggest that the deepening, freshening, and cooling of isopycnals are occurring in the broad expanse of the North Pacific subtropical zones. I can also see cooling and freshening of isopycnals being

commensurate with warming on isobaths in the subtropical zone of the 165°E section that is the focus of this work (Figs. 2-4a, 2-4b, and 2-5). It is thought that this deepening, freshening, and cooling will also modulate biogeochemical fields such as dissolved O_2 concentrations on isopycnal horizons. This effect can be quantified in a manner detailed in the text that follows.

When temperature at a depth "Z_A" rises from θ_A to θ_A' as a consequence of increases in OHC, the density at this depth decreases from σ_A to σ_A' (for simplicity, the vertical profile of salinity is assumed unchanged with time) and the depth of the isopycnal horizon of σ_A moves from Z_A to a deeper depth Z_B (Fig. 2-C1). For the case where freshening as a consequence of a net transfer of freshwater to the surface ocean occurs concurrently, the decrease of density at depth Z_A from σ_A to σ_A' and the deepening of the depth at density σ_A from Z_A to Z_B are reinforced. As the density is functionally determined by temperature and salinity ($\sigma = f(\theta, S)$), the density of an isopycnal horizon, σ_A, is expressed as (C1) before and (C2) after warming, respectively.

$$\sigma_A = f(\theta_A,\ S_A) \qquad \text{(before warming)} \qquad \text{(C1)}$$

$$= f(\theta_B',\ S_B) \qquad \text{(after warming)} \qquad \text{(C2)}$$

S_A and S_B represent salinity at depth Z_A and Z_B, respectively. θ_B' denotes temperature at σ_A at Z_B after warming. To satisfy (C1) and (C2), Z_B is determined. In the region where salinity decreases with depth (e.g., above the salinity minimum layer of NPIW), $S_A > S_B$, and therefore, $\theta_A > \theta_B$'. It means that the potential temperature on an isopycnal horizon rather decreases as a result of warming. It also implicates that the biogeochemical properties on an isopycnal horizon should be expected to change.

For the case where a vertical profile of a certain parameter "X" with respect to depth does not change with time (e.g., salinity in Fig. 2-C1c), a temporal change of X on potential density σ_A is attributed to an apparent change induced by the deepening of the isopycnal

horizon from the depth Z_A to Z_B:

$$\frac{\partial X}{\partial t} = \left(\frac{\partial X}{\partial z} \bullet \frac{\partial z}{\partial t} \right), \tag{C3}$$

where $\partial X/\partial t$ represents the rate of change in X observed on a density σ_A (as shown with gray arrows in Fig. 2-C1), z the depth at σ_A, $\partial X/\partial z$ the vertical gradient of X with respect to the depth (assumed to be unchanged with time in the equation), and $\partial z/\partial t$ the rate of increase in the depth of density σ_A. $\partial X/\partial z \cdot \partial z/\partial t$ denotes the effect of deepening (as shown with white arrows in Fig. 2-C1 as a difference in symbols between closed square and closed circle).

Alternatively, for the case where a vertical profile of another parameter "Y" changes with time and the warming occurs simultaneously, the change of Y at density σ_A is observed as a combination of the apparent change induced by the deepening of the isopycnal horizon from depth Z_A to Z_B and the net temporal change of Y, $(\partial Y/\partial t)_{net}$ between the time before and after warming:

$$\frac{\partial Y}{\partial t} = \left(\frac{\partial Y}{\partial z} \bullet \frac{\partial z}{\partial t} \right) + \left(\frac{\partial Y}{\partial t} \right)_{net}. \tag{C4}$$

Therefore, in order to evaluate net change $(\partial Y/\partial t)_{net}$ (as seen in Fig. 2-C1 as black or textured arrows of a difference in symbols between closed square and open square), it is necessary to evaluate the contribution of the temporal change of Y due to the deepening of the isopycnal horizon and to subtract it from the change of Y observed at density σ_A. For instance, the change of O_2^{sat} in Fig. 2-C1f is observed as a gray arrow after warming. However, this change includes an apparent change induced by the deepening of an isopycnal horizon (white arrow). Therefore, the net change (textured arrow) is obtained as a difference between the observed change and deepening effect.

The concentration of dissolved O_2 can be expressed as

$$O_2 = O_2^{sat} - AOU \quad \text{(C5)}$$

where O_2^{sat} denotes the saturation concentration and AOU denotes "apparent oxygen utilization." The value of O_2^{sat} is determined as a function of temperature and salinity, and AOU represents the net concentration of dissolved O_2 utilized through biological activity subsequent to subduction. AOU is also thought to include a contribution from undersaturation and supersaturation of oxygen when the water parcel was last contact with the atmosphere (this contribution is minor since AOU in a surface water is typically close to zero).

According to (C4), the change in O_2 at a specific density for a fixed station is expressed as

$$\frac{\partial O_2}{\partial t} = \left(\frac{\partial O_2}{\partial z} \cdot \frac{\partial z}{\partial t} \right) + \left(\frac{\partial O_2}{\partial t} \right)_{net} . \quad \text{(C6)}$$

Similarly, the changes in O_2^{sat} and AOU are expressed as

$$\frac{\partial O_2^{sat}}{\partial t} = \left(\frac{\partial O_2^{sat}}{\partial z} \cdot \frac{\partial z}{\partial t} \right) + \left(\frac{\partial O_2^{sat}}{\partial t} \right)_{net} , \quad \text{(C7)}$$

and

$$\frac{\partial (AOU)}{\partial t} = \left(\frac{\partial (AOU)}{\partial z} \cdot \frac{\partial z}{\partial t} \right) + \left(\frac{\partial (AOU)}{\partial t} \right)_{net} , \quad \text{(C8)}$$

respectively. $(\partial O_2^{sat}/\partial t)_{net}$ has a certain value with respect to warming as O_2^{sat} changes as a function of temperature. If AOU does not change with time, i.e., the change in O_2 concentration is attributed only to the change in O_2^{sat}, $\partial(AOU)/\partial t$ is expressed as (C3) and $(\partial(AOU)/\partial t)_{net}$ is zero. On the other hand, if AOU changes with time, $\partial(AOU)/\partial t$ is expressed as (C4) and $(\partial(AOU)/\partial t)_{net}$ is not zero, as shown in Fig. 2-C1g as dashed gray line.

As the concentration of dissolved O_2 is expressed as (C5), net change in O_2 concentration, $(\partial O_2/\partial t)_{net}$, on an isopycnal horizon is expressed as

$$\left(\frac{\partial \mathrm{O}_2}{\partial t}\right)_{\mathrm{net}} = \left(\frac{\partial \mathrm{O}_2^{\mathrm{sat}}}{\partial t}\right)_{\mathrm{net}} - \left(\frac{\partial(\mathrm{AOU})}{\partial t}\right)_{\mathrm{net}}. \qquad \text{(C9)}$$

According to (C6) and (C9), the change in dissolved O_2 on an isopycnal horizon is represented by

$$\frac{\partial \mathrm{O}_2}{\partial t} = \left(\frac{\partial \mathrm{O}_2}{\partial z} \cdot \frac{\partial z}{\partial t}\right) + \left(\frac{\partial \mathrm{O}_2^{\mathrm{sat}}}{\partial t}\right)_{\mathrm{net}} - \left(\frac{\partial(\mathrm{AOU})}{\partial t}\right)_{\mathrm{net}} \qquad \text{(C10)}$$

as described in equation (1) in the main text. Each term in (C10) corresponds to an arrow in Fig. 2-C1e: the four terms in (C10) are represented, respectively, with a gray arrow, a white arrow, a textured arrow with diagonal lines (identical to Fig. 2-C1f), and a textured arrow with checkers (otherwise identical but reversed with respect to Fig. 2-C1g), as one moves from left to right. Consequently, (C10) is replaced by (C11), using (C7) and (C8) as described in equation (2) in the main text:

$$\frac{\partial \mathrm{O}_2}{\partial t} = \left(\frac{\partial \mathrm{O}_2}{\partial z} \cdot \frac{\partial z}{\partial t}\right) + \left(\frac{\partial \mathrm{O}_2^{\mathrm{sat}}}{\partial t} - \frac{\partial \mathrm{O}_2^{\mathrm{sat}}}{\partial z} \cdot \frac{\partial z}{\partial t}\right) - \left(\frac{\partial(\mathrm{AOU})}{\partial t} - \frac{\partial(\mathrm{AOU})}{\partial z} \cdot \frac{\partial z}{\partial t}\right). \qquad \text{(C11)}$$

In reality, vertical profiles of hydrographic and biogeochemical parameters in the ocean are fluctuating significantly with time due to variability in the physical state of the ocean such as the passage of eddies, internal waves, and planetary waves. Therefore, (C11) is in practice not applicable to the infrequently occupied stations since it is difficult to determine both the mean vertical profiles with respect to depth ($\partial X/\partial z$, $\partial Y/\partial z$) and the rate of deepening of a particular isopycnal horizon due to warming/freshening ($\partial z/\partial t$) with confidence. Additionally, the variation of $\partial z/\partial t$ is affected by a meander of a front if it is located near the station. By contrast, in regions where the nearest front is distant enough to have negligible impact on the variation of $\partial z/\partial t$ and in the interior of the subtropical gyre where the horizontal gradient of a parameter on an isopycnal horizon is small (see Fig. 2-4), the influences of gyre wobble in the ocean circulation on $\partial z/\partial t$ is considered minor. At 25°N–30°N along the 165°E section, a

large number of time-series of hydrographic and biogeochemical data are available over the last decades. Therefore, the mean vertical profile and mean rate of isopycnal deepening due to warming can be determined by smoothing out the short-term fluctuations in the vertical profile, thereby (C11) is thought to be applicable to determine the net change of parameters for decades. The region between 20°N and 25°N along 137°E described by *Takatani et al.* [2012] is also considered as such a region where (C11) is applicable.

Figures of Chapter 2

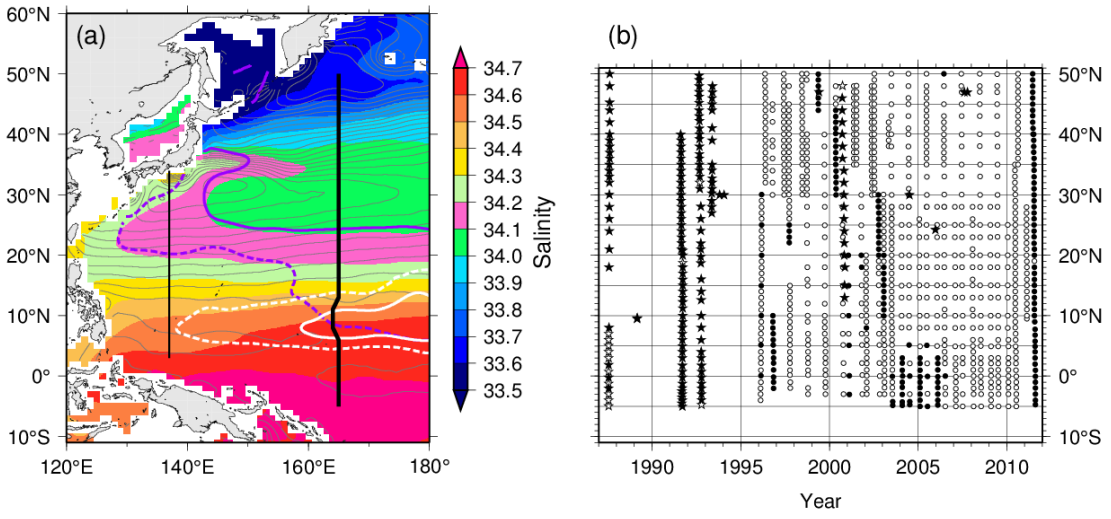

Fig. 2-1. (a) Location map of the repeat hydrographic sections of WHP-P13 (165°E) studied in this work (thick black line) and P09 (137°E) studied in Takatani et al. [2012] (thin black line). Colors and gray contours show climatological salinity and acceleration potential referred to 1500 dbar on 26.8σ_θ, respectively, from the World Ocean Atlas 2009 (WOA09) [*Antonov et al.*, 2010; *Locarnini et al.*, 2010]. Solid and dashed white (purple) lines indicate isolines of climatological dissolved O_2 at 50 and 70 μmol kg^{-1} on 26.8σ_θ (27.4σ_θ), respectively, from WOA09 [*Garcia et al.*, 2010]. (b) Time-latitude distributions of hydrographic stations with dissolved O_2 measurements along the 165°E section. Circles and stars denote the stations occupied by the JMA and the other organizations, respectively. Closed (open) symbols indicate the stations where the maximum depth of measurement was deeper (shallower) than 2100 m.

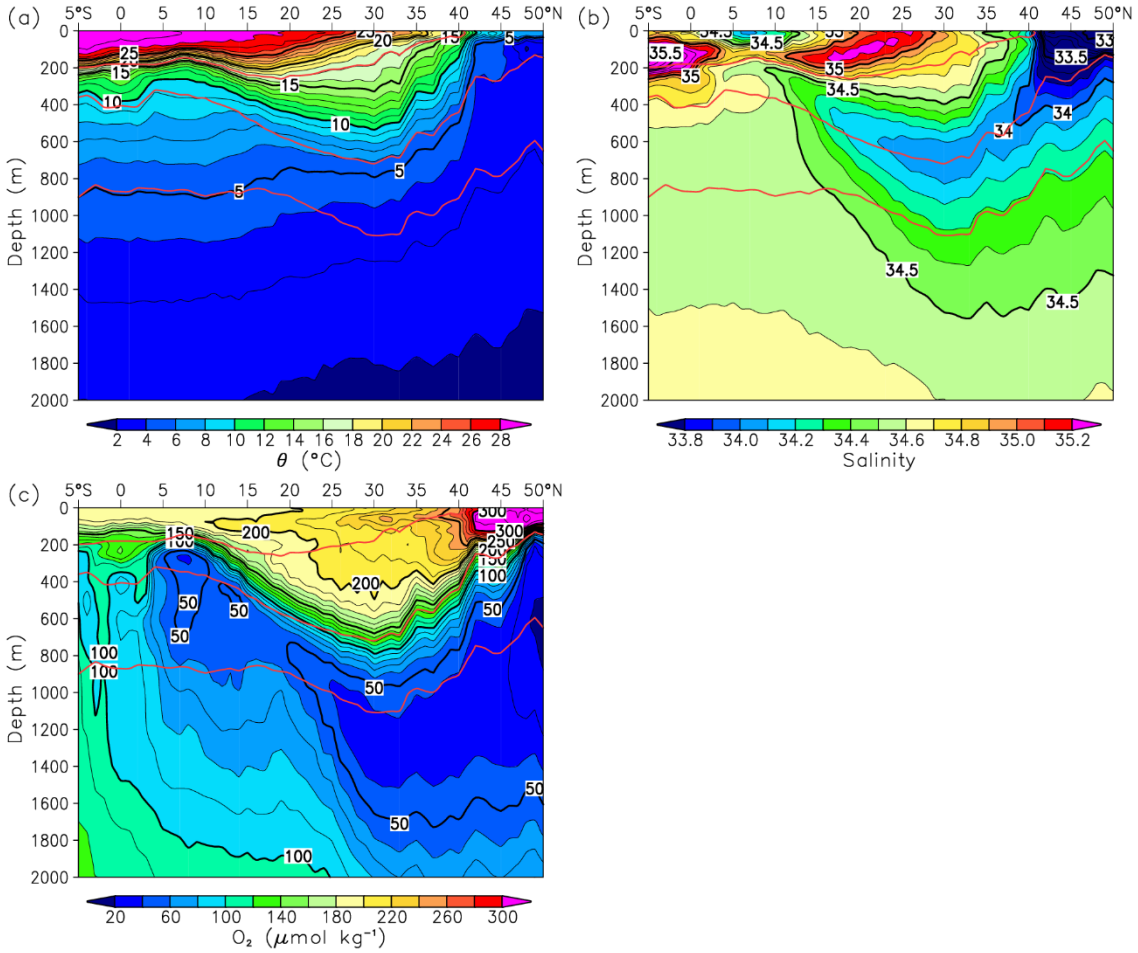

Fig. 2-2. Vertical sections of the mean (a) potential temperature, (b) salinity, and (c) dissolved O_2 for 1987–2011 at 165°E. Red lines denote isopycnal horizons of 25.3σ_θ, 26.8σ_θ, and 27.3σ_θ that intersect the density ranges of NPSTMW, NPIW, and the subtropical OML, respectively.

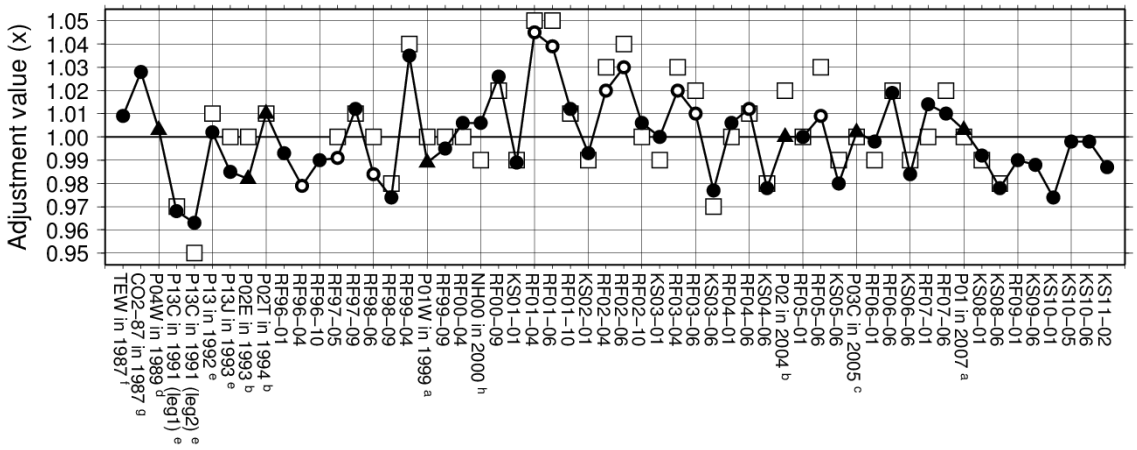

Fig. 2-3. Multiplicative adjustment values of dissolved O_2 for each cruise evaluated in this study. Circles indicate cruises along the 165°E section. Open circles denote cruises in which the maximum depth of observation was shallower than 2100 m, and the distribution of stations is confined to the north of 28°N at 165°E. Triangles represent the cruises for zonal sections crossing with 165°E. Open squares indicate the adjustment values that have been evaluated in PACIFICA. Initial character of cruises “RF” and “KS” represents the cruises of *R/V Ryofu Maru* and *R/V Keifu Maru* conducted by the JMA. The cruises with superscripts of a, b, c, d, and e–h are those of 47°N, 30°N, 24°N, 9/10°N, and 165°E, respectively. Data from cruises a–f are available from the Climate Variability and Predictability/Carbon Hydrographic Data Office (CCHDO; http://cchdo.ucsd.edu/). The cruise g is from *Wisegarver et al.* [1993]. The cruise h is the WEST-COSMIC cruise. This data set is available from the Japan Oceanographic Data Center (JODC; http://www.jodc.go.jp/).

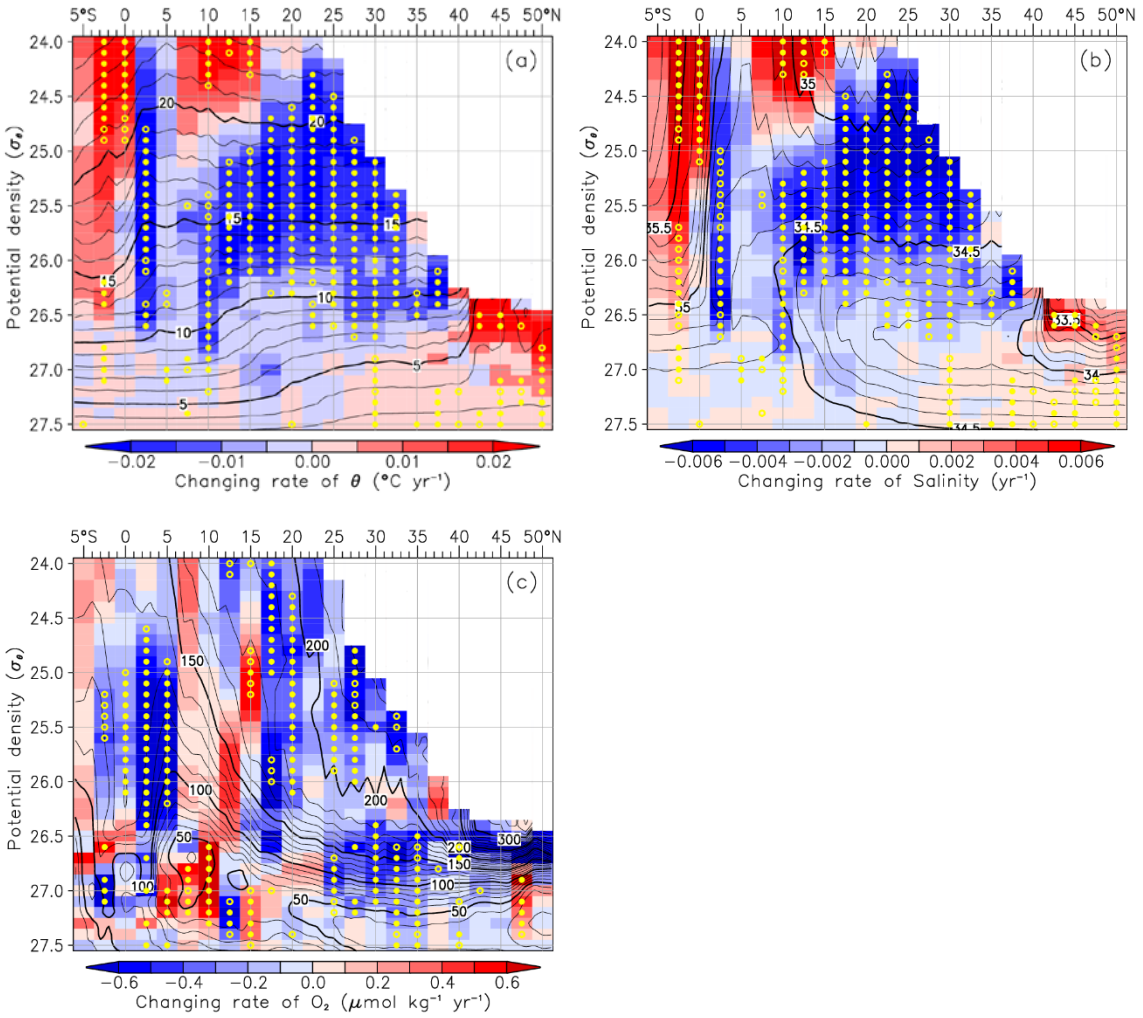

Fig. 2-4. Linear rate of change in (a) potential temperature, (b) salinity and (c) dissolved O_2 on each isopycnal horizon at intervals of $0.1\sigma_\theta$ at each 2.5°of latitude at the 165°E section. Yellow closed (open) circles indicate the grid in which the rate of change is significantly different from zero at 95% (90%) confidence intervals. Contour lines represent the mean values for 1987–2011 at intervals of $0.1\sigma_\theta$ at each 1°of latitude. Grids at which potential density is lighter than that in winter mixed layer calculated from WOA09 have been masked.

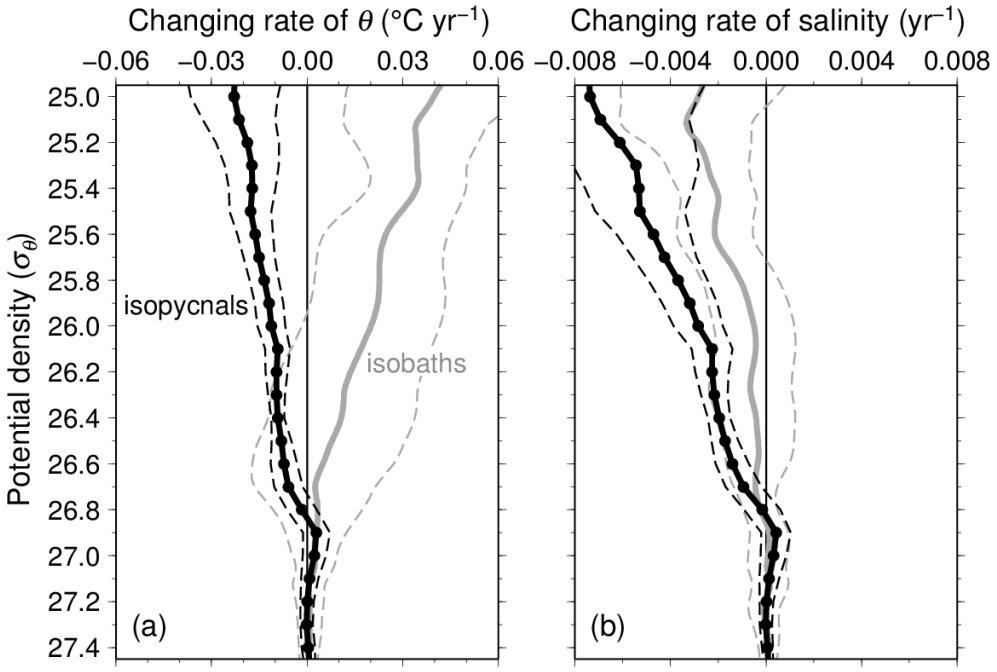

Fig. 2-5. Rates of change in (a) potential temperature and (b) salinity with respect to the potential density at 25°N–30°N. Thick black lines with black dots indicate the rates calculated on isopycnal horizons. Thick gray lines show the rates calculated on isobaths plotted against the mean density on each pressure. Thin broken lines show confidence intervals of 95%.

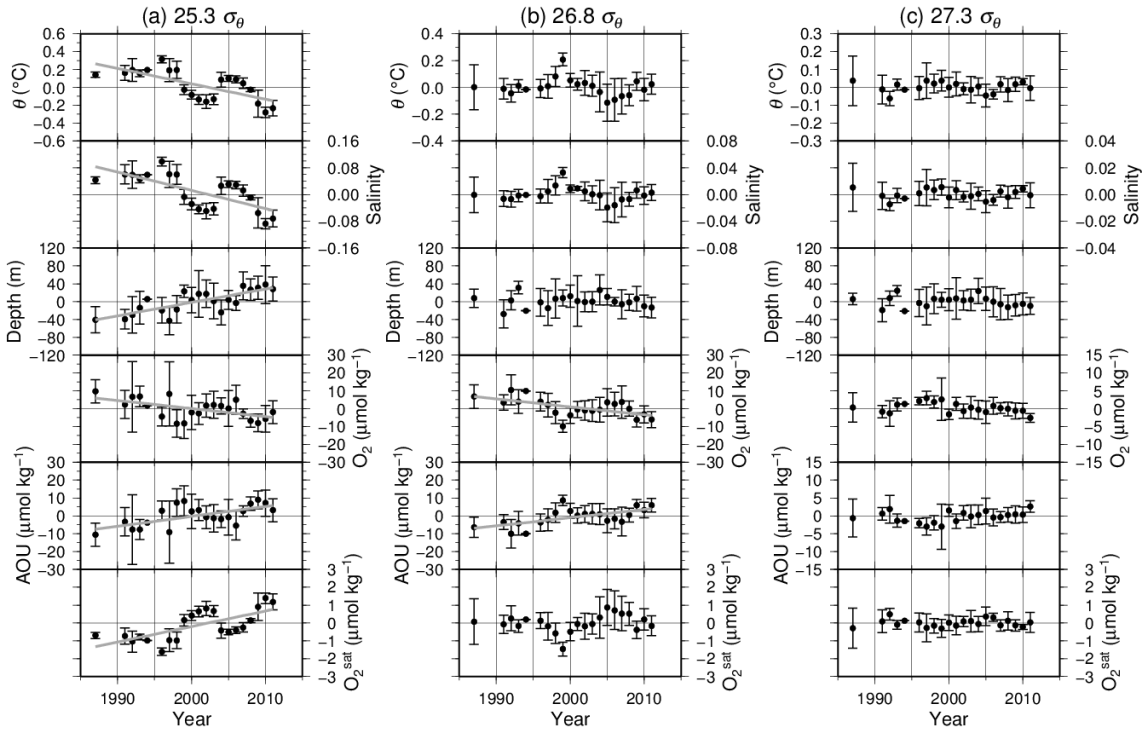

Fig. 2-6. Time series of physical and oxygen parameters averaged over 25°N–30°N at 165°E on (a) 25.3σ_θ, (b) 26.8σ_θ, and (c) 27.3σ_θ. Gray lines indicate the linear trends with confidence level greater than 95%.

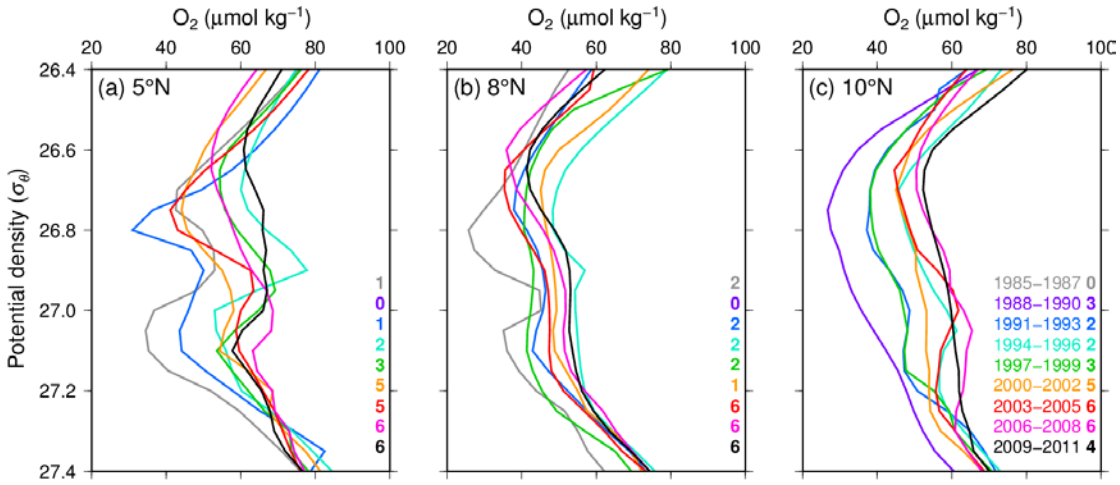

Fig. 2-7. Time-variation of 3 year mean dissolved O_2 concentrations with respect to the potential density at each 1°of latitude at (a) 5°N, (b) 8°N, and (c) 10°N at 165°E. The numbers in bold indicate total stations used to calculate mean profile.

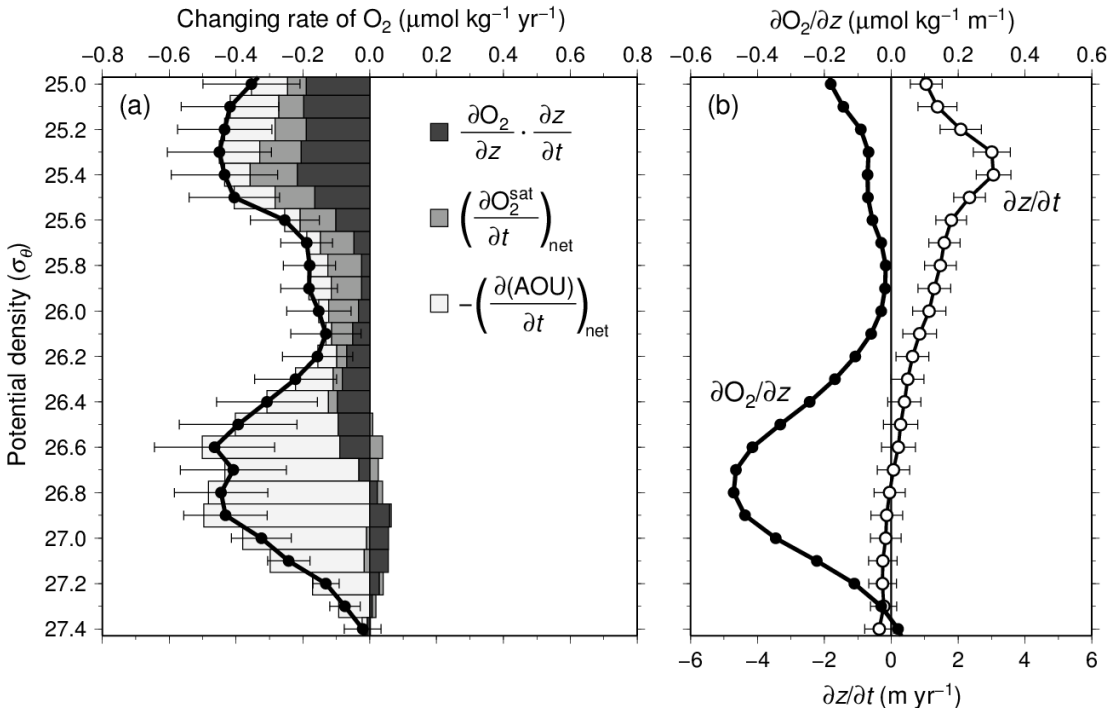

Fig. 2-8. (a) Rate of change of dissolved O_2 on each potential density at 25°N–30°N, 165°E. Closed circles with thick black line denote the rate of observed dissolved O_2 changes. Error bars denote ±1 standard error. Also shown are the contributions of the deepening effect of isopycnal horizon [ii], the net change in O_2^{sat} [iii – iv] and the net change in AOU [v – vi], respectively, to O_2 changes (see section 2.4). (b) Profiles of components in equation (2). Closed and open circles indicate vertical gradient of dissolved O_2 ($\partial O_2/\partial z$) and the rate of change in the depth of isopycnal horizon ($\partial z/\partial t$), respectively.

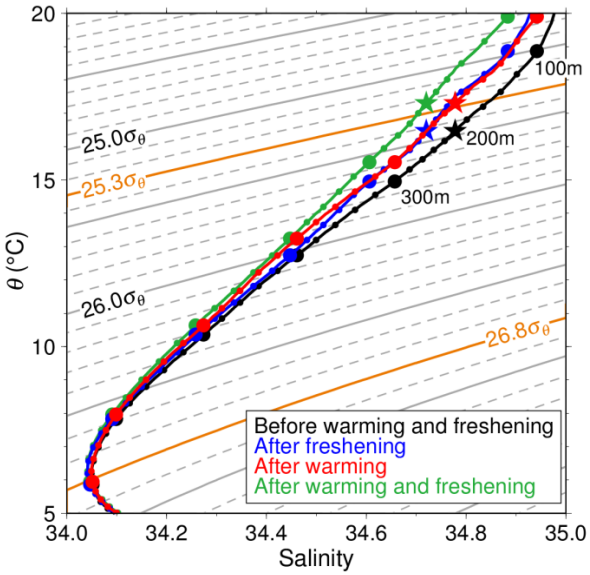

Fig. 2-9. Potential temperature-salinity diagram for 25°N–30°N at 165°E. Each parameter for a given year is reconstructed from long-term trends on isobath surfaces: $X=a \cdot y + b$, where "X" is reconstructed data, "y" is year, and "a" and "b" are the slope (shown in Fig. 2-6 as a gray line) and intercept, respectively. Black line denotes the reconstructed data in 1987 (before warming and freshening). Green line indicates the reconstructed data in 2011 (after warming and freshening). Red (blue) line is drawn with the reconstructed data from temperature in 2011 (1987) and salinity in 1987 (2011) to show the effect of warming (freshening). Large and small dots are plotted at intervals of 100 m and 20 m, respectively. Stars indicate the data at the depth of 200 m. Gray and orange contours denote potential density.

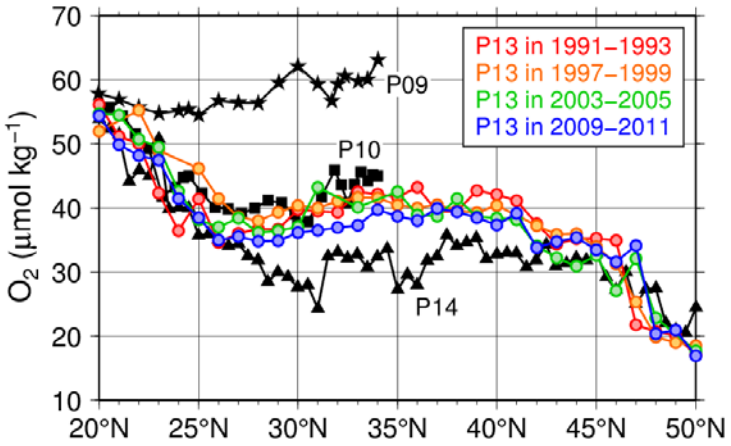

Fig. 2-10. Meridional distributions of 3 year mean dissolved O_2 concentration on $27.3\sigma_\theta$ in the section of P13 (165°E) for 1991–1993 (red), 1997–1999 (orange), 2003–2005 (green), and 2009–2011 (blue), respectively. Also shown are the dissolved O_2 on $27.3\sigma_\theta$ in the sections of WHP-P09 (137°E) in 2010 (star), P10 (150°E) in 2005 (square), and P14 (179°E) in 2007 (triangle), respectively. Data from P10 and P14 that are subjected to secondary quality control have been stored in the PACIFICA (http://cdiac.ornl.gov/oceans/PACIFICA/). Data from P09 have been acquired by the JMA (http://www.data.kishou.go.jp/kaiyou/db/vessel_obs/data-report/html/ship/ship_e.php).

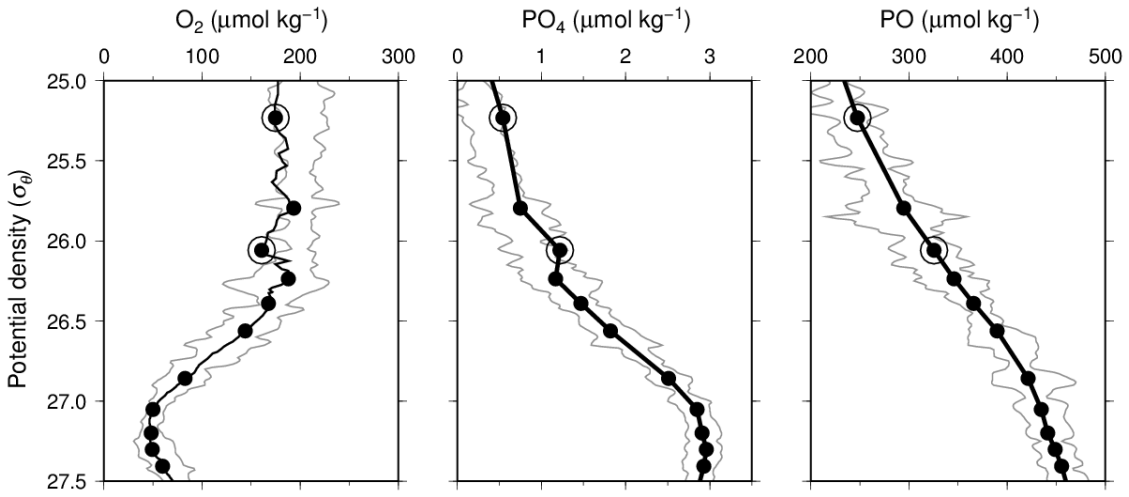

Fig. 2-A1. Profiles of (a) dissolved O_2, (b) PO_4, and (c) PO at 21°N, 165°E, in July 2011 with respect to potential density. Filled circles indicate data from discrete samplings. Highlighted with larger circle are the data flagged by primary QC procedures with only dissolved O_2. The thin line in Fig. 2-A1a represents upcast O_2 sensor data taken with RINKO III (JFE Advantech, Ltd). Gray lines indicate the range of mean ±3SD at 21°N ± 2.5° calculated at each potential density bands at intervals of $0.05\sigma_\theta$.

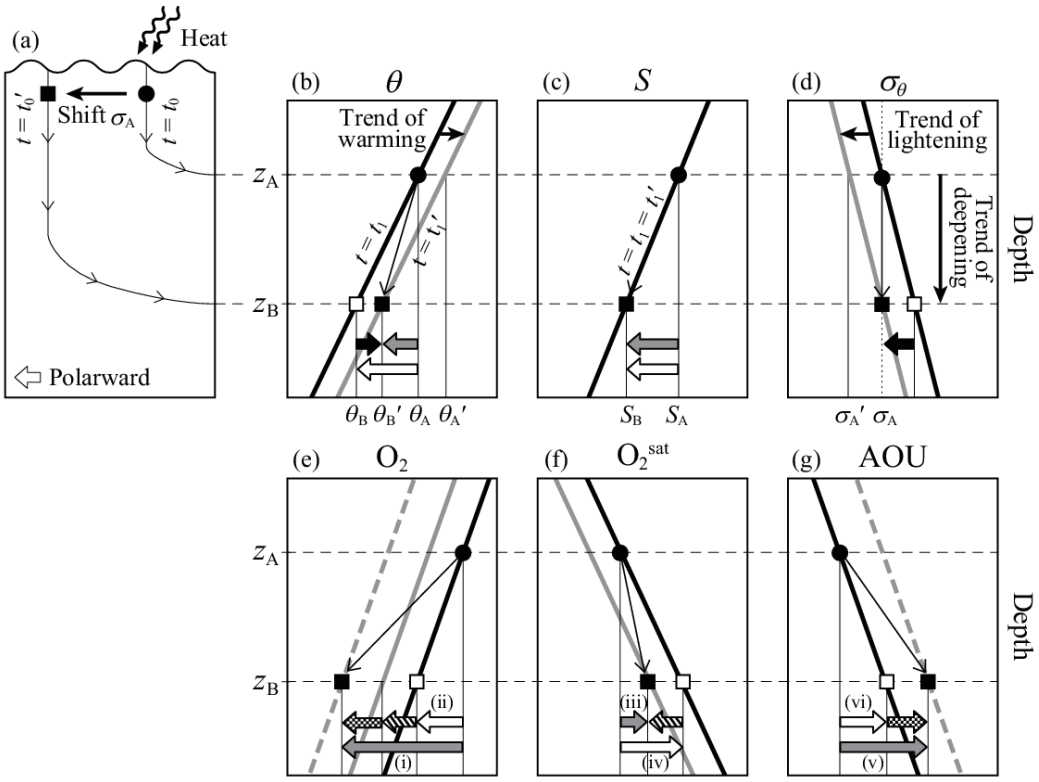

Fig. 2-C1. Schematics of temporal evolution of parameters on a typical (a) isopycnal horizon above a salinity minimum layer. (b) θ, (c) S, (d) σ_θ, (e) dissolved O_2, (f) O_2^{sat}, (g) AOU. Thick black (gray) lines indicate the profiles before (after) warming at a time t_1 (t_1'). Dashed gray lines denote the profiles after warming with concurrent AOU increase. Dotted line in Fig. 2-C1d represents an isopycnal horizon considered here. Closed circles (squares) denote parcels observed at a depth Z_A (Z_B) at a time t_1 (t_1') on an isopycnal horizon σ_A. Open squares indicate parcels at a depth Z_B before warming expected from the relation between parcels of closed circles and squares. Time of t_0 means the time before each parcel was submerged. Gray arrows indicate observed changes on a density horizon ($\partial X/\partial t$). White arrows denote changes by the deepening effect ($\partial X/\partial z \cdot \partial z/\partial t$). Large black and textured arrows represent net change (= gray arrow – white arrow). The textured arrows with the same pattern are identical. The arrows with Roman figures correspond to the terms in equation (2).

Chapter 3
Decrease with Bidecadal Oscillations of Oxygen in the Oyashio region and its propagation to the western North Pacific

3.1. Introduction

The distribution of dissolved oxygen (O_2) concentration in the ocean is controlled by biological and physical processes. In a surface layer, while O_2 concentration is produced by phytoplankton photosynthesis, O_2 is typically kept to be roughly equal to the saturation concentration (O_2^{sat}) through air-sea interaction. A water parcel mixed in surface layer is taken into permanent thermocline through subduction or entrainment, and transported by ocean circulation. After departure from euphotic zone, O_2 concentration is gradually decreased with time due to remineralization by bacterial activities which is reflected to the increase in apparent oxygen utilization (AOU; defined as the difference between measured O_2 concentration and O_2^{sat}). Therefore, O_2 concentration in the ocean interior is used as an indicator of water masses. In the past of few decades, decrease trends of dissolve O_2 have been observed in the North Pacific [*Keeling et al.,* 2010, and references therein]. It is important to understand controlling factors of deoxygenation because oxygen is a fundamental parameter in biogeochemical cycle in the ocean. Additionally, because changes in dissolved O_2 reflect reverse changes in dissolve inorganic carbon (DIC) through biological activity, it is useful to distinguish the change in DIC due to biological activity from the anthropogenic CO_2 invasion in to the ocean interior [e.g. *Gruber et al.,* 1996]

The Oyashio is the western boundary current of the Western Subarctic Gyre (WSAG) in the western North Pacific and flows southwestward along the Kuril Islands chain to the eastern coast of northern Japan. The Oyashio is one of the important water to understand the distribution of chemical parameters in the western North Pacific because the Oyashio water is presumed as one of the source water of North Pacific Intermediate Water (NPIW), which is widely distributed as the salinity minimum layer ($S < 34.2$) centered at $26.8\sigma_\theta$ in the North

Pacific subtropical gyre [*Yasuda*, 1997]. NPIW is formed in the subsurface of the Kuroshio-Oyashio Interfrontal Zone in the region offshore of northern Japan [*Talley*, 1993]. NPIW plays an important role to transport low salinity and nutrient rich water from subarctic to subtropical gyre into the intermediate depths of the North Pacific [e.g. *Yasuda et al.*, 1996; *Ono et al.*, 2003].

In the Oyashio region, *Ono et al.* [2001] have showed increasing trends in AOU using time series data between 26.7σ_θ and 27.2σ_θ for the period of 1968–1998 in winter. They speculated that diminishing in vertical exchange of water in the upper layers contributed to the decreases in O_2. In the western North Pacific, predominant decreases in dissolved O_2 were found in NPIW between 26.6σ_θ and 26.9σ_θ. *Kouketsu et al.* [2010] have documented AOU increase on isopycnal density horizons near the core of NPIW (~26.8σ_θ) at several repeat sections in the western North Pacific (25°N–40°N, west of 170°W from 1980s to 2000s). *Takatani et al.* [2012] identified O_2 decrease in NPIW between 1985 and 2010 based on the time-series hydrographic and biogeochemical measurements along the meridional section of 137°E which were routinely conducted by Japan Meteorological Agency (JMA). *Sasano et al.* [2015] also identified decrease trends in O_2 in NPIW between 1987 and 2011 using another time-series section of 165°E by JMA, and suggested the decreases in NPIW over the western North Pacific was attributed to the change in the Oyashio water because the signal of decreasing O_2 seems to be propagated from the Oyashio region to downstream along the subtropical gyre. Furthermore, in the eastern North Pacific, decreasing O_2 have been reported on isopycnal horizons centered on around 26.6σ_θ [*Emerson et al.*, 2004; *Mecking et al.*, 2008]. Because this density is corresponding to the maximum density that outcrop to the atmosphere in western North Pacific [*Reid*, 1965], they attributed the decrease in O_2 to a reduction of ventilation in this region. Therefore, understanding the change in the Oyashio region is

important to consider the change in the intermediate water of not only the western but also the eastern North Pacific. However, only by the reduction of ventilation, it may be insufficient to account for the decrease trends in O_2 in the western North Pacific. First, O_2 decreasing trends in the Oyashio region were determined up to the isopycnal horizons of $27.2\sigma_\theta$ [*Ono et al.*, 2001], but this density is much deeper than that of $26.7\sigma_\theta$ outcropped in the western North Pacific. Second, the relationship between the changes in potential temperature and AOU to the west of 170°W is different from that to the east of 170°W over the latitudinal band of 25°N–40°N [*Kouketsu et al.*, 2010], suggesting that O_2 change in the western North Pacific may not propagate directly to the eastern North Pacific. Furthermore, the changing rates on an isopycnal horizons are necessary to be considered with vertical distributions of temperature and salinity especially in upper layers because these changes in time induce a misleading of net change in water properties due to the deepening of the isopycnal horizons induced by warming/freshening [*Takatani et al.*, 2012; *Sasano et al.*, 2015]. Therefore, it is necessary to reconsider attentively the change in dissolve O_2 in the Oyashio region with renewed insight.

The Oyashio water has its origins in the two source waters; the Okhotsk Sea Intermediate Water (OSIW) and Western Subarctic Water (WSAW). In particular, OSIW plays an important role to control dissolved O_2 concentration in the North Pacific because OSIW is considered as the main ventilation source of NPIW [*Warner et al.*, 1999]. In the northwestern shelf polynya in the Sea of Okhotsk, sea ice is actively produced in winter. The sea ice forming leads to production of dense shelf water (DSW) due to brine rejection [*Martin et al.*, 1998; *Gladyshev et al.*, 2000]. Because DSW has cold and oxygen-rich properties with relatively high densities of $26.8\sigma_\theta$–$27.0\sigma_\theta$, DSW supplies high O_2 and low temperature water to deep layer where atmospheric infection such as winter convention

cannot reach normally. Additionally, diapycnal mixing is another key process to distribute DSW to deeper layer, which is driven by the tidal mixing around the Bussol' Strait. It is known that diurnal tides currents are strong around the Kuril Straits where the Sea of Okhotsk is separated from the North Pacific [*Nakamura et al.*, 2000]. This strong current induces water mass exchange between the Sea of Okhotsk and the western North Pacific, and induces diapycnal mixing especially around the Bussol' Strait [*Ono et al.*, 2007]. The strong diapycnal mixing provides particular field to affect water properties such as temperature, salinity, and dissolved O_2. *Yamamoto-Kawai et al.* [2004] have shown chlorofluorocarbons (CFCs) distributions in OSIW up to 27.4σ_θ and suggested mechanisms of ventilation combined in two ways; through DSW in the upper OSIW, and through diapycnal mixing around the Bussol' Strait in the lower OSIW. It means that dissolved O_2 is similarly ventilated in OSIW.

In the both source waters of the Oyashio water, the decrease trends in dissolved O_2 has also been reported [e.g. *Andreev and Watanabe*, 2002; *Nakanowatari et al.*, 2007]. *Nakanowatari et al.* [2007] documented that changing rates of temperature (for the period 1955–2004) and dissolved O_2 (for the period 1960–2004) in OSIW were higher than those in the Oyashio water and WSAW in the range in 26.6σ_θ–27.4σ_θ and suggested that these signals in the Oyashio region were propagated from OSIW. Based on shrinking trend of sea ice extension in the northwestern part of the Sea of Okhotsk, they suggested that the cause of these changes was reduction of DSW through weakening trend of sea ice production in the northwestern part of the Sea of Okhotsk. Recently, the reduction of DSW has been quantitatively reported by *Ohshima et al.* [2014]. It means that decrease trend in O_2 in OSIW is significantly attributed to the decrease of production in DSW. Therefore, it is important to understand the connection between OSIW and the Oyashio region.

The bidecadal variability is known as a notable feature in the western subarctic Pacific [e.g. *Andreev and Kusakabe*, 2001; *Watanabe et al.*, 2003; *Osafune and Yasuda*, 2006]. *Ono et al.* [2001] have suggested that AOU was decreasing superimposed distinctly on the bidecadal oscillations in the Oyashio region between 26.7σ_θ and 27.2σ_θ. They pointed out that the oscillations showed a negative correlation with the North Pacific Index (NPI) which indicates the strength of the Aleutian Low (AL). Practical mechanism between them can be explained by changing in mixing ratio between OSIW and WSAW due to variation in the ocean circulation associated with variation in the AL [*Takatani et al.*, 2007]. Another possibility is that the 18.6-yr period nodal tidal cycle could be related with bidecadal variability in the North Pacific [*Yasuda et al.* 2006]. As mentioned above, diurnal tides currents are strong around the Kuril Straits and induce diapycnal mixing. It is known that the amplitude of the tidal currents is varied by 20% due to the 18.6-year cycle [*Loder and Garrett*, 1978]. *Osafune and Yasuda* [2006] investigated that the relationships of the 18.6-year nodal tide to in the changes in physical and chemical parameters in the subarctic region of the Oyashio region, East Kamchatka Current, and the Sea of Okhotsk. Furthermore, in the Alaskan Gyre in the eastern subarctic Pacific, the bidecadal oscillations of O_2 were detected on 26.9σ_θ and 27.0σ_θ with comparable amplitude and with a lag of ~7 years to the Oyashio region [*Whitney et al.*, 2007]. However, because these studies were based on observations in the specific area in the subarctic region, the extent of the bidecadal oscillations in the North Pacific has been unclear. *Sasano et al.* [2015] pointed out the decadal-like variability in 25°N–30°N along the 165°E section and connection with the Oyashio region, but have not discussed in detail. Additionally, because in the previous studies about the oscillations the periodicity was assumed as a constant in 18.6-year or was calculated simply by fitting to nonlinear curve, the evaluations of the periodicity of O_2 variation remain insufficient.

Understanding the bidecadal oscillations and its propagation to the North Pacific are necessary to evaluate the trend based on the multidecadal observations in the subarctic Pacific Ocean.

As another feature of the Oyashio region, the Oxygen Minimum Layer (OML; O_2 < 70 μmol kg^{-1}) is domains between 27.10σ_θ–27.64σ_θ (about 500–1800 m) with the core at around 27.37σ_θ (about 900 m). In the North Pacific, two tongues of low O_2 penetrate sluggishly westward from the coastal zone of the North America as the tropical OML near 26.8σ_θ (around 250 m at the 165°E section) and the subtropical OML at approximately 27.4σ_θ (about 600–1300 m) (see Fig. 2-1a). Furthermore, the subtropical OML is gently separated into two tongues by relatively high O_2 water expanding to the east at around 36°N (Fig. 3-1). In fact, along the 165°E section, two cores of low O_2 are identified in the subtropical OML (not appeared the vertical section of the mean O_2 in Fig. 2-1a due to interval of isolines, but isolines of 35 μmol kg^{-1} distinctly is separated into the two cores centered at 30°N and the northern end of the section). The northern one of the OMLs, hereinafter the subarctic OML, penetrates from the eastern Kamchatka Peninsula along the east side of the Kuril Islands chain (Fig. 3-1). In the subtropical OML, which is the other one of the separated OMLs, long-term decrease of O_2 have been observed in the western North Pacific [*Takatani et al.*, 2012; *Sasano et al.*, 2015]. AS for the tropical OML, decline in O2 concentration and the vertical expansion of the layer have been reported by several studies [e.g. *Stramma et al.*, 2008; *Czeschel et al.*, 2011]. However, for the subarctic OML, little to date has been published regarding an O_2 change. *Sasano et al.* [2015] identified an increasing trend in O_2 in the subarctic OML in 47.5°N along the 165°E section. However, because this change would be affected by a northward shift of WSAG, it would not reflect long-term change in water properties. Because an O_2 decline in the OML would impact the biogeochemical cycle such as nitrogen through

an increase of denitrification [e.g. *Codispoti et al.*, 2001], further investigation will be needed to identify and understand scientifically the O_2 changes in the OML, particularly in poorly studied regions such as in the subarctic OML.

JMA has been conducting hydrographic/biogeochemical observations in the Oyashio region since 1940s. After 1954, the observations was routinely conducted in time. In this study, the O_2 changes in the Oyashio region were analyzed using quality controlled data over the past 61 years during the period 1954–2014, which is twice as long as the previous study by *Ono et al.* [2001]. Since long data set can reduce the influence of short-term noises due to perturbation, it is expected to detect smaller changes in trends and oscillations on isopycnals. Long-term data set also enables to detect trends on isobaths. While the analysis on isobaths includes large uncertainty due to fluctuation in depth over a range of time scales by ocean circulation processes, it could exclude apparent change induced by the deepening of isopycnal horizons due to ocean warming (see Appendix C). Additionally, spectrum analysis is applied to time-series data set of O_2 in the Oyashio region to evaluate a periodicity with more reliable method. This study focused on the density range from $26.6\sigma_\theta$ which was usually below the density in surface water in winter ($26.49 \pm 0.07\sigma_\theta$ on the average ± 1SD at 10 m, the maximum $26.62\sigma_\theta$ through the period) to $27.5\sigma_\theta$ which was the deepest density observed almost continuously through the analysis period used in this study. These analyses will advance understanding of the O_2 change in the Oyashio region. Furthermore, this study attempts to examine the oscillations in the northern part of the section of 165°E because there are no report about the extension of oscillations in the North Pacific. To investigate oscillations both in the Oyashio region and along the 165°E section, we can understand extension of the oscillations from the western to the eastern North Pacific, and would obtain a new information about O_2 trend and its propagation.

3.2. Data and Methods

3.2.1. Data Sources

The hydrographic/biogeochemical observations in the Oyashio region were routinely conducted by R/V *Ryofu Maru* since 1954, and the observations had been conducted mainly by R/V *Kofu Maru* from 1963 to 2010. After 2010, data in this region have been acquired by R/V *Ryofu Maru* and R/V *Keifu Maru*. In this study, the Oyashio region was defined as shown in Fig. 3-1, which is almost the same area as *Ono et al.* [2001], and defined the Oyashio water as water with temperature lower than 5°C at 100 m [*Kawai*, 1972]. Over the period 1954–2014, the observations have been usually conducted in every season (Fig. 3-2). As a result, data from a total of 1332 stations from 266 cruises between 1954 and 2014 were used in this study.

Methods of measurements have been summarized in *Takatani et al.* [2012]. Analysis of dissolved O_2 was made by the Winkler titration method until 1994 [*Winkler*, 1888]. After that, the analysis has been conducted with a modified Winkler's titration [*Carpenter et al.*, 1965, 1966]. Before 2003 its standard deviation (SD) was less than 1.6 μmol kg^{-1} and after 2004 that was 0.60 μmol kg^{-1} [*Takatani et al.*, 2012], reflecting differences in sampling procedures for the evaluation of SD and precision enhancements in O_2 measurements. Until 1989, temperature and pressure at the sampling depths had been measured by means of a reversing mercury thermometer attached on each of the Nansen bottles. Since 1990, temperature and salinity were measured with a Seabird SBE-911 plus CTD system manufactured by Sea-Bird Electronics, Inc. Data after 1965 is available from webpage in

JMA (http://www.data.jma.go.jp/gmd/kaiyou/db/vessel_obs/data-report/html/ship/ship_e.php). Data including before 1964 are also available from World Ocean Database 2013 (WOD13) [*Boyer et al.*, 2013].

In the analysis, annual mean on isopycnal horizons was used. In the Oyashio water, seasonal variations of dissolved O_2 were found above $26.7\sigma_\theta$. For potential temperature, the variations were found up to $26.8\sigma_\theta$ (Fig. 3-3). However, annual mean of water properties were basically used for analysis of long-term trends and oscillations in the Oyashio region in this study because the measurements were nearly evenly distributed in seasons (Fig. 3-2). For the 165°E section, this study used the same data set used in *Sasano et al.* [2015] but extended the period to 1987–2014; this data set consists of the annual mean in each 2.5° band which is calculated from anomalies of the mean value at intervals of 1° for the entire period.

3.2.2. Data Quality Control

As mentioned above, the Oyashio water was defined as water with temperature lower than 5°C at 100 m [*Kawai*, 1972]. Moreover, additional selection was applied to remove the effect of other water mass because this region is close to the Kuroshio-Oyashio Interfrontal Zone and because warmer water is sometimes distinctly observed in the Oyashio region due to the penetration of the Kuroshio water. Sometimes, water which have strongly influenced by WSAW was observed in the Oyashio region. To extract information of the Oyashio water, the layer data in which temperature was higher than the mean +1SD in the same layer of WSAW was rejected because temperature in Kuroshio is generally higher than that in WSAW. The WSAW region was selected in the subarctic region along the 165°E section and 158°E – 165°E along the P1 section (see Fig. 3-1), in which observations have been conducted by JMA period 1996–2014. The region WSAW in 165°E was identified in 49°N–50°N which is

located in upstream region for the Oyashio region because potential temperature in temperature minimum layer around 47.5°N is the coolest among the subarctic region (indicating the center of WSAG; see the vertical section of the mean potential temperature in 165°E in Fig. 2-2a with the coolest temperature minimum layer in subsurface among the subarctic region although the center seems to be located in 45°N based on geostrophic stream lines in Fig. 3-1).

Generally, observation data includes outliers due to analytical error. Therefore, quality control (QC) is a critical process in assuring the highest possible quality of data. However, outlying data may reflect large natural variability in ocean tracer fields. To reject outliers in dissolved O_2 only due to analytical error, statistical method proposed by *Sasano et al.* [2015] was applied as primary QC, which excludes outliers and additionally considers natural variability based on quasi-conservative parameters of NO and PO [*Broecke*r, 1974]. Moreover, this study also apply the same statistical method of excluding outliers for temperature and salinity data acquired by discrete water samples before 1989. When these data were rejected, data of dissolved O_2 acquired in the same layer was also rejected. On the basis of above QC method, 686 data out of 25544 data (2.69%) were rejected in O_2 data. The data that have passed through the primary QC were interpolated vertically at intervals of 5 m and $0.05\sigma_\theta$ for each station using the Akima spline method [*Akima,* 1991].

Along with primary QC, correction of systematic offsets between cruises is also important as secondary QC. *Sasano et al.* [2015] proposed the statistical method to evaluate the offsets along a single section based on the assumption that water properties in deep water are stable over time, following the procedure of CARINA [*Tanhua et al.*, 2010] and PACIFICA [*Suzuki et al.*, 2013]. However, it is difficult to apply this method for the Oyashio data because in some cruises the maximum depth of measurement was too shallow to evaluate

offset value, especially the cruises before 1988 (maximum depth is ~1200 dbar corresponding to isopycnal horizon of 27.5σ_θ). Furthermore, this method might judge natural variability as artificial offsets because in the northern part of the western North Pacific dissolved O_2 in the depth range 1500–2100 m includes natural variability [*Sasano et al.*, 2015]. Therefore, secondary QC is not applied to data in this study. *Takatani et al.* [2012] have evaluate the offset among cruises conducted by JMA as 3 μmol kg^{-1} between 1967 and 2010 based on the standard deviation of dissolved O_2 on 2000 m and 27.65σ_θ surface along the 137°E section. According to this, 3 μmol kg^{-1} is used in this study as a benchmark to judge whether the variability and change are significant or not. As the same as the Oyashio region, the secondary QC is not applied to data in 165°E. Although in the offset correlation the amplitude of oscillations was typically reduced (e.g. the amplitude on 26.8σ_θ was decreased at 1.2 μmol kg^{-1} on average between 30°N and 42.5°N), the result of calculation of O_2 oscillations was typically independent on whether secondary QC was applied or not.

3.2.3. Computation of Long-term Change

In the Oyashio region, linear rates of physical and oxygen parameters were calculated based on general linear least squares method at intervals of 5 m and 0.05σ_θ. Additionally, for dissolved O_2, trends with bidecadal oscillations were calculated at intervals of 0.05σ_θ by applying the following equation,

$$X = A \cdot (t - t_0) + B + C \cdot \sin\{2\pi(t - t_0 - D)/E\} \quad (1)$$

where X represents O_2 concentration, t year, and t_0 a reference year in 2000. Coefficients of A–E indicate trend, offset, amplitude, phase lag, and periodicity, respectively. After binomial 5-year low-pass filtered, time series data were fitted to equation (1) by nonlinear least squares (NLS) method. To get the best fitting curve (that is, the smallest residuals), the calculations

were made in a few hundred times as the following two processes; (1) two methods of NLS (the quasi-Newton method and the Levenberg-Marquardt method) were applied, and (2) each computation was repeated in over a hundred combinations with change in the initial coefficients because the solution of NLS depends on initial coefficients. The significances of trends and oscillations (95% confidence level) were judged in the standard errors of coefficients in trend and amplitude, respectively. To certify the oscillations determined by NLS, power spectral analysis (Maximum Entropy Method: MEM) was also applied to O_2 data in the Oyashio region. For the analysis of time series data along the 165°E section, trends and oscillations were calculated as the same method of above NLS. In the calculation, data with time gap over 3 years were not used, meaning that data with time gap within 2 years were used for NLS after 5-year low-pass filtered.

These calculation was based on data of annual mean, and for the 165°E section the data period was short as 19–24 years. This indicates that these results might include a large uncertainty in the calculation in the oscillation and its lag to discuss strict relationships between the oscillations. However, these results have sufficient consistency in vertical and horizontal extension of bidecadal oscillations not only in the Oyashio region but also along the 165°E section. Therefore, the calculation of oscillations is sufficiently reliable to evaluate the oscillations.

3.3. Results

3.3.1. Linear Trends of Physical and Oxygen Parameters in the Oyashio Region

In the western subarctic region, a winter mixed layer could be colder than underlying

water due to the presence of a strong halocline. In early spring, as surface water begin to warm, temperature minimum layer (i.e., the dichothermal layer [*Uda*, 1963]) is formed in subsurface layer, meaning that the dichothermal layer is the remnant of the mixed layer from the preceding winter. Temperature maximum layer (i.e., the mesothermal layer [*Uda*, 1963]) is also observed under of the dichothermal layer through a year because a temperature minimum exists in a subsurface layer. Therefore, the dichothermal layer and the mesothermal layer are generally seen in the North Pacific subarctic region [*Ueno and Yasuda*, 2000]. In the Oyashio region, the dichothermal layer and temperature maximum layer are usually observed at around $26.7\sigma_\theta$ and $27.1\sigma_\theta$, respectively (Figs. 3-3, 3-4). However, temperature on $26.7\sigma_\theta$ in winter is warmer than those in the other seasons (compare with representative seasonal profiles in subarctic Pacific of Fig. 3 in *Ueno and Yasuda* [2000]), though temperature in winter almost is uniformed vertically due to winter convection. It means that the dichothermal layer observed in the seasons except for winter is maintained by lateral penetration from upstream regions. *Stabeno et al.* [1994] have reported that daily mean velocities of Oyashio along the Kuril Islands is approximately 15 cm s^{-1} with surface drifters. It indicates that the Oyashio water formed around the Kuril Islands arrives at the Oyashio region within a few months. Therefore, observed changes in the dichothermal layer except for winter represent winter condition of somewhere in the upstream regions because the dichothermal layer is considered as a proxy of the proceeding winter mixed layer.

Annual mean rates of temperature and salinity changes on isopycnal horizons were significantly observed between $26.80\sigma_\theta$ and $27.45\sigma_\theta$ (Figs. 3-5a and 3-5b). Since a density is functionally determined by temperature and salinity, changes in them are perfectly correlated with each other to remain on a constant density. The changing rates of temperature and salinity on $26.7\sigma_\theta$ were almost zero, and those on upper densities were decreased. On the

other hand, the rates of temperature calculated on isobaths were increased above 27.4σ_θ (significantly in 27.00σ_θ–27.35σ_θ). The rates of salinity on isobaths were not significant but decreasing trends were found in a slightly deeper depth corresponding to isopycnal horizon of 26.8σ_θ than those on isopycnals. The disagreement in the rates between on isopycnals and isobaths were found especially in temperature above 26.7σ_θ. Furthermore, the disagreement were determined up to 27.1σ_θ. This would be attributed to the deepening effect of isopycnal horizons due to warming/freshening [*Takatani et al.*, 2012; *Sasano et al.*, 2015]. In fact, depth of isopycnal horizons tended to deepen above 27.2σ_θ, and significantly deepened between 26.60σ_θ and 26.75σ_θ (Fig. 3-5c). On 26.7σ_θ, the depth of isopycnal horizon was significantly deepened at the rate of 0.41 ± 0.14 (1SD) m yr^{-1}. Because the density of 26.7σ_θ is roughly corresponded to the core of dichothermal layer (that is, inflection point of vertical gradient in temperature), changing direction of temperature and salinity due to the effect toward either increase or decrease would be alternated at this density. A detailed discussion of the effect is described in section 3.4.1. In winter, the changing rates of temperature and salinity on isopycnal horizons were different from the other seasons above 26.8σ_θ. In particular, the rates showed positive values above 26.7σ_θ on which the rates showed negative values. However, the rates of temperature on isobaths denote positive values as the same as those in annual mean, but were slightly higher. The disagreements between isopycnals and horizons were attributed to the presence of temperature minimum layer which affects the direction of the deepening effect of isopycnal horizons.

Linear decrease trends in dissolved O_2 were significantly determined through densities from 26.6σ_θ to 27.5σ_θ (Fig. 3-5d). The highest change in O_2 was found on 26.7σ_θ at the rate of -0.72 ± 0.11 μmol kg^{-1} yr^{-1}. Although O_2 concentration represented seasonal variations on the density (Fig. 3-3), decreasing trends were determined in each season as almost equal

changing rates (Fig. 3-6). The decrease rates were gradually diminished with depth. On isobaths, annual mean rates of O_2 change also significantly decreased through the same densities. However, the rates were slightly lower than those on isopycnal horizons between $26.6\sigma_\theta$ and $27.1\sigma_\theta$ which were corresponding to the densities where disagreements of temperature and salinity between isopycnals and isobaths were found. The highest decreasing rate was found on isopycnal horizon of $26.7\sigma_\theta$, but diminished on isobaths and the rates were almost uniformed between $26.7\sigma_\theta$ and $26.9\sigma_\theta$. It means that these disagreement of changing rates between isopycnals and isobaths would be attributed to the deepening effect of isopycnal horizons. For AOU, increase trends were also determined and were approximately mirror image of those of O_2, indicating that the contribution of change in O_2^{sat} to change in O_2 was minor (Figs. 3-5d and 3-5e). Indeed, although the decreasing trends of O_2^{sat} were determined on isobaths, the contributions to decline in O_2 were quite small (Fig. 3-5f). Through comparison of these changes on isobaths, the contributions were evaluated at 5% around $26.8\sigma_\theta$ and at 10% around $27.1\sigma_\theta$. It means that O_2 decline in the Oyashio region is predominantly controlled by change in AOU. This was well agreed with the controlling factor of O_2 change in NPIW along the sections of 137°E [*Takatani et al*., 2012] and 165°E [*Sasano et al.*, 2015] which were downstream of the Oyashio region.

3.3.2. Trends and Oscillations of Oxygen in the Oyashio Region

In the Oyashio region, dissolve O_2 have been decreasing superimposed distinctly on the bidecadal oscillations on isopycnals from $26.6\sigma_\theta$ (about 125 m) near surface layers to $27.4\sigma_\theta$ (about 950 m) in the subarctic OML for the period 1954–2014 as results from NLS (Fig. 3-7). Although O_2 concentration represented seasonal variations up to $26.7\sigma_\theta$ (about 170

m), the bidecadal oscillations on 26.7σ_θ were synchronously determined in each season (Fig. 3-6). Through the densities from 26.6σ_θ to 27.4σ_θ, the cycles of oscillations of O_2 were almost constant (16.4–19.6 year) (Fig. 3-8). As another method of evaluation for the cycles, the MEM analysis of power spectral revealed predominant periods at about 20 years between 26.6σ_θ and 27.4σ_θ (Fig. 3-9). This result supported the result of NLS of bidecadal oscillations in O_2 variations. On deeper isopycnal horizon in 27.5σ_θ (about 1260 m) in the subarctic OML, changes in trend (-0.09 ± 0.02 μmol kg^{-1} yr^{-1}) for 61 years sufficiently exceeded the benchmark as 3 μmol kg^{-1} and amplitude of oscillations (1.58 ± 0.38 μmol kg^{-1} in amplitude, meaning the cyclic change was twice as large as amplitude) was slightly higher than the benchmark. The MEM analysis could not detect predominant period on this isopycnal horizon because the decadal oscillations was probably small to be detected by spectrum analysis. However, the bidecadal oscillations on 27.5σ_θ were well synchronized with upper horizons at the cyclic period at 18.3 year (Fig. 3-4d). Through isopycnal horizons, the phases were well synchronized with a lag of 0–1 year, which were evaluated by time-lagged correlation analysis from data on 26.6σ_θ (Fig. 3-10a). This means that bidecadal oscillations are synchronously extended at least from 26.6σ_θ to 27.5σ_θ in the Oyashio region.

Through densities on from 26.6σ_θ to 27.5σ_θ, annual mean rates of O_2 change based on NLS were significantly determined as the same as based on linear fitting. On 26.7σ_θ, the mean rate of O_2 decrease was the highest at -0.72 ± 0.11 μmol kg^{-1} yr^{-1} among all isopycnal horizons considered (Fig. 3-8). The changing rate of AOU on 26.7σ_θ in this study at 0.74 ± 0.06 μmol kg^{-1} was much smaller than that reported by *Ono et al.* [2001] at 1.28 ± 0.47 μmol kg^{-1}. Through densities from 26.7σ_θ and 27.2σ_θ, the trends were much smaller in 52–68% than the previous study. It would reflect data extension in time in the present study. The largest amplitude of oscillations of dissolved O_2 was found on 26.7σ_θ at 14.4 ± 1.5 μmol kg^{-1} and the

amplitudes were gradually diminished with depth (Fig. 3-8). It is likely that the cyclic oscillation is considered to be ascribed in change in mixing ratio between the source waters of WSAW and OSIW [*Takatani et al.*, 2007]. However, the magnitude of amplitude also reflects the differences in O_2 concentration between the source waters. Therefore, it is difficult to mention the impact of the source waters to the amplitude of O_2 in the Oyashio region. At least, the presence of oscillations can indicate that the water consists in the two source waters and mixing ratio between them is periodically varied in time. However, the detection of oscillation in deep isopycnal horizon up to 27.5σ_θ in the subarctic OML is one of the new findings in this study.

3.3.3. Bidecadal Oscillations of Oxygen along the 165°E Section

Along the section of 165°E, bidecadal oscillations in dissolved O_2 on 26.8σ_θ were determined between 30°N and 42.5°N (Fig 3-11). This density is corresponding to the core of NPIW although in north of 40°N it cannot be observed as a salinity minimum in an intermediate layer (Fig. 2-2b). Although these periodicities showed large variability in 12.4–24.3 year, it is probably attributed to the calculation error from short period of data (in 19–24 years) and small amplitudes in oscillations. Nevertheless, the oscillations were appeared to be changed synchronously high in early 1990s and late 2000s, and were low in early 2000s and early 2010s. Additionally, using time-lagged correlation analysis, the phases in these region was be correlated with those in the Oyashio region with a lag of 1–3 years (Fig. 3-10b). The amplitudes of oscillations were much smaller (3.6–6.9 μmol kg^{-1}) than those in the Oyashio region (17.7 μmol kg^{-1} on 26.8σ_θ). In 50°N of the northernmost region in this study, bidecadal oscillations were also determined with preceding 2–4 years to those in the Oyashio region while unfiltered data exhibited very large interannual variation (Figs. 3-10b and 11).

In the region in 47.5°N, shorter oscillations were determined. Because the region is located in the center of WSAG (see section 3.2.2), the oscillations could exhibit the different pattern.

The bidecadal oscillations of dissolved O_2 found in 40°N at the subarctic region were relatively distinct because of large amplitude at 6.1 μmol kg^{-1} (Fig. 3-11b). It would reflect the difference in the location which is close to downstream of the Oyashio region (Fig. 3-1). The bidecadal oscillations of O_2 were detected vertically from 26.8σ_θ to 27.5σ_θ (Fig. 3-12a). The periodicities on these densities were 16.5–18.7 years. The amplitudes were diminished with depth but the amplitude on 27.5σ_θ was sufficiently determined at 1.7 ± 0.2 μmol kg^{-1}. While data acquired in 1987 were not included in the calculation due to data gap, these data looked like on extrapolated oscillation lines in time. Through these densities, the oscillations were changed synchronously in high and low phases. The oscillations determined in 40°N were well correlated with those in the Oyashio region with a lag of 2–5 years compared on the same density, and the lag for the oscillations in the Oyashio region appeared to be late with depth. (Fig. 3-10c). On the other hand, the bidecadal oscillations found in 30°N on 26.8σ_θ in NPIW were correlated to those of Oyashio region with a lag about 3 years while the decadal-like oscillations found in the subtropical OML were not well correlated (Fig. 3-10d). These results indicate that the oscillations have been extended horizontally to the density of 26.8σ_θ in 30°N–42.5°N corresponding to NPIW and vertically to the subarctic region including OML in the western North Pacific.

3.4. Discussion

3.4.1. Change in Physical Parameters in the Oyashio Region

Temporal changes of physical and biogeochemical parameters are classically quantified on isopycnals rather than on isobaths. This is because the mixing and transport usually occur along the path of circulation of isopycnal horizons, and analysis on isopycnals could cancel out vertical fluctuation in depth due to ocean circulation processes. However, as *Sasano et al.* [2015] have pointed out, this conventional approach begins to waver as changes in temperature and salinity on constant density horizons would drive isopycnal displacements in the upper layers of the oceans due to the deepening effects of isopycnal horizon. First, therefore, net changes of temperature and salinity on isobaths are discussed, and then the deepening effect on isopycnals are considered to consider O_2 trends on isopycnal horizons.

In the Oyashio region, potential temperature on isobaths was increasing above depth corresponding to $27.4\sigma_\theta$ (about 950 m) (Fig. 3-5a). Although ocean heat content have rather decreased at around 40°N in the North Pacific, it represents shift of the large-scale front [*Levitus et al.*, 2005, 2012]. By contrast, the changing rates in temperature in the present study, which extracted data with the Oyashio water, might exclude the shift of the front, and therefore reflect pure warming process in the Oyashio water. Above the dichothermal layer corresponding to the density at $26.7\sigma_\theta$, the warming would be mainly caused through global warming progress because the layer is the remnant of winter convection, meaning that the layer is a typical limit to propagate the signal from atmosphere. Below the layer, the increasing trends in temperature were also determined especially in $27.00\sigma_\theta$–$27.35\sigma_\theta$ with confidence level greater than 95%. The signal in the Oyashio region would be propagated from OSIW which is attributed to less overturning due to reduction of DSW [*Nakanowatari et al.*, 2007]. For salinity, the decreasing trends were determined above depth corresponding to $26.8\sigma_\theta$ (about 230 m) (Fig. 3-5b). It would reflect the freshening in the subarctic North

Pacific because of amplification of the global hydrological cycle [*Hosoda et al.*, 2009; *Durack and Wijffels*, 2010]. The combination of these controlling factors would be contributed to the long-term trend in temperature and salinity. On the other hand, these long-term changes could be explained by change in the mixing ratio between the two source waters of WSAW and OSIW. Because WSAW is warmer and salter than OSIW, increase in the contribution of WSAW to the Oyashio water results simultaneously in warming and salting in the Oyashio region. Indeed, both warming and salting trends were determined below depth corresponding to $26.8\sigma_\theta$. Furthermore, the change in mixing ratio between the source waters compatibly accounts for long-term trends in the AL and other water properties in the Oyashio region such as in dissolved O_2 and isopycnal thickness (details are discussed in section 3.4.2). It suggests that the long-term changes in temperature and salinity observed in the Oyashio region may be attributed to an increase in the contribution of WSAG due to the strengthening of the AL.

Next, based on the net changes on isobaths, the deepening effect of isopycnal horizons is examined. With the effect, lightening (weighting) changes in density by warming/freshening (cooling/salting) displace the isopycnal surface to deeper (shallower) layer, and changes in temperature/salinity on this isopycnal horizon depend on whether the other parameter related to calculation of density as salinity/temperature vertically increases or decreases in the deeper (shallower) layer. The explanations were detailed in Appendix C. Although their explanation was mainly described with the subtropical region, it can apply to the subarctic region. The underlying processes are described in Appendix D. Because time-series data set of six decades used in this study was sufficiently long to reduce fluctuations in depth over a range of time scales by ocean circulation processes, the rates on isobaths would be expected to reflect qualitatively a real change in spite of large uncertainty. To evaluate the

contributions of warming and freshening to the effect, reconstructed data based on linear trends of potential temperature (θ) and salinity (S) with depth were evaluated, indicating the temporal evolution within a θ-S diagram and these profiles (Fig. 3-13).

Above the dichothermal layer on around $26.7\sigma_\theta$ in annual mean, temperature was cooling on isopycnals but warming on isobaths (Fig. 3-5a). By contrast, salinity was freshening both on isopycnals and isobaths (Fig. 3-5b). In reconstructed data above $26.7\sigma_\theta$, θ-S line shifts to low temperature and low salinity on isopycnal horizons as a consequence of both warming (change from θ_0 to θ_1) and freshening (change from S_0 to S_1) (Fig. 3-13). As a consequence of warming alone (taking the combination of θ_1 and S_0), changes in temperature and salinity on isopycnal horizons were not induced. Although warming on isobaths is expected to induce warming/salting on isopycnals qualitatively, gradient of isopycnals is almost even for change in temperature to suppress the induction (Fig. 3-13). On the other hand, when only the contribution from freshening (taking the combination of θ_0 and S_1) is considered, changes in temperature and salinity on isopycnal horizons have induced cooling/freshening on isopycnals. It means that changes in temperature and salinity found on isopycnals above the dichothermal layer are predominantly controlled by change in salinity. This would be largely affected by the vertical structure in the subarctic region where halocline is strongly developed in surface layers. Depth of isopycnal horizons of $26.7\sigma_\theta$ deepened from 1954 to 2014 at the rate of 0.42 ± 0.14 m yr^{-1}, and the rate was contributed by 70% in freshening and by 30% in warming (Fig. 3-13). In winter, increasing trends of temperature above the dichothermal layer were observed both on isopycnals and on isobaths. The observed changes on isopycnal horizons were caused by the deepening effect while the change pattern in winter was contrasted with that in annual. This was attributed to the differences in vertical profile of temperature; in winter freshening was not contributed to

change on isopycnals because temperature was vertically uniformed. Rather, warming trends on isobaths were exhibited as salting on isopycnal horizons whose contribution to the deepening effect was not found in annual mean due to inferior to that of freshening (Fig. 3-5b). This change was confirmed in a θ-S diagram with reconstructed data (not shown).

Below $26.7\sigma_\theta$ through $27.4\sigma_\theta$, temperature and salinity increased on isopycnal horizons. On the other hand, on isobaths temperature also decreased through these densities but salinity was not changed above $27.05\sigma_\theta$ while increase below $27.1\sigma_\theta$. In reconstructed data below $26.7\sigma_\theta$, a θ-S line distinctly shifts to high temperature as a consequence of warming alone (taking the combination of θ_1 and S_0) (Fig. 3-13). It means that changes in temperature and salinity found on isopycnals in the Oyashio region are controlled by change in temperature on isobaths between $26.7\sigma_\theta$ and $27.4\sigma_\theta$. By contrast, the deepening effect of isopycnal horizons to changes on isopycnal horizons would contribute to changes in temperature and salinity up to $27.1\sigma_\theta$ corresponding to the mesothermal layer because the changes on isopycnals below above $27.1\sigma_\theta$ mostly consisted with those on isopycnals. It might reflect that vertical gradients of temperature and salinity were relatively gentle (Fig. 3-3a). Although the changing rate in depth of isopycnal horizon is within the uncertainty range of the estimate, the contribution of the effect is supported by the same patterns in O_2 of disagreement in changing rates between isopycnals and isobaths which is independent for change in a vertical structure.

As mentioned above, the deepening effect of isopycnal horizons can explain the differences of change in water properties between on isopycnals and on isobaths. However, in the case that observed changes in temperature and salinity involves in displacement with another water parcel, the deepening effect of isopycnal horizons should not be applied (see Appendix D). The Oyashio water is originally formed as mixture between WSAW and OSIW.

If the mixing ratio between them is not changed but these properties are changed, the deepening effect is distinguishable. By contrast, if these properties are not changed but the mixing ratio is changed, the concept of the effect should not be applied. Unfortunately, however, it is impossible to distinguish between these two cases. It means that it is difficult to evaluate quantitatively the contribution of the effect observed as changes on isopycnal horizons in the Oyashio region. Nevertheless, because simultaneous increase or decrease on isopycnal horizons are not determined in temperature and salinity above $27.1\sigma_\theta$ and disagreements of the changes between isopycnals and isobaths are not determined below $27.1\sigma_\theta$, it is speculated that the imponderable contribution of the deepening effect of isopycnal horizons due to the displacement with another water parcel is minor.

3.4.2. Oxygen Decline in the Oyashio Region

For dissolved O_2, significant trends were determined through densities from $26.6\sigma_\theta$ to $27.5\sigma_\theta$ both on horizons and on isobaths, and these changes were mainly attributed to changes in AOU (Figs. 3-5d to 3-5f). The contribution of change in O_2^{sat} was evaluated only up to 10%. One should consider the possibility that increase in AOU contributes to bacterial activity. However, in order to explain the net increase of AOU by bacterial activity, the O_2 utilization would need to be an order of magnitude larger in the change of in situ O_2 utilization rate by an export flux of organic matter or in the remineralization of organic matter [*Watanabe et al.*, 2001]. Meanwhile, although increasing contribution of subtropical water with low O_2 concentration to the Oyashio region can also account for decline in O_2, it cannot be successfully explained in long-term increase in PO_4 in the Oyashio region [*Ono et al.*, 2001]. Here, other controlling factors of change in AOU are discussed.

The trend of dissolved O_2 determined on isopycnal horizons from $26.6\sigma_\theta$ to $27.1\sigma_\theta$

distinctly disagreed with those on isobaths corresponding to the same isopycnals. These ranges were in accord with those in temperature and salinity. It suggests that the deepening effect of isopycnal horizons have affected on changes in O_2 on these isopycnal horizons. The contribution of the effect to change in oxygen is much simpler than those in temperature and salinity because O_2 change invokes no changes in a vertical structure. Furthermore, because layers where the deepening effect is induced due to change in temperature/salinity are typically shallower than oxygen minimum layer on $27.4\sigma_\theta$ (indicating decrease O_2 with depth; see Fig. 3-3a), deepening isopycnal horizon contributes only to direction of decreasing O_2 on an isopycnal horizon. Although the highest changing rate in O_2 was found on $26.7\sigma_\theta$, the largest difference in changing rates between isopycnals (-0.72 ± 0.11 μmol kg^{-1} yr^{-1}) and isobaths (-0.48 ± 0.12 μmol kg^{-1} yr^{-1} on comparable depth at 165 m) was also found on this density. It implied that approximately 33% of O_2 decrease was apparent change due to the deepening effect of isopycnal horizon. This was attributed to relatively high changing rate of depth of isopycnal horizons (-0.41 ± 0.14 m yr^{-1}) and to the vertically steepest gradient (-0.97 ± 0.47 μmol kg^{-1} m^{-1}) in O_2 on $26.7\sigma_\theta$ (Fig. 3-8). On lower density at $27.1\sigma_\theta$, the contribution of the effect to O_2 decrease was evaluated at approximately 14% mainly due to warming assuming that the difference between on isopycnals and isobaths was fully attributed to the effect.

Considering the apparent contribution of the deepening effect of isopycnal horizon to O_2 decline, the highest rates of net decreasing O_2 have been determined from $26.7\sigma_\theta$ to $26.9\sigma_\theta$ at about -0.5 μmol kg^{-1} yr^{-1}. Because the density of $26.7\sigma_\theta$ is roughly corresponded to the core of dichothermal layer formed in winter convection, ventilation in winter mixed layer would largely contribute to long-term change in O_2. This may be supported by the fact that vertical gradient of O_2 concentration is the steepest in this density, suggesting that O_2 concentration

on this density is sensitive to variations of winter mixing. In the previous studies, the weakening of vertical water exchange in winter and the reduction of ventilation are considered as predominant factors to control O_2 long-term trend [e.g. *Ono et al.*, 2001; *Mecking et al.*, 2008]. To confirm the contribution of winter convection to O_2 decrease, conditions of winter surface water at 10 m are evaluated (Fig. 3-14). Surface density in winter have significantly been lightening during the period 1954–2014 at -0.0020 ± 0.0005 kg m^{-3} yr^{-1}. This was largely attributed to increase in temperature (+0.0212 ± 0.0083 °C yr^{-1}) while changing rate of salinity was not significant (-0.0001 ± 0.0010 yr^{-1}). The trend of decreasing density in the Oyashio region in winter at 10 m was also shown by *Ono et al.* [2001] although it was accompanied by decrease in salinity. The lightening density implied the weakening ventilation in winter although winter mixed layer depth, defined as the depth at which potential density increases by $0.125\sigma_\theta$ from its 10 m depth value, showed insignificant change being shallow at -0.37 ± 0.34 m yr^{-1} (not shown). However, because the dichothermal layer observed in the Oyashio region except for winter is maintained by lateral penetration from upstream region (Fig. 3-3), the decrease in winter surface density could not give direct evidence of the weakening ventilation locally in the Oyashio region. Nevertheless, O_2 concentration on $26.7\sigma_\theta$ exhibited decreasing trends in spite of seasonal variations (Fig. 3-6). Considering the dichothermal layer is formed in winter convection in a subarctic region, decreasing trends on $26.7\sigma_\theta$ observed locally in the Oyashio region in all seasons implied that the signals of the weakening ventilation were penetrated from upstream region and the decrease in winter surface density in the Oyashio might represent a proxy of the weakening ventilation in the subarctic region. It might be supported by the distribution of the dichothermal layer in the subarctic Pacific which the densest water of temperature minimum is found along the Kuril Straits and the Oyashio region [*Ueno and Yasuda*, 2000; *Ueno and*

Yasuda, 2005].

Another critical issue to consider O_2 decline is change in disequilibrium of oxygen in air-sea interaction because intensified stratification due to ocean warming may induce the change in a span of exposure of water in mixed layer to atmosphere. In particular, winter surface water in a subarctic region are typically undersaturated, reflecting high O_2^{sat} due to low temperature and deep convection which moves up low O_2 water from deeper layer to take more time to equilibrate. Although the importance of the disequilibrium is recognized, it is difficult to evaluate the contribution to long-term trends in O_2 due to lack in data of winter surface. In this study, in the Oyashio region the long-term trend of AOU in winter surface water showed no significant change at -0.01 ± 0.01 μmol kg^{-1} yr^{-1} during the period 1954–2014 while decreasing O_2 were largely attributed to decrease in O_2^{sat} due to warming. It indicated that disequilibrium of oxygen in air-sea interaction have been no temporal change at least during the six decades in the Oyashio region, suggesting that the disequilibrium would be not contributed to O_2 decline in spite of progress in ocean warming.

Through a typical winter convection, the signals of winter mixed layer would not reach only to $26.7\sigma_\theta$ at most. *Ono et al.* [2007] have indicated that winter convection around the Bussol' Strait reached indirectly to the depth of $26.8\sigma_\theta$ isopycnal horizon due to diapycnal mixing induced by tidal mixing. It means that reduction of ventilation in sea surface accounts for O_2 decrease up to $26.8\sigma_\theta$. However, these processes related to winter convection could not account for the decreasing trend in O_2 observed in the Oyashio region up to $27.5\sigma_\theta$. For the ventilation source of O_2 of deep layer of the western North Pacific, OSIW is considered through water exchange in the Kuril Straits. Furthermore, DSW is considered as ventilation source of OSIW because DSW has cold and oxygen-rich properties with densities of $26.8\sigma_\theta$–$27.0\sigma_\theta$ [*Martin et al.*, 1998; *Gladyshev et al.*, 2000]. DSW is produced through sea ice

production in the northwestern shelf of the Sea of Okhotsk. Recently, *Ohshima et al.* [2014] have quantitatively reported the reduction of DSW by approximately 30% through sea ice decline and freshening in the Sea of Okhotsk during the past four decades. This would affect the decreasing trend in O_2 in OSIW [*Nakanowatari et al.*, 2007]. However, the decreasing trends in O_2 in OSIW are determined up to 27.4σ_θ while the process of reduction of DSW production would reach only to the density of 27.0σ_θ. Recently, diapycnal mixing induced by tidal mixing around the Kuril Straits is noticed to contribute to biogeochemical cycle in the ocean. *Ono et al.* [2007] have indicated that diapycnal mixing at the Bussol' Strait is important process to control vertical distribution of water properties because water properties of the lower part in intermediate water in 27.3σ_θ–27.6σ_θ at the Bussol' Strait can be explained only by the diapycnal mixing. Their suggestion was confirmed by direct observation of turbulent diffusivity up to 27.5σ_θ in the Bussol' Strait [*Yagi and Yasuda*, 2012]. *Nishioka et al.* [2013] showed the importance of diapycnal mixing around the Bussol' Strait, which extends high dissolved iron originated in DSW to intermediate water with the range of 26.6σ_θ–27.5σ_θ in the western North Pacific. These studies suggest that diapycnal mixing in the Bussol' Strait is important process to control not only vertical distribution of O_2 concentration but also vertical propagation of the signal of O_2 decline originated in the reduction of DSW up to 27.5σ_θ. This might be also supported by the fact that bidecadal oscillations were synchronously detected up to 27.5σ_θ in the Oyashio region because the oscillations possibly implied footprint of tidal mixing. As a result, to account for decreasing trends in O_2 in the Oyashio region in lower densities up to 27.5σ_θ, the combination of the reduction of DSW and its propagation by diapycnal mixing from the Sea of Okhotsk is likely to contribute.

The Oyashio water is originating from OSIW and WSAW. In comparison, OSIW has water properties of higher O_2, lower temperature, and lower salinity than those of WSAW.

Furthermore, OSIW has lower potential vorticity (PV) than WSAW, especially between 26.6σ_θ and 27.0σ_θ [*Yasuda*, 1997; *Yasuda et al.*, 2002]. *Takatani et al.* [2012] supposed that the long-term decreases in O_2 in the Oyashio region were attributed to an increase in the contribution of low-O_2 WSAW due to strengthening of the AL. Indeed, the intensity of the AL, which is defined as the sea level pressure minimum with in a region of 30°N–60°N and 150°E–150°W in winter mean field [*Sugimoto and Hanawa*, 2009] and is substituted for NPI in this study, have strengthened during 1950–2015 in agreement with *Sugimoto and Hanawa* [2009] (Fig. 3-15). It suggests the increasing contribution of WSAW to the Oyashio water due to strengthening of the AL. To examine this, the changing rate of isopycnal thickness (proportional to the reciprocal of PV) was analyzed as a proxy of PV between 26.9σ_θ and 27.0σ_θ where the difference of PV is large but the density is sufficiently below winter mixed layer depth. The reasons of using not PV but isopycnal thickness are that before 1989 discrete measurement of temperature and salinity could include a large estimation error to calculate PV. The thickness has been significantly decreasing at -0.13 ± 0.02 m yr^{-1} (Fig. 3-15). This trend well agrees with the previous studies [*Osafune et al.*, 2006; *Takatani et al.*, 2007]. Additionally, increase in the contribution of WSAW to the Oyashio region concurrently accounts for long-term increase in temperature in the Oyashio region (Fig. 3-15d) because temperature in WSAW is warmer than in OSIW. These facts support the possibility that the long-term decreases in O_2 in the Oyashio region could be attributed to the increasing in the contribution of WSAW due to strengthening AL through ocean circulation during the past six decades. However, the question still remains whether the AL have been strengthening in the past decades. Based on measurements of sea level from the satellite in 1993–2009, intensifying trends were seen in the north of WSAG but weakening in the south of WSAG [*Qiu et al.*, 2012]. Additionally, in model experiments in 1980–2008, the similar patterns

were seen in trend of water transport [*Nakanowatari et al.*, 2015]. They also showed the weakening AL in the period based on climatological data. These results seem to be disagreement with this study. However, it might be attributed to difference of data period because the AL intensity changes with bidecadal oscillation. Further evaluations of the changes due to ocean circulation are needed for the precise contribution on the change in the water properties in the Oyashio region.

3.4.3. Bidecadal Oscillations in Oxygen in the western North Pacific

In the Oyashio region, bidecadal oscillations in dissolved O_2 have been determined synchronously from 26.6σ_θ to 27.5σ_θ during the period 1954–2014 (Fig. 3-7). It has been reported that the bidecadal oscillations in the Oyashio region are negatively correlated with NPI [*Ono et al.*, 2001; *Watanabe et al.*, 2003]. The present study also showed that the bidecadal oscillations in O_2 were well synchronized with the intensity of the AL (Fig. 3-15). The bidecadal oscillations of the intensity of the AL about 20 years have been significantly documented by *Sugimoto and Hanawa* [2009]. Additionally, these oscillations were also synchronized with those of both isopycnal thickness and temperature. These changes are consistently attributed to strengthening in WSAG, which increases mixing ratio of WSAW (high temperature, high salinity, low O_2, and high PV) for OSIW (low temperature, low salinity, high O_2, and low PV). Therefore, the oscillations in the AL intensity through ocean circulation would account for the bidecadal oscillations of the water properties in the Oyashio region.

On the other hand, these oscillations in the Oyashio region also can be attributed to the 18.6-yr period nodal tidal cycle [*Osafune and Yasuda et al.*, 2006; *Yasuda et al.* 2006]. Recently, there is a growing recognition that the 18.6-yr period nodal tidal cycle contributes

to decadal variations in the North Pacific, such as in the western subarctic North Pacific and the Sea of Okhotsk [*Osafune and Yasuda*, 2006] and in the Bering Sea [*Osafune and Yasuda*, 2010]. When tidal current is amplified in the tidal cycle, water exchange between the Sea of Okhotsk and the western North Pacific is activated in the Kuril Straits. Additionally, amplified tidal current induces tidal mixing between densities. In the Bussol' Strait, the diapycnal mixing due to tidal mixing has been observed up to $27.5\sigma_\theta$ [*Ono et al.*, 2007; *Yagi and Yasuda*, 2012]. Therefore, the bidecadal oscillations in dissolved O_2 in the Oyashio region can be attributed to the 18.6-yr period nodal tidal cycle. The period cycles determined from $26.6\sigma_\theta$ to $27.5\sigma_\theta$ at 16.4–19.6 year are well consistent with the nodal cycle. It might be supported by the fact that there are almost no lags in the oscillations through densities because the oscillations are induced in vertically diapycnal mixing in the Kuril Straits. However, in this study, I could not conclude whether the bidecadal oscillations are controlled by atmospheric forcing through change in ocean circulation or the 18.6-yr period nodal tidal cycle because these controlling factors contribute to change in water properties in the same variation. Furthermore, relationship between the nodal cycle and the AL intensity has been discussed. Using a global barotropic tidal model, *Tanaka et al.* [2012] have suggested that the 18.6-yr period nodal tidal cycle contributes to sea surface temperature anomaly known as the Pacific Decadal Oscillation [*Mantua et al.*, 1997], and then amplifies the AL. It suggests that the bidecadal oscillations found in the Oyashio region are attributed to both the 18.6-yr period nodal tidal cycle and the variation in strengthening in WSAG due to atmospheric oscillations. Further consideration about the controlling factor of the oscillations is necessary to evaluate long-term change in the western North Pacific.

Along the 165°E section, the bidecadal oscillations in dissolved O_2 would be extended horizontally on $26.8\sigma_\theta$ between 30°N and 42.5°N (Fig. 3-11). This water is formed in the

subsurface of the Kuroshio-Oyashio Interfrontal Zone [*Talley*, 1993] and is transported eastward as the core of NPIW although in north of 40°N it cannot be observed as a salinity minimum layer in an intermediate depth. These oscillations were well synchronized with those in the Oyashio region with a lag in 1–3 years (Fig. 3-10b). *Ueno and Yasuda* [2003] have shown that water flows on $26.7\sigma_\theta$ and $27.2\sigma_\theta$ take about 1 year from 155°E to 165°E in 40°N–44°N based on particle trajectories. Considering that the bidecadal oscillations are propagated from the Oyashio region to 165°E by 155°E and the longitude of 155°E is located in the middle of the Oyashio region and 165°E section, the observed lags in 165°E would be reasonable. Moreover, the lag in 30°N is later than those in its northern region. This would result in additional travel in flow field in the subtropical gyre because NPIW observed in 30°N is thought to be advectively transported from the west through the Kuroshio recirculation (it can be seen that geostrophic stream lines in Fig. 3-1). The bidecadal oscillations were also determined in 50°N with preceding 2–4 years to those in the Oyashio region. Because unfiltered data exhibited very large interannual variation and time-lagged correlation analysis is not significant, this result might lack of reliability. Nevertheless, since this region is located in the upstream of the Oyashio region, the preceding oscillations possibly are propagated from the Bering Sea where tidal mixing is also strong [*Osafune and Yasuda*, 2010]. In the region in 47.5°N located in the center of WSAG, shorter oscillations were determined in O_2 concentration on $26.8\sigma_\theta$. Along the 165°E section, *Sasano et al.* [2015] identified an increasing trend in O_2 in the subarctic OML in 47.5°N and suggested that this change would be affected by a northward shift of WSAG. While the AL is oscillated with bidecadal timescale in its intensity and longitudinal position, the AL is oscillated with decadal time scale in its latitudinal position [*Sugimoto and Hanawa*, 2009]. It suggests that the oscillations with decadal timescale in 47.5°N might be affected by shift of WSAG position.

The bidecadal oscillations in dissolved O_2 were also determined vertically in 40°N at 165°E on $26.8\sigma_\theta$–$27.5\sigma_\theta$ with the periodicity at 16.5–18.7 years (Fig. 3-12), and were synchronized with a lag within 2–3 years in the intermediate depth for those in the Oyashio region on the same isopycnal surfaces and within 3–5 years in the OML (Fig. 3-10c). This region is corresponding to the gyre boundary in the Kuroshio and Oyashio Extension region, and water flows eastward. As mentioned above, the nearly constant lag with 2–3 years between $26.8\sigma_\theta$ and $27.2\sigma_\theta$ is presumable [*Ueno and Yasuda*, 2003]. It means that the oscillations in O_2 is simply controlled by advection by the mean current. Furthermore, based on ocean model, *Osafune and Yasuda* [2013] have suggested that along vertical 40°N section temperature anomalies with the 18.6 year modulation move eastward with nearly constant lag from the surface to 1000 m at approximately $27.2\sigma_\theta$. These results in model studies are in good agreement with this study. On the other hand, the bidecadal oscillations in O_2 have been determined in much deep layers in $27.3\sigma_\theta$–$27.5\sigma_\theta$ which are corresponding to the OML with the core approximately at $27.4\sigma_\theta$. However, because the OMLs expand sluggishly in places where the ocean circulation stagnates and the expansion have been not yet well understood, it is further difficult to examine the propagation of the oscillations in the OML. Nevertheless, the lag in the OML at 3–5 years seems to be too fast in comparison with flows in the upper layer. One possibility to explain the bidecadal oscillations in the OML in 40°N is that tongue-like distribution of O_2 is oscillated between east and west. Because the AL is oscillated with bidecadal timescale in its intensity and longitudinal position [*Sugimoto and Hanawa*, 2009], swing in the position of WSAG and subsequent shift in a front might be responsible to the oscillation in the OML. Alternatively, the oscillations in the AL might induce movement of the tongue of the OML between east and west. This possibility might be supported by the comparison with variation of O_2 in the OML in 30°N where the bidecadal oscillations have

been not determined (compare Fig. 3-10c to Fig. 3-10d). The lag of the oscillations in O_2 from the Oyashio region is significantly determined in 40°N while this is not seen in 30°N. It would reflect the difference in the upstream region: the OML observed in 40°N seems to penetrate from west to east while that in 30°N from east to west (Fig. 3-1). This means that the OML in 40°N is affected by WSAG in perspective, but that in 30°N is by the subtropical gyre. As a result, the bidecadal oscillations in dissolved O_2 have been determined horizontally and vertically in the region where the impact of the subarctic region can reach. However, these speculations for the bidecadal oscillations in the OML remains uncertain. To understand the long-term change in dissolved O_2, it needs further investigation about the vertical and horizontal expansion of the oscillations.

The amplitudes of O_2 oscillations in 40°N was relatively large at 6.1 ± 0.7 μmol kg^{-1} on 26.8σ_θ along the 165°E section. The large amplitude might implies the high contribution of the Oyashio water. This amplitudes were half as large as those in the Oyashio region on the same density at 12.2 ± 1.0 μmol kg^{-1}. It is assumed that the amplitude is attenuated by mixing process with the other source of NPIW of Kuroshio water in which it is speculated that there are much smaller variation in O_2 even if an interdecadal variability is present. The bidecadal oscillations have also been determined in the eastern subarctic Pacific at Ocean Station Papa (OSP) [*Whitney et al.*, 2007]. Because the oscillations were correlated with those of the Oyashio water with a lag of ~7 years [*Keeling et al.*, 2010], it has been considered that the oscillations were propagated from the Oyashio region. However, the amplitude in OSP is as large as that in the Oyashio region (see Fig. 7 in *Keeling et al.* [2010]). It means that another source would contributed to the amplified oscillations in OSP since the 165°E section is located between the Oyashio region and OSP. This consideration is reasonable to explain differences of the trend of O_2 decline between the western and eastern North Pacific. *Kouketsu*

et al. [2010] have pointed out that the relationship between the change in potential density and that in AOU to the west of 170°W is different from that to the east of 170°W over the latitudinal band of 25°N–40°N. *Ueno and Yasuda* [2005] have shown that the horizontal distribution of the dichothermal layers found around 26.6σ_θ in WSAG becomes shallow to approximately 26.2σ_θ toward east. It suggests that the O_2 changes on 26.6σ_θ in the western North Pacific would not propagate directly to the eastern North Pacific. It sufficiently supports the possibility of another water source of O_2 in the eastern North Pacific.

3.5. Conclusions

In the Oyashio region, decreasing trends in dissolved O_2 were significantly identified between 26.6σ_θ and 27.5σ_θ during 1954–2014. The highest rate of decreasing O_2 was determined on the 26.7σ_θ at the rate of -0.72 ± 0.11 μmol kg^{-1} yr^{-1} although the trends would be apparently attributed to deepening effect of isopycnal horizon by approximately 33% due to freshening and warming. This density is roughly corresponding to the core of the dichothermal layer which is formed in winter convection. Although the layer is not locally affected by surface water of the Oyashio region except for winter, it is clear that the layer is formed anywhere in the upstream region through winter convection. Therefore, secular trends found on 26.7σ_θ would reflect changing condition in winter, and the decreasing O_2 on 26.7σ_θ would be largely contributed by the reduction of ventilation. This is supported by decreasing trend in density in surface at 10 m in winter. On the other hand, O_2 decrease below 26.7σ_θ could not account for a reduction of ventilation. Because the isopycnal horizons denser than 26.7σ_θ is not widely outcropped in the open North Pacific, the signal of surface cannot reach

to 27.5σ_θ only by winter convection. Even with considering the contribution of diapycnal mixing near surface layer around the Bussol' Strait [*Ono et al.*, 2007], the signal of ventilation reaches only to the depth of 26.8σ_θ isopycnal horizon. This missing can be explained by the dynamics of OSIW and DSW which play as a source of O_2 to the deep layer. As *Yamamoto-Kawai et al.* [2004] have shown deep ventilation for CFCs up to 27.4σ_θ in OSIW, ventilation for O_2 together with decrease trends is controlled by combined two mechanisms; directly ventilation in the upper OSIW through DSW supply, and diapycnal mixing driven by the strong tidal mixing around the Bussol' Strait. This process related to tidal mixing can sufficiently explain decreasing trends up to 27.5σ_θ in the Oyashio region. In fact, *Nakanowatari et al.* [2007] have reported decreasing trends in O_2 in 27.4σ_θ in OSIW at the rate of -0.23 μmol L^{-1} yr^{-1} which is larger than those in the Oyashio region. The change was attributed to decrease of DSW production in the Sea of Okhotsk due to warming of autumn air temperature [*Kashiwase et al.*, 2014] and freshening [*Ohshima et al.*, 2014] in the northwest of the Sea of Okhotsk. Furthermore, considering the fact that tidal mixing around the Bussol' Strait extends to 27.5σ_θ [*Ono et al.*, 2007; *Yagi and Yasuda*, 2012], and that bidecadal oscillations are determined in the isopycnal horizon of 27.5σ_θ in this study, it is reasonable to assume that the signal of OSIW is propagated up to 27.5σ_θ in the Oyashio region. As a result, except for the apparent contribution of the deepening effect, O_2 decreases in the Oyashio region can largely attributed to the reduction of ventilation in winter in upper layer and the reduction of DSW production due to ocean warming and freshening in lower layer. These finding suggest that dissolved O_2 in the Oyashio region will continue to decrease in the coming decades as global warming progresses. On the other hand, the trends in the Oyashio region in deep layer up to 27.5σ_θ might be also explained by an increase in contribution of WSAW to the Oyashio region due to the strengthening of WSAG because O_2 concentration

in WASG is lower than that in OSIW. This circulation change might be supported by long-term strengthening in the AL. However, the relationship between ocean circulation and global warming is not yet well understood. Additionally, it needs further consideration about the strengthening in ocean circulation.

In the Oyashio region, the bidecadal oscillations in dissolved O_2 were synchronously determined between 26.6σ_θ to 27.5σ_θ. In the layer on 26.7σ_θ, where O_2 concentration varied seasonally, the bidecadal oscillations were detected in spite of seasons. Furthermore, the bidecadal oscillations were determined horizontally on 26.8σ_θ between 30°N and 42.5°N along the 165°E section with a lag of 1–3 years and vertically in the OML in 40°N at 165°E with a lag of 3–5 years. It means that the bidecadal oscillations in O_2 were expanded to the region where the subarctic water influences. These findings are the first to characterize the extension of the bidecadal oscillations to the western North Pacific. Furthermore, through the comparison of the amplitude of oscillations between the western and eastern subarctic Pacific, it is pointed out that O_2 source other than the western North Pacific is contributed to the eastern North Pacific. It means that the oscillations is possibly useful to evaluate variations in the ocean.

Generally, the oscillations disturb determinations of long-term trends because it is necessary to distinguish secular trends from oscillations with a large number of observation data. The deepening effect of isopycnal horizons also disturbs the determinations because this do not involved net change and because it is difficult to detect in short-period. However, because these signals in dissolved O_2 is more detectable than those in temperature and salinity and O_2 data are archived over the long period with relatively good qualities, the determination of the signals from ocean observation is advantage of analysis in O_2. The results in this study will help to understand of long-term trends in physical and other biogeochemical parameters.

In particular, it would be useful for the parameters which have relatively short data period such as DIC. Therefore, analysis in long-term trends with the bidecadal oscillations in O_2 would provide answers to interpret the accumulation of anthropogenic CO_2 in the ocean.

Appendix D

In the subtropical North Pacific, potential temperature is typically decreasing with depth, while salinity is also decreasing with depth but is turned to be increasing in intermediate layer with salinity minimum layer. For example, above the salinity minimum, warming on isobaths induces cooling/freshening on isopycnal horizons. Because warming makes density of a water parcel light, depth of isopycnal horizon shifts to deeper layer than that before warming where salinity is fresher due to its vertical distribution. According to changing parameter and vertical structure, induced changes are different; increase in temperature on isobath induces cooling/freshening on isopycnals above salinity minimum but warming/salting below it due to vertical structure of salinity; decrease in salinity on isobaths induces cooling/freshening both above and below it due to vertical structure of temperature. More details are described in Appendix C.

In the subarctic North Pacific, salinity is typically increasing with depth while temperature has minimum (dichothermal) and maximum (mesothermal) layers. These structures are quite different from those in the subtropical region. It implies that the deepening effect of isopycnal horizons generates different contributions by either warming or freshening. If temperature in vertical profile is increasing (salinity is assumed unchanged with time), changes of temperature/salinity on isopycnals always show increasing trends due to the

vertical distribution of salinity. On the other hand, if salinity in the vertical profile is decreasing (temperature is assumed unchanged with time), changes of temperature/salinity on isopycnals show decreasing trends above the dichothermal layer, increasing between dichothermal and mesothermal layers, and decreasing below the mesothermal layers due to the distribution of potential temperature as theoretical change. However, the magnitude of change resulting in temperature and salinity is dependent on their relationships with density (see density contour lines in Fig. 3-13a). If opposing actions are induced between changes in temperature and salinity, predominant contribution to change in density emerges as a consequent change on isopycnal horizon.

As mention above, the deepening effect of isopycnal horizons is affected to changes on isopycnal horizons if temperature and/or salinity changes. This concept is useful to distinguish apparent change due to change in temperature/salinity. However, it should not be applied to the situation that a water parcel is displaced by other (for example, subtropical water is displaced to subarctic one) because changes in temperature and salinity invoke no change due to long-term trends in warming/cooling and freshening/salting. In this case, changes in temperature and salinity would differ between on isopycnals and isobaths and are attributed to be displaced by other water parcels which just has different temperature and salinity. The concept of the deepening effect can apply to correct vertical displacement of depth of isopycnal horizons due to long-term changes in temperature/salinity.

Figures of Chapter 3

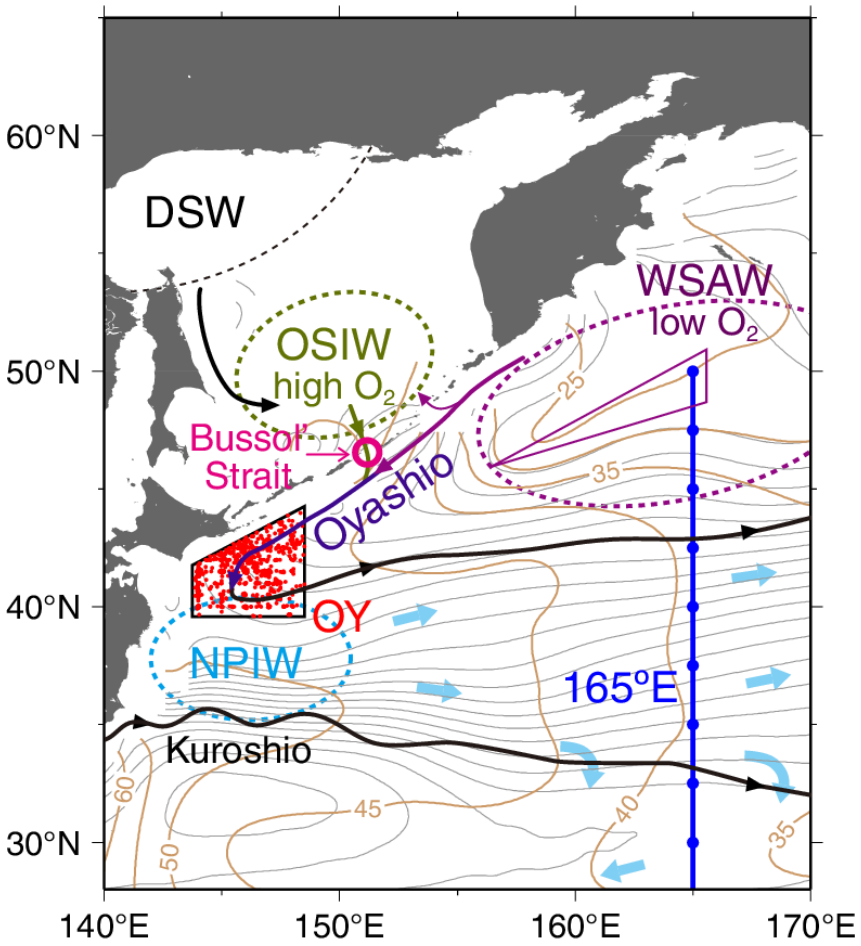

Fig. 3-1. Schematic representation of the currents and distributions of water masses in the western North Pacific. Red dots bounded by a black line represent hydrographic stations in the Oyashio region (OY) defined in this study. A blue line with dots denote the repeat hydrographic section of 165°E and the central positions to calculate annual mean in each 2.5° band. Gray contours show climatological acceleration potential referred to 1500 dbar on 26.8σ_θ from the World Ocean Atlas 2009 (WOA09) [*Antonov et al.*, 2010; *Locarnini et al.*, 2010]. Brown contours denote climatological dissolved O_2 on 27.4σ_θ from WOA09 [*Garcia et al.*, 2010]. A purple solid line indicates the area used in primary QC as WSAG along the P1 section (see section 3.2.2).

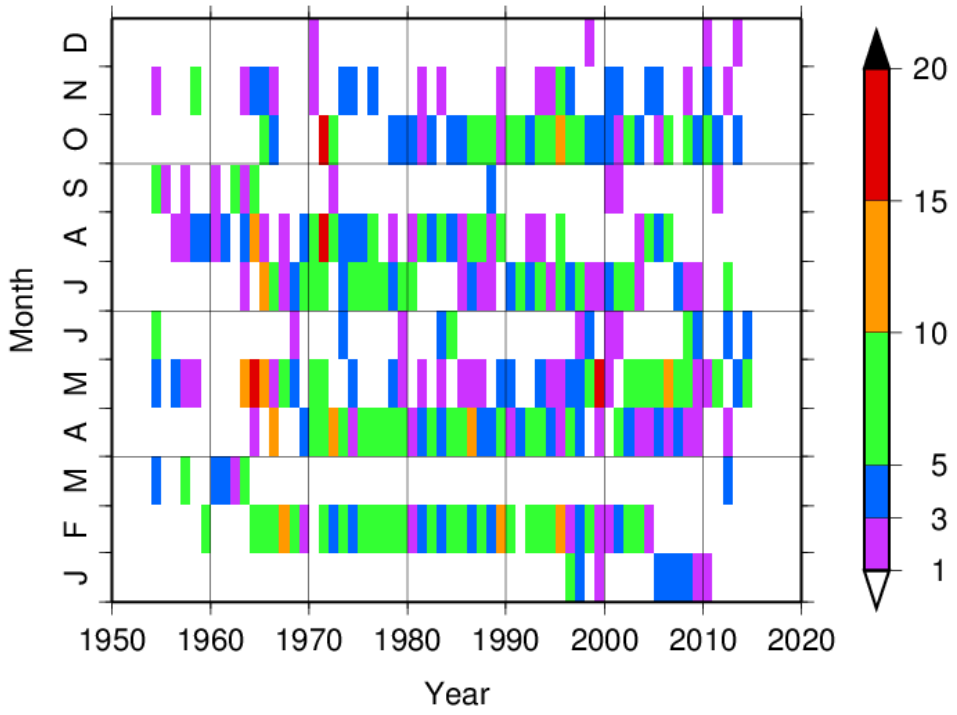

Fig. 3-2. Year-month distributions of hydrographic stations with dissolved O_2 measurements in the Oyashio region.

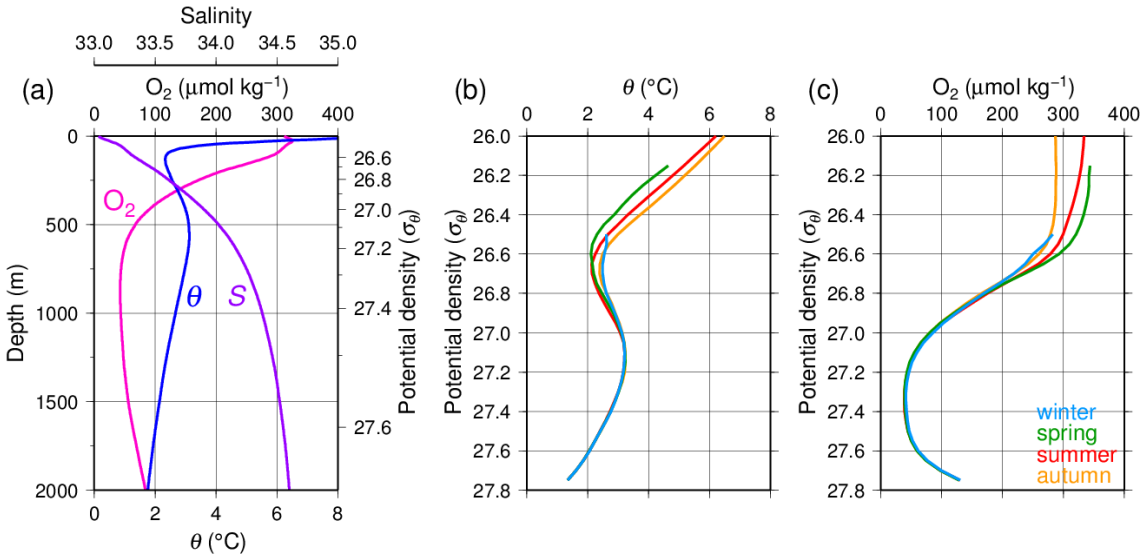

Fig. 3-3. (a) Profiles of the mean O_2, potential temperature and salinity for 1954–2014 with respect to depth. (b) Profiles of the seasonal mean potential temperature for 1954–2014 with respect to potential density. (c) Profiles of the seasonal mean O_2 for 1954–2014 with respect to potential density. For (b) and (c), data above season mean density in 10 m are not shown.

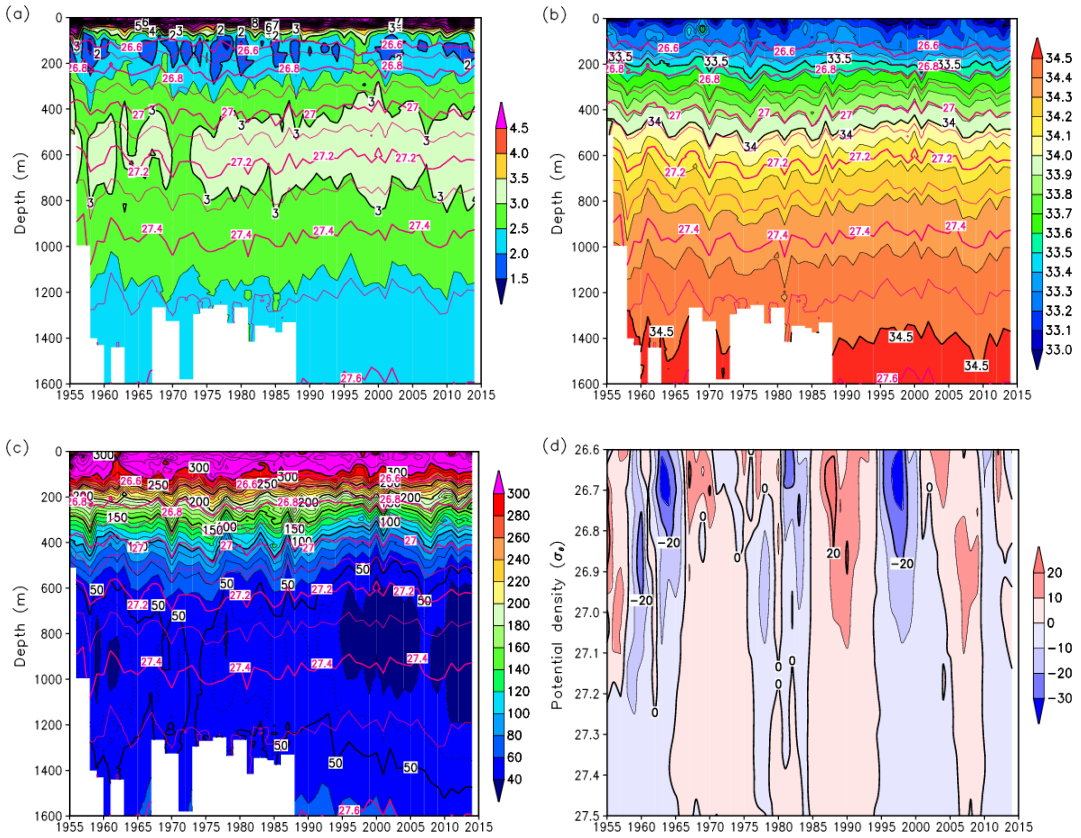

Fig. 3-4 Time–depth distributions of annual mean (a) potential temperature, (b) salinity, and (c) dissolved O_2. Pink lines indicate isopycnal horizons below 26.6σ_θ. (d) Time–density distributions of anomalies of oscillations from trends of dissolved O_2.

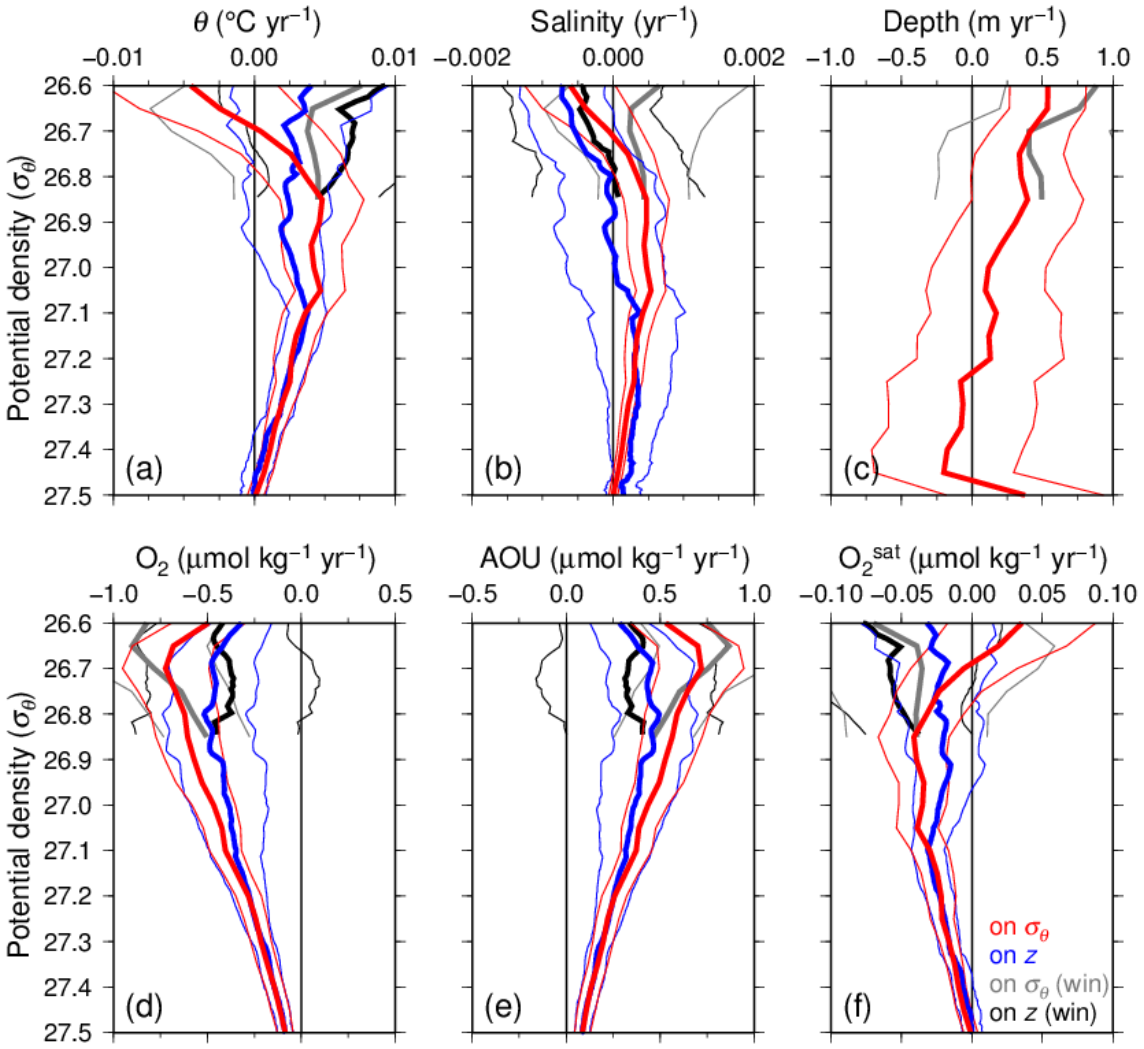

Fig. 3-5. Linear rates of changes in (a) potential temperature, (b) salinity, (c) depth of isopycnal horizon, (d) dissolved O_2, (e) AOU, and (f) O_2^{sat} with respect to the potential density in the Oyashio region. Thick red lines represent annual mean rate of change calculated on isopycnal horizons at intervals at $0.05\sigma_\theta$. Thick blue lines indicate the rates calculated on isobaths at intervals at 5 m plotted against the mean density on each depth. Thin lines show confidence intervals of 95%. Gray and black lines are the same as red and blue lines, respectively, but in winter mean rate of change above $26.8\sigma_\theta$. The lines related to isobaths are smoothed out by averaging in ±5 m.

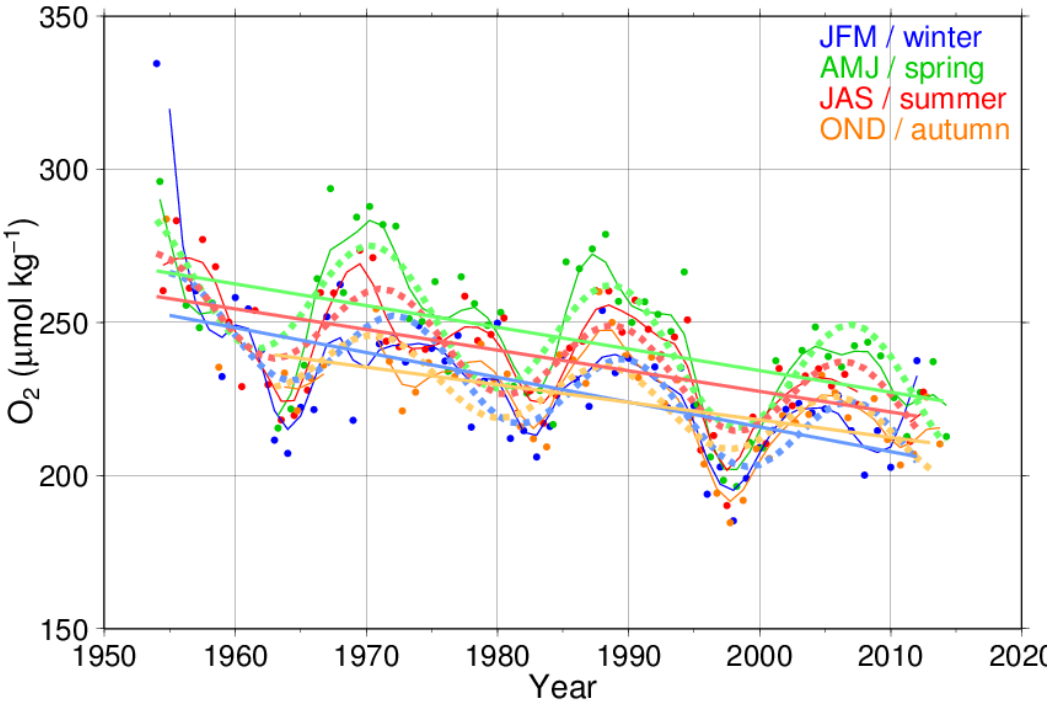

Fig. 3-6. Time series of dissolved O_2 on 26.7σ_θ in each season averaged in year. Thick broken and solid lines with lighter color indicate the trends and oscillations fitted by nonlinear least squares method with confidence level greater than 95%. Thin lines with darker color denote data with 5-year low pass filter.

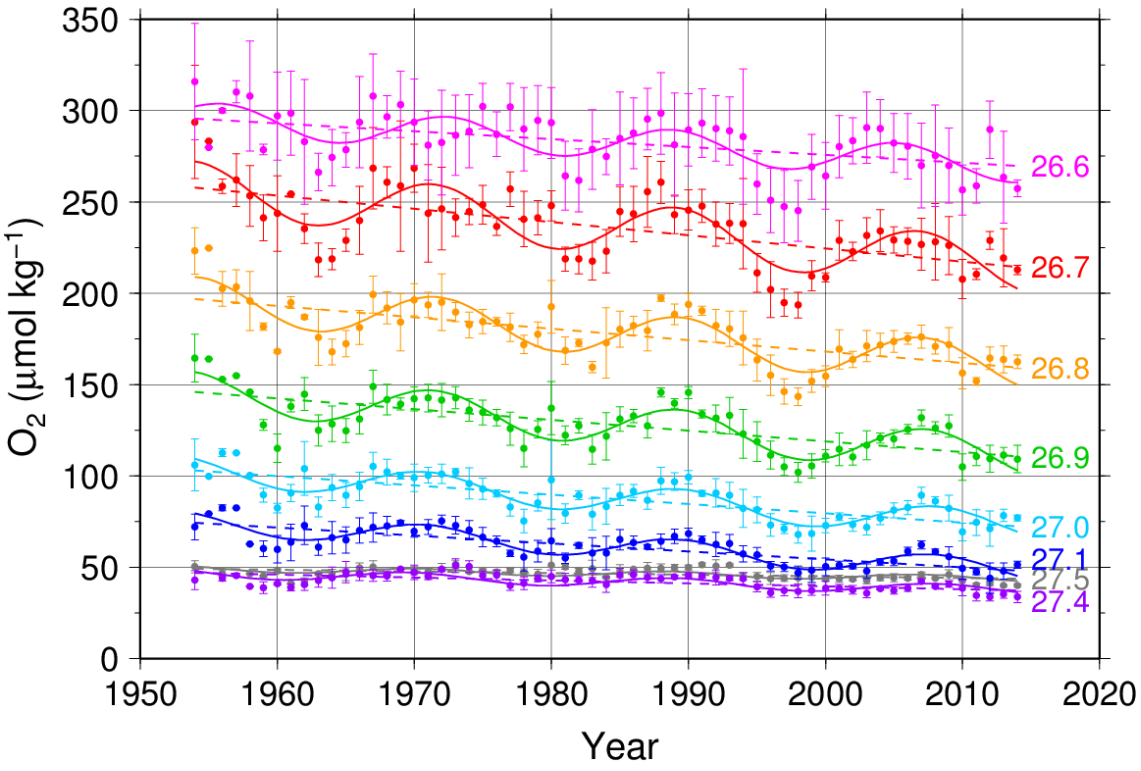

Fig. 3-7. Time series of dissolved O_2 on isopycnal horizons in the Oyashio region. Plots and error bars indicate annual means and their standard deviations in each year. Linear and curve lines indicate the trends and oscillations fitted by nonlinear least squares method with confidence level greater than 95%.

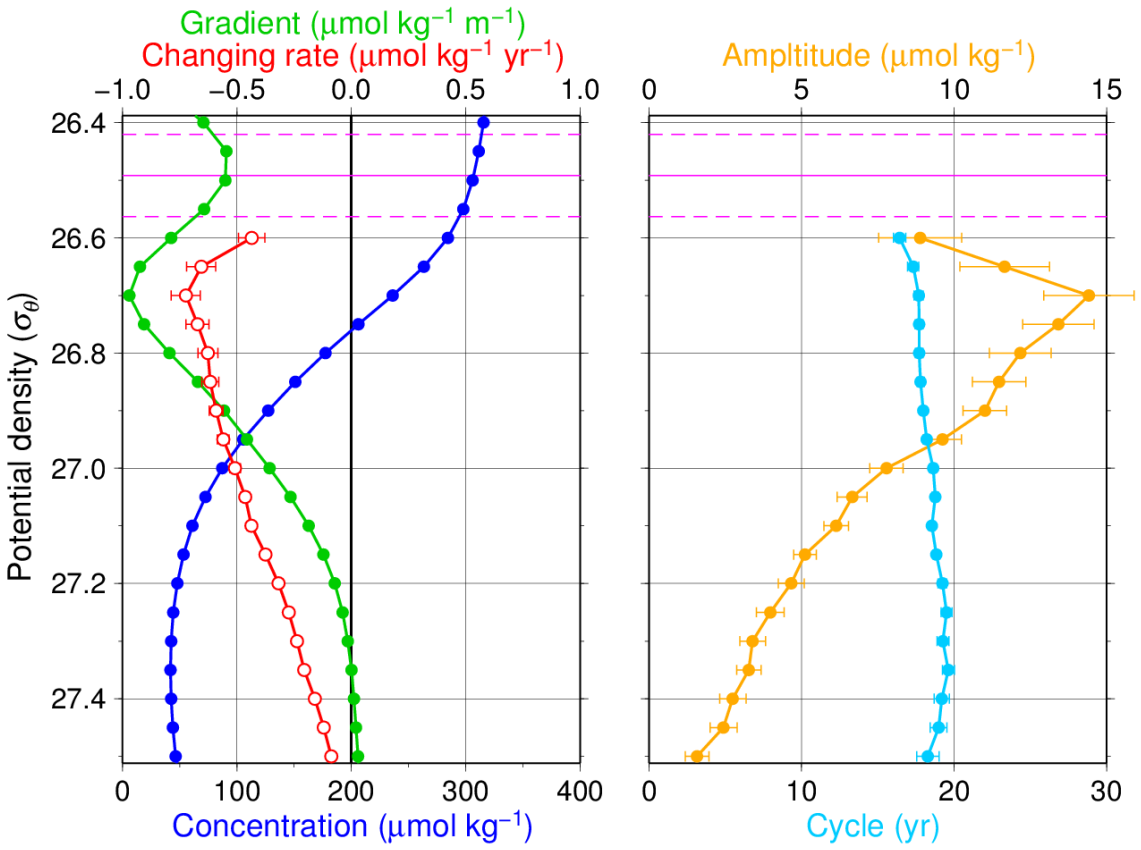

Fig. 3-8. Vertical profiles of dissolved O_2 with respect to the potential density in the Oyashio region. Red, yellow, and light blue circles indicate the coefficients of A (changing rate), C (amplitude), and E (cycle) in equation (1), respectively. Blue and green circles denote annual mean and its gradient. Error bars denote ±1 standard error. Red opened circles represent the trends with confidence level greater than 95%. Solid and broken lines with pink indicate the densities of winter mean and mean ±1SD at 10m.

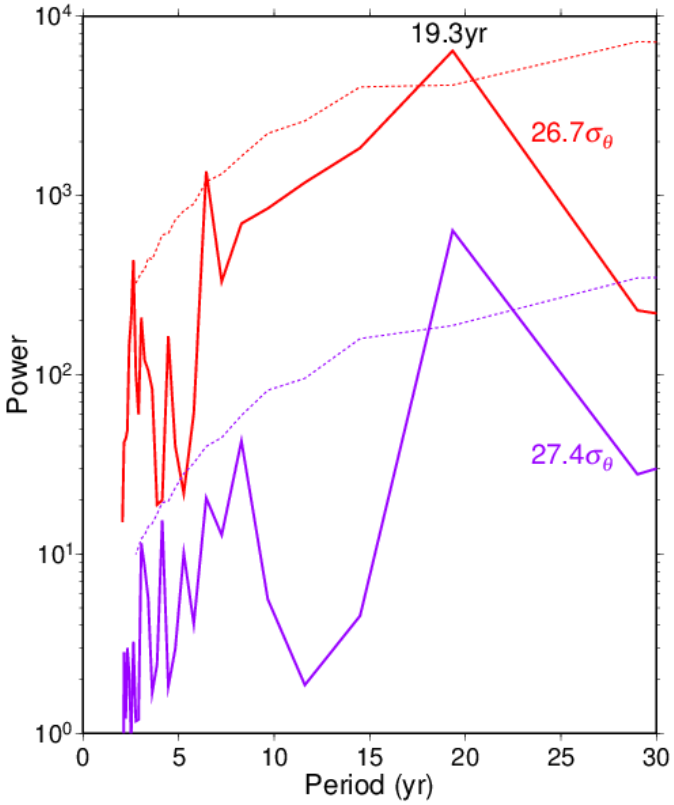

Fig. 3-9. Power spectra of dissolved O_2 on $26.7\sigma_\theta$ and $27.4\sigma_\theta$ in the Oyashio region. Dotted lines show 95% confidence level obtained with the Monte Carlo simulation based on a red-noised (AR-1) model for the observed lag-1 correlation coefficient using a 10,000 surrogate time series.

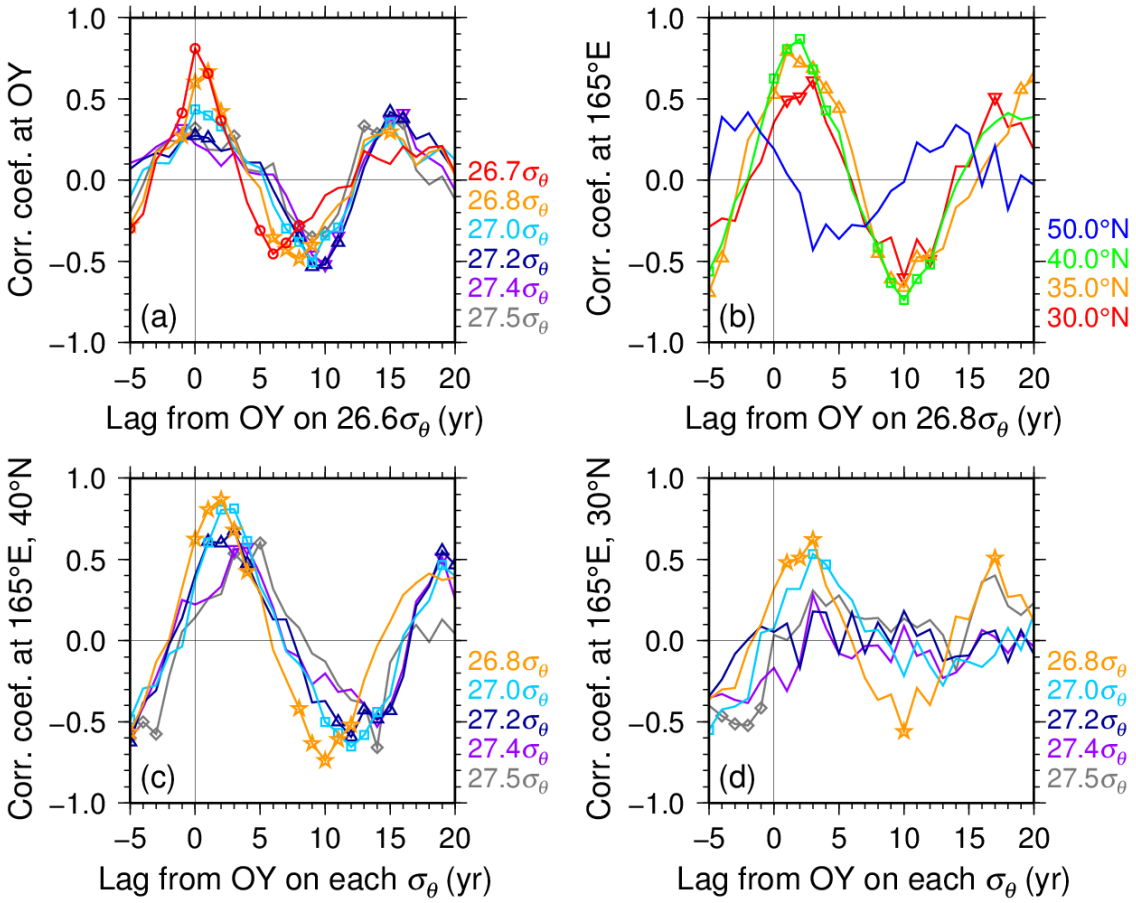

Fig. 3-10. Lagged correlation of dissolved O_2 of (a) the Oyashio region (OY) on each isopycnal horizon from OY on 26.6σ_θ, (b) the 165°E section on 26.8σ_θ from OY on 26.8σ_θ, (c) 40°N in 165°E from OY on the same isopycnal horizon, and (d) 30°N in 165°E from OY on the same isopycnal horizon. Symbols indicate that the correlations are significant at the 95% confidence level. These calculations are based on detrended annual mean data with no-filter.

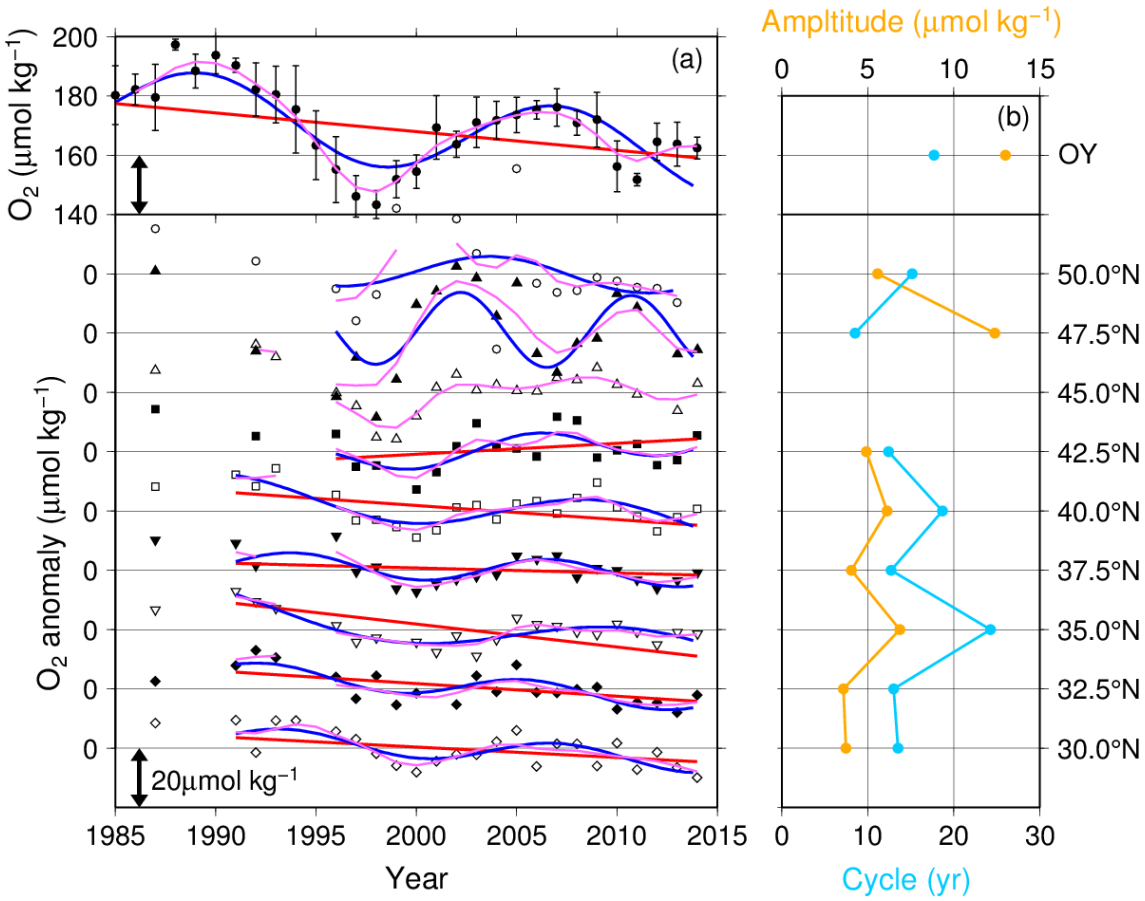

Fig. 3-11. (a) Time series of dissolved O_2 on 26.8σ_θ along the 165°E section between 30°N and 50°N and in the Oyashio region (OY) (labels of latitude are denoted on right side of (b)). Plots indicate annual means in each year. Pink lines denote annual means with 5-year low pass filter used in the NLS calculation. Red and blue lines represent the trends and oscillations fitted by NLS with confidence level greater than 95%. (b) Spatial distributions of the coefficients of C (amplitude) with yellow and E (cycle) with light blue in equation (1) in dissolved O_2 on 26.8σ_θ with respect to latitude along the 165°E section.

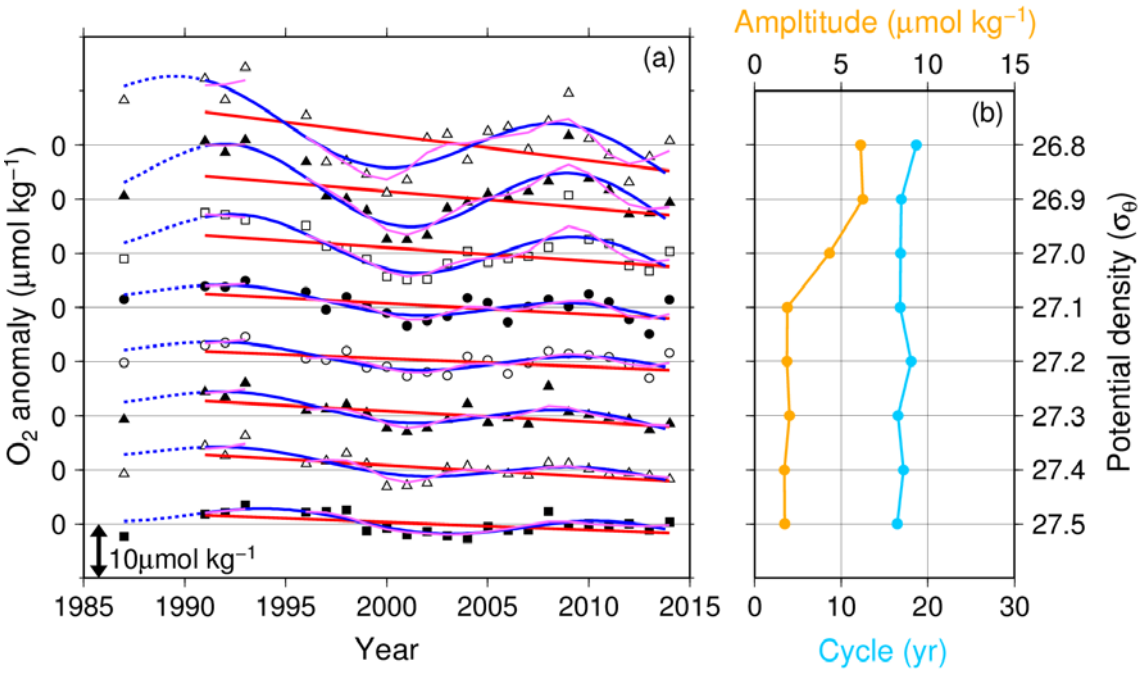

Fig. 3-12. Time series of dissolved O_2 on 26.8σ_θ–27.5σ_θ along the 165°E section in 40°N (labels of density are denoted on right side on (b)). Plots indicate annual means in each year. Pink lines denote annual means with 5-year low pass filter used in the NLS calculation. Red and blue lines represent the trends and oscillations fitted by NLS with confidence level greater than 95%. Dotted lines indicate time extrapolated oscillations to data which is not included in the NLS calculation due to data gap. (b) Vertical distributions of the coefficients of C (amplitude) with yellow and E (cycle) with light blue in equation (1) in dissolved O_2 with respect to the potential density along the 165°E section in 40°N.

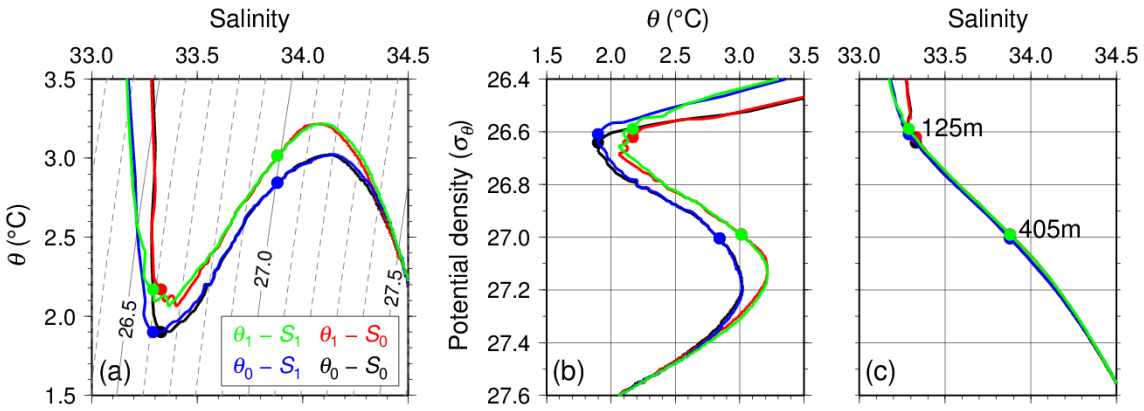

Fig. 3-13. (a) Potential temperature-salinity diagram, (b) profiles of potential temperature with respect to potential density, and (c) profiles of salinity with respect to potential density in the Oyashio region. Each parameter for a given year is reconstructed from long-term trends on isobath surfaces: $X=a \cdot y + b$, where "X" is reconstructed data, "y" is year, and "a" and "b" are the slope (shown in Figs. 3-5a and 3-5b as blue lines) and intercept, respectively. Black line denotes the reconstructed data in 1954 (before warming θ_0, and before freshening S_0). Green line indicates the reconstructed data in 2014 (after warming θ_1, and after freshening S_1). Red (blue) line is drawn with the reconstructed data from θ_1 (θ_0) and S_0 (S_1) to show the effect of warming (freshening). Circles indicate data at the depth of 125 m (corresponding to mean depth of 26.6σ_θ) and 405 m (27.0σ_θ). Gray contours denote potential density.

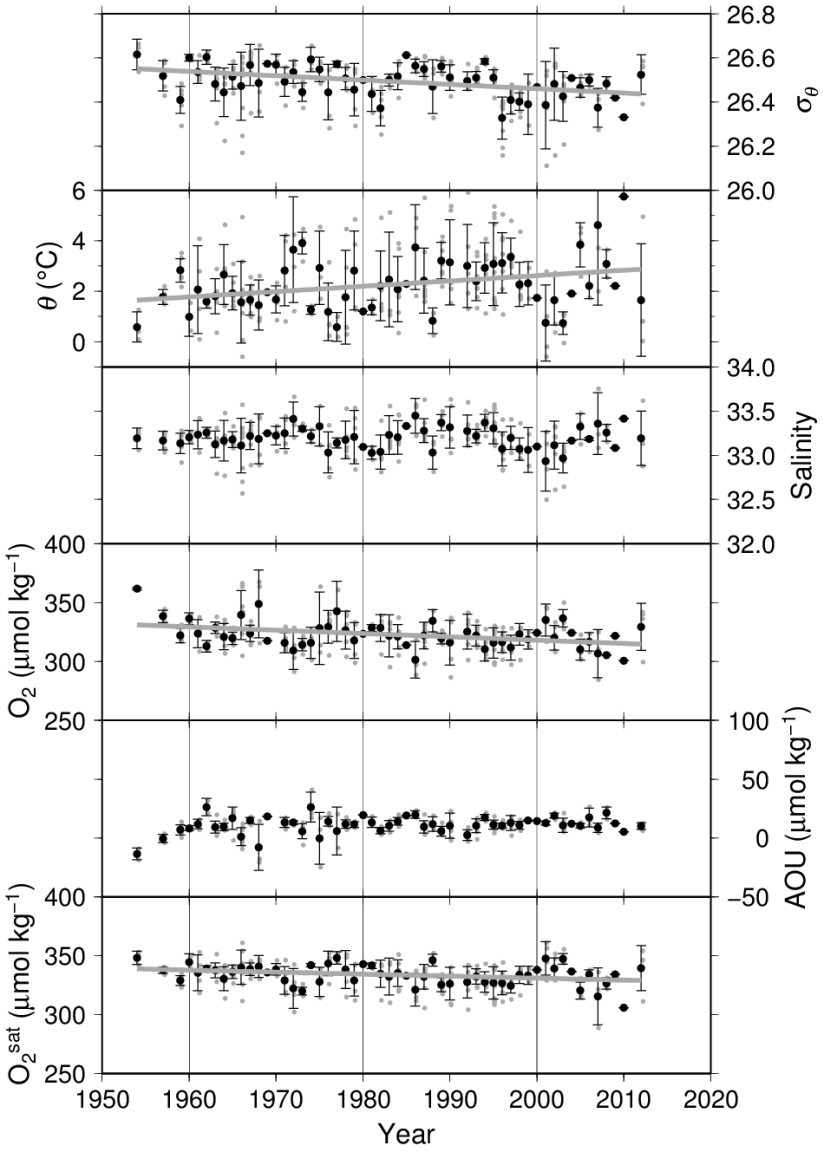

Fig. 3-14. Time series of physical and oxygen parameters in 10 m in winter in the Oyashio region. Plots and error bars indicate annual means and their standard deviations in each year. Gray lines indicate the linear trends with confidence level greater than 95%.

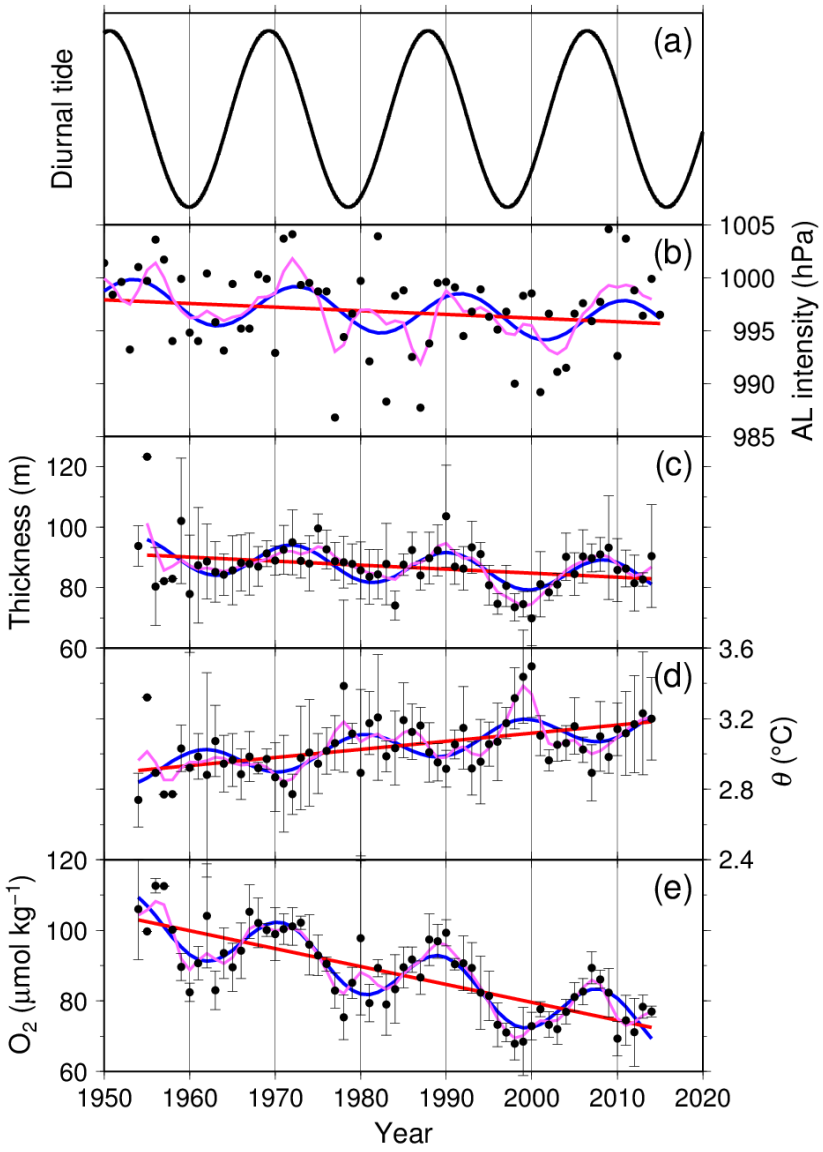

Fig. 3-15. Time series of (a) strength of the diurnal tide in the 18.6-year nodal tidal cycle, (b) intensity of AL, (c) thickness (m) between $26.9\sigma_\theta$ and $27.0\sigma_\theta$, (d) potential temperature on $27.0\sigma_\theta$, and (e) dissolved O_2 on $27.0\sigma_\theta$. Plots and error bars indicate annual means and their standard deviations in each year. Pink lines denote annual means with 5-year low pass filter. Red and blue lines represent the trends and oscillations fitted to equation (1) by nonlinear least squares method with confidence level greater than 95%. Intensity of AL (b) is calculated for the period 1950–2014 from NCEP reanalysis dataset [*Kalnay et al.*, 1996] in accordance with *Sugimoto and Hanawa* [2009].

General discussion

In the world's ocean, dissolved O_2 have been decreased over the past few decades. In particular, there are many studies in the North Pacific based on snapshot observations on the same sections or on time series measurements in the same regions (summarized in Fig. GD-1). In this study, secular trends in O_2 were determined in the western North Pacific based on long-term hydrographic and hydrochemical observations. Furthermore, the present study has also provided the novel findings related to bidecadal oscillations in the western North Pacific. Although there are some reports about oscillations in O_2 in the North Pacific (summarized in Fig. GD-1), this study have first represented the expansion of the bidecadal oscillations in O_2 from the Oyashio region to downstream region.

The controlling factors of O_2 decline are different among the water masses and spread over the western North Pacific (summarized in Fig. GD-2). In NPSTMW, reduction in O_2^{sat} largely contributes to O_2 decrease except for apparent changes due to the deepening effect of isopycnal horizons. Decreasing O_2 in NPIW, which is widely determined in the western North Pacific, are further ascribed to weakening ventilation in the subarctic region (upper NPIW) and the reduction of DSW in the Sea of Okhotsk (lower NPIW). These factors are directly associated with ocean warming, and therefore theses O_2 decline will continue in the coming decades. As for the reduction of O_2^{sat}, the contribution to O_2 decrease is not so serious because the contribution of O_2^{sat} decreases due to warming is small roughly from 3 μmol kg^{-1} $°C^{-1}$ in a subtropical region to 8 μmol kg^{-1} $°C^{-1}$ in a subarctic region based on solubility [*Garcia and Gordon*, 1992]. By contrast, weakening ventilation would contribute to serious O_2 decrease because it causes residence time to increase steadily. It is conceivable that O_2 concentration could decrease continuously in the future with ocean warming.

However, considering that an OML, which has little opportunity to mix with other water, and therefore has the water mass age at more than a few hundred years, is located in a confined region in the ocean, it is speculated that serious depletion in dissolved O_2 due to weakening ventilation is still to come. On the other hand, it is also possible that change in ocean circulation contributes to O_2 decline in such as the Oyashio region and the subtropical OML. However, long-term change in ocean circulation remains unclear. Moreover, because the relationship between global warming and ocean circulation has not been clarified, it is difficult to forecast its contribution to O_2 decline. Further studies with considering changes in large scale are needed in order to understand O_2 change associated with climate change.

To evaluate the long-term trends, the changes in temperature and salinity were also evaluated to understand changes as physical field in this study. Classically, long-term variations of biochemical parameters are preferred to be analyzed on density-axis to cancel out fluctuations in depth-axis due to heaving by shorter-term natural variability in ocean circulation processes. However, in the upper layers of oceans, this conventional approach begins to waver as changes in temperature and salinity on constant density horizons would drive isopycnal displacements. This might induce serious misleading about long-term change. Fortunately, however, a layer where the deepening effect of isopycnal horizons is largely involved due to warming/freshening is limited to relatively upper one. In past studies based on the repeat measurements on the same sections made several years apart, it is difficult to deconvolve the long-term secular trend from shorter-term natural variability [e.g. *Kouketsu et al.*, 2010]. By contrast, long-term data was used for the 165°E section in 25 years, and in the Oyashio region in 61 years. This have a large advantage to analyze long-term changes in water properties not only on isopycnals but also on isobaths because long-term data can reduce fluctuations in depth over a range of time scales. Through the comparison of changes

between isopycnals and isobaths, apparent changes induced by a deepening effect of isopycnal horizons can be distinguished from the net change in water properties. For the evaluation of the effect, it is assumed that dissolved O_2 may be more suitable than temperature and salinity. The reasons is that change in O_2 do not involve change in vertical structure like temperature and salinity. Of course, temperature and salinity are the most important parameters to understand climate change because their changes reflect ocean warming and change in ocean dynamics. However, these changes involve displacement of isopycnals by a deepening effect of isopycnal horizons. Furthermore, as another variability, while bidecadal oscillations in temperature have been determined in the Oyashio region, the signal is much paler than that in O_2 [*Osafune and Yasuda*, 2006] (see also Fig. 3-15). It means that in some cases O_2 is superior to temperature and salinity to detect long-term variations. It might detect much longer variations through O_2 measurement such as pentadecadal climate oscillations documented by *Minobe* [1999] or undiscovered variation longer than centennial oscillations.

The secular trends and natural climate variability are naturally involved in those in other biogeochemical parameters. Because changes in dissolved O_2 reflect reverse changes in DIC and nutrients, the variation of long-term trends and bidecadal oscillations in these parameters are expected to be mirror image of those of O_2. Indeed, long-term trends with bidecadal oscillations in PO_4 reported in the Oyashio region [*Tadokoro et al.*, 2009] seems to be consistent reversely with those of O_2. However, considering observation platform of measurements with precision and development in a sensor, study in variations in O_2 have a great advantage. In particular, it would be critical to investigate variations in DIC. Since DIC measurement requires high precision and accuracy to detect climate change, it is unfamiliar enough to hydrographic observation. Additionally, because DIC measurements in high precision and accuracy are initiated in the mid of 1990s, the data record is not so long.

Although long-term trends in DIC have been identified in several repeat sections [e.g. *Kouketsu et al.*, 2013], it is difficult to comprehensively consider a deepening effect of isopycnal effects and bidecadal oscillations. To identify controlling factors of secular trends and natural climate variability in DIC, it is useful to consider variations in DIC together with those in dissolved O_2.

This study focused on the western subtropical and subarctic North Pacific. In particular, the western subarctic North Pacific is an important region because the region is located close to the area where the densest density is outcropped and thereby supplies an O_2-rich water to the western subtropical and eastern subarctic North Pacific. It would be critical to detect climate change in this region. To consider O_2 change definitely, it is also necessary to observe long-term trends in O_2 change in the Sea of Okhotsk because the Sea is the key to understand the biogeochemical cycle in various water properties in the North Pacific [e.g. *Yamamoto-Kawai et al.*, 2004; *Nishioka et al.*, 2013]. However, it is difficult to conduct a continuous observation for a long period because of problem in the location. To complement this missing information, it underscores the need to improve our understanding of the trends, as well as impacts through an optimization of the ocean observing network for physics, biogeochemistry, and biology and through models. Besides, it is necessary to improve analytical precision and accuracy in O_2 measurement because there are no certified reference material of dissolved O_2 to achieve detectable measurement of long-term trends. Some organizations have already attempted to keep high data quality in measurements as in GO-SHIP Repeat Hydrography cruises. Furthermore, application of the O_2 sensor is another key to improve understanding of O_2 change. As mentioned in Chapter 3, the subarctic region is an important area to consider O_2 change. However, it is difficult to detect long-term trends in the subarctic region because the layer where variations are expected to be distinct is corresponding to that vertical gradient

is steep. It means that observation based on discrete water sample will include an analytical errors due to interpolation to a certain density. Therefore, development in availability of O_2 sensor is effective since the sensor allow continuous automated observations and thus the determination of O_2 variability in great detail. In nearly a decade, Argo profiling floats with attached O_2 sensors have been deployed in the oceans, thus facilitating the collection of high spatial and temporal density datasets in space and time. More recently, an autonomous underwater glider with attached O_2 sensors have been deployed in the ocean [e.g. *Nicholson et al.*, 2015]. These autonomous instruments with O_2 measurement system also help to understand winter condition of ocean which is critical to consider O_2 change due to seasonal deep convection because in winter it is difficult to be achieved by shipboard hydrographic observations in rough oceanic condition. In next few decades, the combination of continuously hydrographic and hydrochemical observations with high frequency by ships with the autonomous instruments will clarify the picture of O_2 variation in the ocean. Thereby, the study of dissolved O_2 will promote the better understanding of the ocean biochemistry and climate change, and this leads to more suitable prediction of future ocean environment.

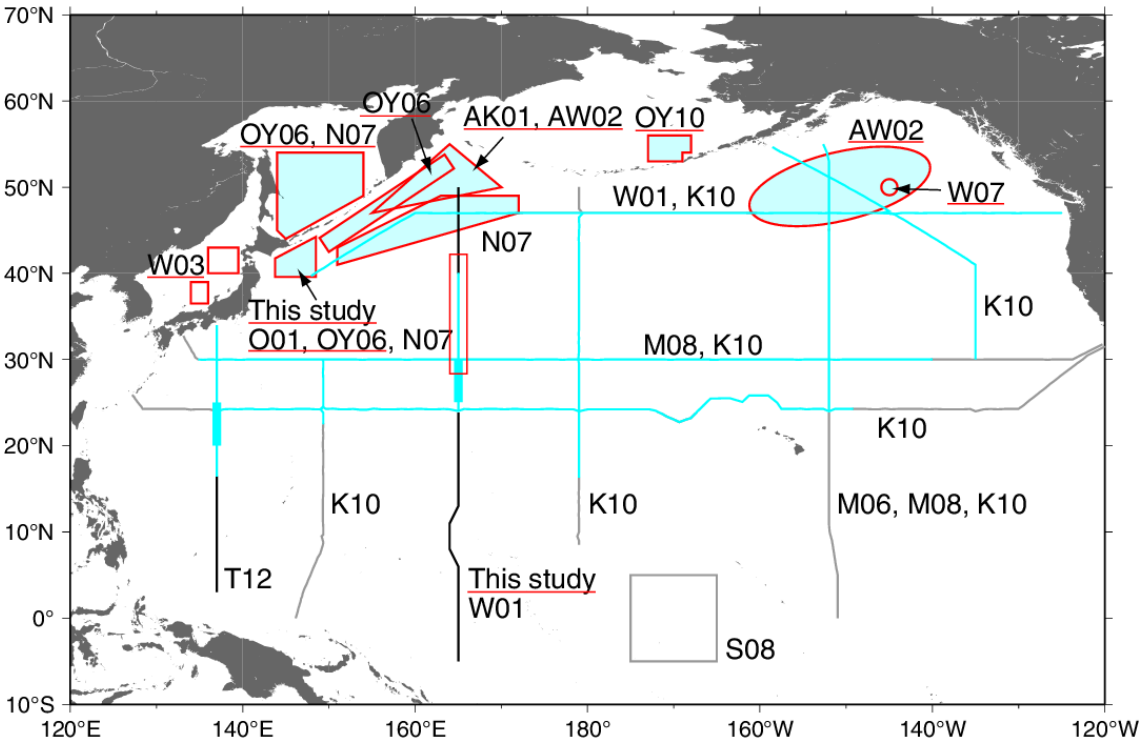

Fig. GD-1. Location of studies about secular trends in dissolved O_2 in the open North Pacific and its marginal seas. Lines and regions with light blue indicate where O_2 decrease has been documented on $26.6\sigma_\theta$–$27.0\sigma_\theta$. The studies which have also mentioned oscillations in O_2 are highlighted with a red line. Labeling indicates a literature about each line or region as follows: AK01 [*Andreev and Kusakabe*, 2001], AW02 [*Andreev and Watanabe*, 2002], K10 [*Kouketsu et al.*, 2010], M06 [*Mecking et al.*, 2006], M08 [*Mecking et al.*, 2008], N07 [*Nakanowatari et al.*, 2007], O01 [*Ono et al.*, 2001], OY06 [*Osafune and Yasuda*, 2006], OY10 [*Osafune and Yasuda*, 2010], S08 [*Stramma et al.*, 2008], T12 [*Takatani et al.*, 2012], W01 [*Watanabe et al.*, 2001], W03 [*Watanabe et al.*, 2003], and W07 [*Whitney et al.*, 2007].

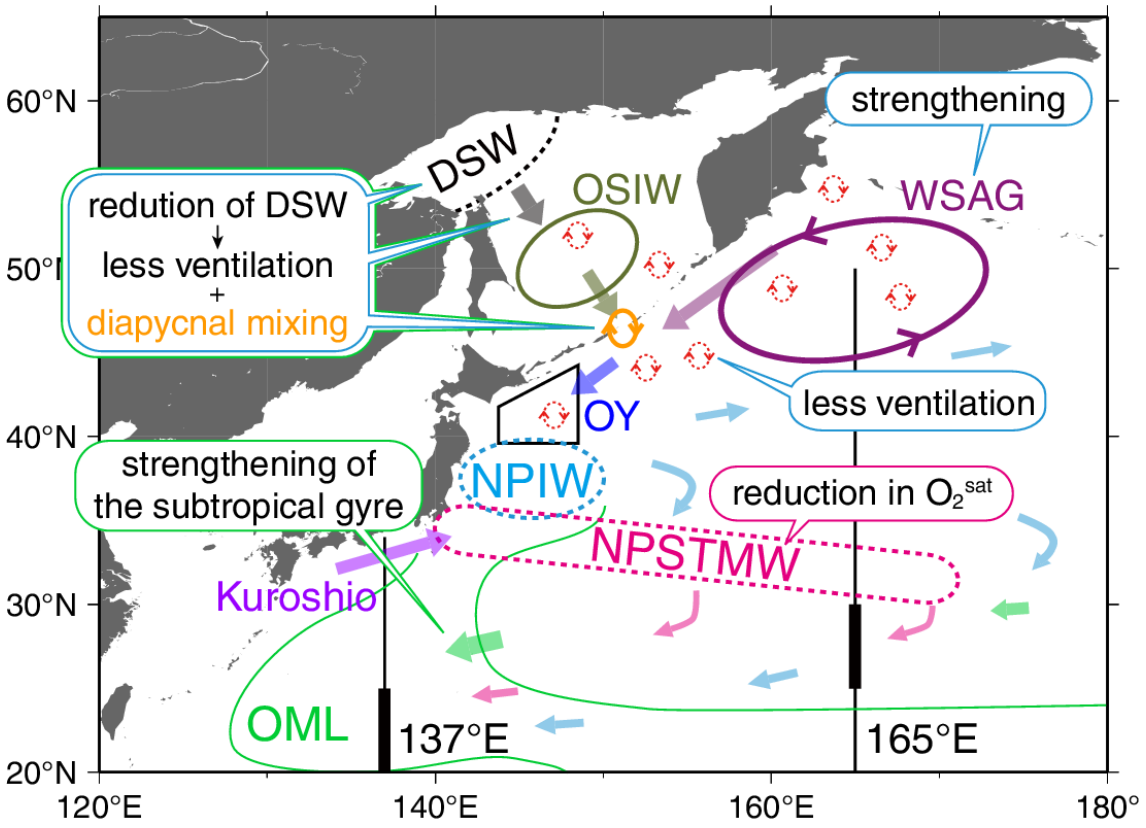

Fig. GD-2. Schematic diagram of O_2 decline in the western North Pacific. Balloons with pink, light blue, and green borders indicate controlling factors of O_2 decrease related to NPSTMW, NPIW and the OML, respectively. The circles with a dotted line denote the areas where each water is formed.

Acknowledgments

I would like to express my gratitude to Professor Takeo Hama of Life and Environmental Sciences, University of Tsukuba for his generous support, suggestion and encouragement. Special thanks are extended to Dr. Masao Ishii of the Meteorological Research Institute for invaluable advices and supports. I owe my sincere thanks to Professor Ueda Hiroaki and Associate Professor Mitsuru Hirota of University of Tsukuba for reviewing this manuscript and providing advices.

I also thank to Dr. Midorikawa of the Meteorological Research Institute for many fruitful comments. Many valuable discussions with Dr. Toshiya Nakano and Yusuke Takatani of the Japan Meteorological Agency and Naohiro Kosugi of the Meteorological Research Institute are greatly appreciated. The researches in this dissertation could not completed without their helpful suggestions and kind supports.

I am much obliged to Assistant Professor Shigeki Wada and Assistant Professor Yuko Omori of University of Tsukuba for their encouragements. I am also grateful to Dr. K. B. Rodgers for helpful comments during the course of this study.

I would like to thank captains, officers and crew of R/V *Ryofu Maru*, *Keifu Maru*, *Kofu Maru*, and all other ships on which measurements of dissolved oxygen have been made and contributed to this work for their laudable long-term observation efforts.

I also thank to all colleagues in the Meteorological Research Institute of Oceanography and Geochemistry Research Department, and the Japan Meteorological Agency of Global Environment and Marine Department for their help during this work.

Finally, I would like to express my heartfelt gratitude to my wife Kazumi and my son Kohei for their encouraging supports in many ways.

References

Akima, H. (1991), A method of univariate interpolation that has the accuracy of a third-degree polynomial, *ACM Trans.Math0 Software*, 17(3), 341-366.

Andreev, A. G. and M. Kusakabe (2001), Interdecadal variability in dissolved oxygen in the intermediate water layer of the Western Subarctic Gyre and Kuril Basin (Okhotsk Sea), *Geophys. Res. Lett.*, 28(12), 2453–2456, doi:10.1029/2000GL012688.

Andreev, A. and S. Watanabe (2002), Temporal changes in dissolved oxygen of the intermediate water in the subarctic North Pacific, *Geophys. Res. Lett.*, 29(14), 1680, doi:10.1029/2002GL015021.

Antonov, J. I., D. Seidov, T. P. Boyer, R. A. Locarnini, A. V. Mishonov, H. E. Garcia, O. K. Baranova, M. M. Zweng, and D. R. Johnson (2010), *World Ocean Atlas 2009, Volume 2*: *Salinity*, NOAA Atlas NESDIS, vol. 69, edited by S. Levitus, 184 pp., NOAA, Silver Spring, Md.

Aoyama, M. et al., 2008, Marine biochemical response to a rapid warming in the main stream of Kuroshio in the western North Pacific, *Fish. Oceanogr.*, 17(3), 206-218.

Bindoff, N. L., and T. J. McDougall (1994), Diagnosing climate change and ocean ventilation using hydrographic data, *J. Phys. Oceanogr.*, *24*, 1137–1152.

Bopp L, C. Le Quéré, M. Heimann, A. C. Manning, and P. Monfray (2002), Climate-induced oxygen fluxes: Implications for the contemporary carbon budget, *Global Biogeochem. Cycles*, 16(2), 1022 doi:10.1029/2001GB001445.

Boyer, T. P., Levitus, S., Antonov, J. I., Locarnini, R. A., and Garcia, H. E. (2005), Linear trends in salinity for the World Ocean, 1955–1998, *Geophys. Res. Lett.*, 32, L01604, doi:10.1029/2004GL021791.

Boyer, T. P. et al. (2013), *World Ocean Database 2013*, NOAA Atlas NESDIS 72, S. Levitus, Ed., A. Mishonov, Technical Ed.; Silver Spring, MD, 209 pp., http://doi.org/10.7289/V5NZ85MT.

Brewer, P. G. (1978), Direct observation of the oceanic CO_2 increase, *Geophys. Res. Lett*, 5(12), 997-1000, doi:10.1029/GL005i012p00997.

Broecker, W. S. (1974), "NO", a conservative water-mass tracer, *Earth Planet. Sci. Lett., 23*, 100-107.

Broecker, W. S., and T. H. Peng (1974), Gas exchange rates between air and sea, *Tellus*, 26, 21–35, doi:10.1111/j.2153-3490.1974.tb01948.x.

Byrne, R. H., S. Mecking, R. A. Feely, and X. Liu (2010), Direct observations of basin-wide acidification of the North Pacific Ocean, *Geophys. Res. Lett.*, 37, L02601, doi:10.1029/2009GL040999.

Carpenter, J. H. (1965), The Chesapeake Bay Institute technique for the Winkler dissolved oxygen method, *Limnol. Oceanogr.*, 10, 141–143, doi:10.4319/lo.1965.10.1.0141.

Carpenter, J. H. (1966), New measurements of oxygen solubility in pure and natural water, *Limnol. Oceanogr.*, 11, 264–277, doi:10.4319/lo.1966.11.2.0264.

Christian, J. R., and D. M. Karl (1995), Bacterial ectoenzymes in marine waters: Activity ratios and temperature responses in three oceanographic provinces, *Limnol. Oceanogr.*, *40*, 1042-1049.

Codispoti, L. A., J. A. Brandes, J. P. Christensen, A. H. Devol, S. W. A. Naqvi, H. W. Paerl, and T. Yoshinari (2001), The oceanic fixed nitrogen and nitrous oxide budgets: Moving targets as we enter the anthropocene?, *Sci. Mar.*, 65, 85–105.

Czeschel, R., L. Stramma, F. U. Schwarzkopf, B. S. Giese, A. Funk, and J. Karstensen (2011), Middepth circulation of the eastern tropical South Pacific and its link to the oxygen

minimum zone, *J. Geophys. Res.*, 116(C1), C01015, doi:10.1029/2010JC006565.

Deutsch, C., S. Emerson, and L. Thompson (2005), Fingerprints of climate change in North Pacific oxygen, *Geophys. Res. Lett., 32*, L16604, doi:10.1029/2005GL023190.

Deutsch, C., S. Emerson, and L. Thompson (2006), Physical-biological interactions in North Pacific oxygen variability, *J. Geophys. Res., 111*, C09S90, doi:10.1029/2005JC003179.

Diaz, R. J., and R. Rosenberg (2008), Spreading dead zones and consequences for marine ecosystems, *Science*, 321, 926–929, doi:10.1126/science.1156401.

Durack, P. J., and S. E. Wijffels (2010), Fifty-Year Trends in Global Ocean Salinities and Their Relationship to Broad-Scale Warming, *J. Clim.*, 23(16), 4342–4362, doi:10.1175/2010JCLI3377.1.

Emerson, S., Y. Watanabe, T. Ono, and S. Mecking (2004), Temporal trends in apparent oxygen utilization in the upper pycnocline of the North Pacific: 1980-2000, *J. Oceanogr*., 60, 139 – 147.

Fujii, Y., T. Nakano, N. Usui, S. Matsumoto, H. Tsujino, and M. Kamachi (2013), Pathways of the North Pacific Intermediate Water identified through the tangent linear and adjoint models of an ocean general circulation model, *J. Geophys. Res. Oceans*, 118, 2035–2051, doi:10.1002/jgrc.20094.

Garcia, H. E., and L. I. Gordon (1992), Oxygen solubility in seawater: Better fitting equations, *Limnol. Oceanogr.*, 37, 1307–1312, doi:10.4319/lo.1992.37.6.1307.

Garcia, H. E., R. A. Locarnini, T. P. Boyer, J. I. Antonov, O. K. Baranova, M. M. Zweng, and D. R. Johnson (2010), *World Ocean Atlas 2009, Volume. 3, Dissolved Oxygen, Apparent Oxygen Utilization, and Oxygen Saturation*, *NOAA Atlas NESDIS*, vol. 70, edited by S. Levitus, 344 pp., NOAA, Silver Spring, Md.

Gladyshev, S., S. Martin, S. Riser, and A. Figurkin (2000), Dense water production on the

northern Okhotsk shelves: Comparison of ship-based spring-summer observations for 1996 and 1997 with satellite observa- tions, *J. Geophys. Res.*, 105, 26281–26299.

Grantham, B., F. Chan, K. Nielsen and D. Fox (2004), Upwelling-driven nearshore hypoxia signals ecosystem and oceanographic changes in the northeast Pacific, *Nature*, 429(6993), 749–754, doi:10.1038/nature02612.1.

Gruber, N. (1998), Anthropogenic CO_2 in the Atlantic Ocean. *Global Biogeochem. Cycles*, 12(1), 165–191.

Gruber, N. (2011), Warming up, turning sour, losing breath: Ocean biogeochemistry under global change, *Philos. Trans. R. Soc. A*, *369*(1943), 1980-1996, doi:10.1098/rsta.2011.0003.

Gruber, N., S. C. Doney, S. R. Emerson, D. Gilbert, T. Kobayashi, A. Körtzinger, G. C. Johnson, K. S. Johnson, S. C. Riser, and O. Ulloa, (2007), The argo-oxygen program. A white paper to promote the addition of oxygen sensors to the international Argo float program.

Gruber, N., J. L. Sarmiento, and T. F. Stocker (1996), An improved method for detecting anthropogenic CO2 in the oceans, *Global Biogeochem. Cycles*, 10(4), 809-837, doi:10.1029/96GB01608.

Hanawa, K., and L. D. Talley (2001), Mode waters, in *Ocean Circulation and Climate*, edited by G. Siedler and J. Church, and J. Group, pp. 373-386, Academic, San Diego, Calif.

Hosoda, S., T. Suga, N. Shikama, and K. Mizuno (2009), Global surface layer salinity change detected by Argo and its implication for hydrological cycle intensification, *J. Oceanogr.*, 65(4), 579–586, doi:10.1007/s10872-009-0049-1.

Japan Meteorological Agency (1999), Manual of Oceanographic Observations, Part 1.

Kalnay, E., et al. (1996), The NCEP/NCAR 40-year reanalysis project, *Bull. Am. Meteorol.*

Soc., 77, 437–471.

Kashiwase, H., K. I. Ohshima, and S. Nihashi (2014), Long-term variation in sea ice production and its relation to the intermediate water in the Sea of Okhotsk, *Prog. Oceanogr*., 126, 21–32, doi:10.1016/j.pocean.2014.05.004.

Kawai, H. (1972), Hydrography of the Kuroshio extension, in *Kuroshio: physical aspects of the Japan Current*, ed., edited by H. Stonmel and K. Yoshida, pp.235-352, Univ. of Washington Press., Seattle.

Keeling, R. F., A. Körtzinger, and N. Gruber (2010), Ocean deoxygenation in a warming world, *Annu. Rev. Mar. Sci., 2*, 199-229, doi:10.1146/annurev.marine.010908.163855.

Key, R. M., A. Kozyr, C. L. Sabine, K. Lee, R. Wanninkhof, J. Bullister, R. A. Feely, F. Millero, and C. Mordy, T.H. Peng (2004), A global ocean carbon climatology: Results from GLODAP, *Global Biogeochem. Cycles*, 18, GB4031, doi:10.1029/2004GB002247.

Körtzinger, A., U. Send, D. W. R. Wallace, J. Kartensen, and M. DeGrandpre (2008), Seasonal cycle of O_2 and pCO_2 in the central Labrador Sea: Atmospheric, biological, and physical implications. *Global Biogeochem. Cycles*, **22**, GB1014, doi:10.1029/2007GB003029.

Kouketsu, S., M. Fukasawa, D. Sasano, Y. Kumamoto, T. Kawano, H. Uchida, and T. Doi (2010), Changes in water properties around North Pacific intermediate water between the 1980s, 1990s and 2000s, *Deep Sea Res., Part II, 57*, 1177–1187, doi:10.1016/j.dsr2.2009.12.007.

Kouketsu, S., A. Murata, and T. Doi (2013), Decadal changes in dissolved inorganic carbon in the Pacific Ocean, *Global Biogeochem. Cycles*, 27, doi:10.1029/2012GB004413.

Le Quéré, C. et al. (2013), The global carbon budget 1959-2011, *Earth Syst. Sci. Data*, 5(1), 165–185, doi:10.5194/essd-5-165-2013.

Levitus, S., J. Antonov, and T. Boyer (2005), Warming of the world ocean, 1955–2003, Geophys. Res. Lett., 32(2), L02604, doi:10.1029/2004GL021592.

Levitus, S., J. I. Antonov, T. P. Boyer, H. E. Garcia, R. A. Locarnini, A. V. Mishonov, and H. E. Garcia (2009), Global ocean heat content 1955–2008 in light of recently revealed instrumentation problems, *Geophys. Res. Lett.*, 36, L07608, doi:10.1029/2008GL037155.

Levitus, S., et al. (2012), World ocean heat content and thermosteric sea level change (0–2000 m), 1955-2010, *Geophys. Res. Lett.*, *39*, L10603, doi:10.1029/2012GL051106.

Locarnini, R. A., A. V. Mishonov, J. I. Antonov, T. P. Boyer, and H. E. Garcia (2010), *World Ocean Atlas 2009, Volume 1: Temperature*, *NOAA Atlas NESDIS*, vol. 68, edited by S. Levitus, 184 pp., NOAA, Silver Spring, Md.

Loder, J. W., and C. Garrett (1978), The 18.6-Year Cycle of Sea Surface Temperature in Shallow Seas Due to Variations in Tidal Mixing, *J. Geophys. Res.*, 83(C4), 1967–1970, doi:10.1029/JC083iC04p01967.

Mantua N. J., S. R. Hare, Y. Zhang, J. M. Wallace, and R. C. Francis (1997), A Pacific interdecadal climate oscillation with impacts on salmon production, *Bull Amer Meteor Soc*, 78, 1069–1079.

Martin, J. H., R. M. Gordon, S. Fitzwater, and W. W. Broenkow (1989), VERTEX: phytoplankton/iron studies in the Gulf of Alaska, *Deep Sea Res., Part I*, 36(5), 649–680.

Mecking, S., M. J. Warner, and J. L. Bullister (2006), Temporal changes in pCFC-12 ages and AOU along two hydrographic sections in the eastern subtropical North Pacific, *Deep Sea Res., Part I*, 53(1), 169–187, doi:10.1016/j.dsr.2005.06.018.

Mecking, S., C. Langdon, R. A. Feely., C. Sabine, C. Deutsch, and D.-H. Min (2008), Climate variability in the North Pacific thermocline diagnosed from oxygen measurements: An

update based on the U.S. CLIVAR/CO2 Repeat Hydrography cruises, *Global Biogeochem. Cycles, 22*, GB3015, doi:10.1029/2007GB003101.

Minobe, S. (1999), Resonance in bidecadal and pentadecadal climate oscillations over the North Pacific: Role in climatic regime shifts, *Geophys. Res. Lett.*, 26(7), 855-858.

Murata, A., H. Uchida, and K. Sasaki (2009), R/V Mirai Cruise Report, MR09-01. http://www.jamstec.go.jp/cruisedata/mirai/e/MR09-01_leg1.html.

Nakamura, T., T. Awaji, H. Takaki, K. Akitomo, and T. Takizawa (2000), Tidal exchange through the Kuril Straits, *J. Phys. Oceanogr*., 1622–1644.

Nakano, T. (2010), R/V *Ryofu Maru* Cruise Report: P09. [Available online at: http://cchdo.ucsd.edu/data_access/show_cruise?ExpoCode=49RY20100706.]

Nakano, T. (2012), R/V *Ryofu Maru* Cruise Report: P13. [Available online at: http://cchdo.ucsd.edu/data_access/show_cruise?ExpoCode=49RY20110515.]

Nakano, T., I. Kaneko, T. Soga, H. Tsujino, T. Yasuda, H. Ishizaki, and M. Kamachi (2007), Mid-depth freshening in the North Pacific subtropical gyre observed along the JMA repeat and WOCE hydrographic sections, *Geophys. Res. Lett.*, *34*, L23608, doi:10.1029/2007GL031433.

Nakanowatari, T., T. Nakamura, K. Uchimoto, H. Uehara, H. Mitsudera, K. I. Ohshima, H. Hasumi, and M. Wakatsuchi (2015), Causes of the Multidecadal-Scale Warming of the Intermediate Water in the Okhotsk Sea and Western Subarctic North Pacific, *J. Clim.*, 28(2), 714–736, doi:10.1175/JCLI-D-14-00172.1.

Nakanowatari, T., I. Oshima, and M. Wakatsuchi (2007), Warming and oxygen decrease of intermediate water in the northwestern North Pacific, originating from the Sea of Okhotsk, 1955-2004, *Geophys. Res. Lett., 34*, L04602, doi:10.1029/2006GL028243.

Nicholson, D. P., S. T. Wilson, S. C. Doney, and D. M. Karl (2015), Quantifying subtropical

North Pacific gyre mixed layer primary productivity from Seaglider observations of diel oxygen cycles, *Geophys. Res. Lett.*, 42, 4032–4039, doi:10.1002/2015GL063065.

Nishioka, J. et al. (2013), Intensive mixing along an island chain controls oceanic biogeochemical cycles, *Global Biogeochem. Cycles*, 27(3), 920–929, doi:10.1002/gbc.20088.

Ohshima, K. I., T. Nakanowatari, S. Riser, Y. Volkov, and M. Wakatsuchi (2014), Freshening and dense shelf water reduction in the Okhotsk Sea linked with sea ice decline, *Prog. Oceanogr.*, 126, 71–79, doi:10.1016/j.pocean.2014.04.020.

Oka, E., and B. Qiu (2012), Progress of North Pacific mode water research in the past decade, *Journal of Oceanography*, 68, 5-20.

Oka, E., and T. Suga (2005), Differential formation and circulation of North Pacific central mode water, *J. Phys. Oceanogr*, 35(11), 1997–2011, doi:10.1175/JPO2811.1.

Oka, E., S. Kouketsu, K. Toyama, K. Uehara, T. Kobayashi, S. Hosoda, and T. Suga (2011), Formation and subduction of central mode water based on profilingfloat data, 2003–08, *J. Phys. Oceanogr*, 41(1), 113–129, doi:10.1175/2010JPO4419.1.

Ono, K., K. I. Ohshima, T. Kono, M. Itoh, K. Katsumata, Y. N. Volkov, and M. Wakatsuchi (2007), Water mass exchange and diapycnal mixing at Bussol' Strait revealed by water mass properties, *J. Oceanogr.*, 63(2), 281–291, doi:10.1007/s10872-007-0028-3.

Ono, T., T. Midorikawa, Y. Watanabe, K. Tadokoro, and T. Saino (2001), Temporal increases of phosphate and apparent oxygen utilization in the subsurface waters of western subarctic Pacific from 1968 to 1998, *Geophys. Res. Lett.*, 28 (17), 3285-3288, doi:10.1029/2001GL012948.

Ono, T., K. Sasaki, and I. Yasuda (2003), Re-estimation of annual anthropogenic carbon input from Oyashio into North Pacific Intermediate Water, *J. Oceanogr.*, 59.

Osafune, S. and I. Yasuda (2006), Bidecadal variability in the intermediate waters of the northwestern subarctic Pacific and the Okhotsk Sea in relation to 18.6-year period nodal tidal cycle, *J. Geophys. Res.*, *111*, C05007, doi:10.1029/2005JC003277.

Osafune, S., and I. Yasuda (2010), Bidecadal variability in the Bering Sea and the relation with 18.6 year period nodal tidal cycle, *J. Geophys. Res.*, 115(C2), C02014, doi:10.1029/2008JC005110.

Osafune, S., and I. Yasuda (2013), Remote impacts of the 18.6 year period modulation of localized tidal mixing in the North Pacific, *J. Geophys. Res. Ocean.*, 118(6), 3128–3137, doi:10.1002/jgrc.20230.

Oschlies, A., K. G. Schulz, U. Riebesell, and A. Schmittner (2008), Simulated 21st century's increase in oceanic suboxia by CO_2-enhanced biotic carbon export, *Global Biogeochem. Cycles*, 22, GB4008, doi:10.1029/2007GB003147.

Paulmier, A., and D. Ruiz-Pino (2009), Oxygen minimum zones (OMZs) in the modern ocean, *Prog. Oceanogr.*, 80(3), 113-128.

Qiu, B, and S. Chen (2012), Multidecadal sea level and gyre circulation variability in the northwestern tropical Pacific Ocean, *J. Phys. Oceanogr.*, 42(1), 193-206.

Reid, J. L. (1965), Intermediate waters of the Pacific Ocean, *Johns Hopkins Oceanogr. Stud.*, *2*, 85.

Reid, J. L. (1997), On the total geostrophic circulation of the Pacific Ocean: Flow patterns, tracers, and transports, *Prog. Oceanogr.*, *39*, 263-352, doi:10.1016/S0079-6611(97)00012-8.

Rhein, M. et al. (2013), Observations: Ocean, in *Climate Change 2013: The Physical Science Basis. Contribution of Working Group I to the Fifth Assessment Report of the Intergovernmental Panel on Climate Change*, edited by T. F. Stocker et al., pp. 255–316,

Cambridge Univ. Press, Cambridge, U. K., and New York, doi:10.1017/CBO9781107415324.010.

Stabeno, P. J., R. K. Reed, and J. E. Overland (1994), Lagrangian measurements in the Kamchatka Current and Oyashio, *J. Oceanogr.*, 50(6), 653–662, doi:10.1007/BF02270498.

Stramma, L., G. C. Johnson, J. Sprintall, and V. Mohrholz (2008), Expanding oxygen-minimum zones in the tropical oceans, *Science*, *320*, 655–658, doi:10.1126/science.1153847.

Suga, T., K. Hanawa, and Y. Toba (1989), Subtropical mode water in the 137°E section, *J. Phys. Oceanogr.*, 19, 1605–1618.

Suga T., K. Motoki, Y. Aoki, A. Macdonald (2004), The North Pacific climatology of winter mixed layer and mode waters, *J. Phys. Oceanogr.*, 34, 3–22.

Sugimoto, S., and K. Hanawa (2009), Decadal and Interdecadal Variations of the Aleutian Low Activity and Their Relation to Upper Oceanic Variations over the North Pacific, *J. Meteorol. Soc. Japan*, 87(4), 601–614, doi:10.2151/jmsj.87.601.

Suzuki, T., et al. (2013), *PACIFICA Data Synthesis Project. ORNL/CDIAC-159, NDP-092*, Carbon Dioxide Information Analysis Center, Oak Ridge National Laboratory, U.S. Department of Energy, Oak Ridge, Tennessee., doi:10.3334/CDIAC/OTG.PACIFICA_NDP092.

Tadokoro, K., T. Ono, I. Yasuda, S. Osafune, A. Shiomoto, and H. Sugisaki (2009), Possible mechanisms of decadal‐scale variation in PO4 concentration in the western North Pacific, *Geophys. Res. Lett.*, 36, L08606, doi:10.1029/2009GL037327.

Takatani, Y., T. Iwao, T. Miyao, T. Midorikawa, and K. Saitou (2007), Oyashio water quality: Decadal changes and controlling factors (in Japanese with English abstract), *Umi no*

Kenkyu, 16(1), 23-37.

Takatani, Y., D. Sasano, T. Nakano, T. Midorikawa, and M. Ishii (2012), Decrease of dissolved oxygen after the mid-1980s in the western North Pacific subtropical gyre along the 137°E repeat section, *Global Biogeochem. Cycles*, *26*, GB2013, doi:10.1029/2011GB004227.

Talley, L. D. (1993), Distribution and formation of North Pacific Intermediate Water, *J. Phys. Oceanogr.*, 23, 517–537, doi: 10.1175/1520-0485(1993)023<0517:DAFONP>2.0.CO;2.

Talley, L. D. (2007). *Hydrographic Atlas of the World Ocean Circulation Experiment (WOCE). Volume 2: Pacific Ocean,* in edited by M. Sparrow, P. Chapman and J. Gould, *International WOCE Project Office, Southampton, U.K.*

Tanaka, Y., I. Yasuda, H. Hasumi, H. Tatebe, and S. Osafune (2012), Effects of the 18.6-yr Modulation of Tidal Mixing on the North Pacific Bidecadal Climate Variability in a Coupled Climate Model, *J. Clim.*, 25(21), 7625–7642, doi:10.1175/JCLI-D-12-00051.1.

Tanhua, T., S. van Heuven, R. M. Key, A. Velo, A. Olsen, and C. Schirnick (2010), Quality control procedures and methods of the CARINA database, *Earth Syst. Sci. Data*, *2*(1), 35–49, doi:10.5194/essd-2-35-2010.

Uchida, H., G. C. Johnson, and K. E. McTaggart (2010), CTD Oxygen Sensor Calibration Procedures, GO-SHIP Repeat Hydrography Manual: A collection of expert reports and guidelines. IOCCP Report, (14).

Uchida, H., T. Kawano, I. Kaneko, and M. Fukasawa (2008), In situ calibration of optode-based oxygen sensors. *J. Atmos. Oceanic Technol.*, **25**, 2271-2281, doi:10.1175/2008JTECHO549.1.

Uda, M. (1963), Oceanography of the subarctic Pacific Ocean, *J. Fish. Res.*, 20, 119–179.

Ueno, H., and I. Yasuda (2000), Distribution and formation of the mesothermal structure

(temperature inversions) in the North Pacific subarctic region, *J. Geophys. Res.*, 105(C7), 16,885–16,897.

Ueno, H., and I. Yasuda (2003), Intermediate water circulation in the North Pacific subarctic and northern subtropical regions, *J. Geophys. Res.*, 108(C11), 3348, doi:10.1029/2002JC001372.

Ueno, H., and I. Yasuda (2005), Temperature inversions in the subarctic North Pacific, *J. Phys. Oceanogr*., 35(12), 2444–2456.

Warner, M. J., J. L. Bullister, D. P. Wisegarver, R. H. Gammon, and R. F. Weiss (1996), Basin-wide distributions of chlorofluorocarbons CFC-11 and CFC-12 in the North Pacific: 1985–1989, *J. Geophys. Res.*, 101, 20525-20542, doi:10.1029/96JC01849.

Watanabe, Y. W., M. Shigemitsu, and K. Tadokoro (2008), Evidence of a change in oceanic fixed nitrogen with decadal climate change in the North Pacific subpolar region, *Geophys. Res. Lett*., *35*, L01602, doi:10.1029/2007GL032188.

Watanabe, Y. W., T. Ono, A. Shimamoto, T. Sugimoto, M. Wakita, and S. Watanabe (2001), Probability of a reduction in the formation rate of the subsurface water in the North Pacific during the 1980s and 1990s, *Geophys. Res. Lett.*, *28* (17), 3289-3292.

Watanabe, Y. W., M. Wakita, N. Maeda, T. Ono, and T. Gamo (2003), Synchronous bidecadal periodic changes of oxygen, phosphate and temperature between the Japan Sea deep water and the North Pacific intermediate water, *Geophys. Res. Lett.*, 30(24), 2273, doi:10.1029/2003GL018338.

Whitney, F. A., H. J. Freeland, and M. Robert (2007), Persistently declining oxygen levels in the interior waters of the eastern subarctic Pacific, *Prog. Oceanogr.*, *75*(2), 179-199.

Winkler, L. W. (1888), Die Bestimmung des im Wasser gelösten Sauerstoffes. *Berlin Deut. Chem. Ges.*, 21, 2843–2854.

Wisegarver, D.P., J. L. Bullister, R. H. Gammon, F. A. Menzia, and K. C. Kelly (1993), NOAA chlorofluorocarbon tracer program air and seawater measurements: 1986-1989, *NOAA Data Report ERL PMEL No. 43*.

Yagi, M., and I. Yasuda (2012), Deep intense vertical mixing in the Bussol' Strait, *Geophys. Res. Lett.*, 39(1), L01602, doi:10.1029/2011GL050349.

Yamamoto-Kawai, M., S. Watanabe, S. Tsunogai, and M. Wakatsuchi (2004), Chlorofluorocarbons in the Sea of Okhotsk: Ventilation of the intermediate water, *J. Geophys. Res.*, 109(C9), C09S11, doi:10.1029/2003JC001919.

Yasuda, I. (1997), The origin of the North Pacific Intermediate Water, *J. Geophys. Res.*, 102, 893-909, doi:10.1029/96JC02938.

Yasuda, I., K. Okuda, and Y. Shimizu (1996), Distribution and modification of North Pacific Intermediate Water in the Kuroshio-Oyashio interfrontal zone, *J. Phys. Oceanogr.*, 26, 448–465.

Yasuda, I., S. Kouketsu, K. Katsumata, M. Ohiwa, Y. Kawasaki, and A. Kusaka (2002), Influence of Okhotsk Sea Intermediate Water on the Oyashio and North Pacific Intermediate Water, *J. Geophys. Res.*, 107(C12), 3237, doi:10.1029/2001JC001037.

Yasuda, I., S. Osafune, and H. Tatebe (2006), Possible explanation linking 18.6-year period nodal tidal cycle with bi-decadal variations of ocean and climate in the North Pacific, *Geophys. Res., Lett., 33*, L08606, doi:10.1029/2005GL025237.

Yasuda, T., and K. Sakurai (2006), Interdecadal variability of the sea surface height around Japan, *Geophys. Res. Lett.*, 33, L01605, doi:10.1029/2005GL024920.